Establishment of an *in vitro* test platform for nanoparticle toxicity testing under realistic exposure conditions

Inaugural-Dissertation

to obtain the academic degree

Doctor rerum naturalium (Dr. rer. nat.)

submitted to the Department of Biology, Chemistry, Pharmacy

of Freie Universität Berlin

by

Lars Benedikt Leibrock

from Homburg

2021

This thesis was carried out at the German Federal Institute for Risk Assessment (BfR) in Berlin from April 2016 to November 2020 under the supervision of Prof. Dr. Dr. Andreas Luch.

1st Reviewer: Prof. Dr. Dr. Andreas Luch

2nd Reviewer: Prof. Dr. Burkhard Kleuser

Date of defense: 13.10.2022

Erklärung

Hiermit versichere ich, die vorliegende Dissertation mit dem Titel „Establishment of an *in vitro* test platform for nanoparticle toxicity testing under realistic exposure conditions" selbstständig und ohne Benutzung anderer als der zugelassenen Hilfsmittel angefertigt zu haben. Alle angeführten Zitate sind als solche kenntlich gemacht. Die vorliegende Arbeit wurde in keinem früheren Promotionsverfahren angenommen oder als ungenügend beurteilt.

Lars Benedikt Leibrock

Die Dissertation wurde in englischer Sprache verfasst.

Acknowledgement

First, I would like to thank Prof. Dr. Dr. Luch for his supervision, guidance, and the opportunity to conduct my doctoral in his department at the German Federal Institute for Risk Assessment (BfR). I appreciated his continues support and the opportunity to work freely on this topic.

I would like to thank Prof. Dr. Kleuser for his interest in the project and his role as second reviewer.

I would also like to thank Dr. Laux for his support in administrative questions at BfR and for initiating many contacts in the research community.

I thank Dr. Tentschert for her ongoing interest in my thesis, her advice and the helpful discussions on ALI exposure systems and standardization. This project would certainly not have come about as it did without her support.

Thanks to Dr. Jungnickel for his help in ToF-SIMS analysis.

I would also like to thank Frank Bierkand and Dr. Ajay-Vikram Singh for their continuous interest in the project and a lot of fruitful discussions.

A big thanks to my cooperation partners at National Institute of Standards and Technology, Dr. Elijah Petersen and Blaza Toman. Thank you to Elijah for the great

discussions on data analysis to improve standardization. Those discussions were quite helpful in guiding my research project. I thank Blaza for R-Code development.

Without the professional and technical support of all research assistants at BfR, this work would certainly not have worked so great. Thus, I thank Julian Tharmann for introducing me in ALI systems, Philipp Reichardt, Roman Schmidt and Nadine Dreiack for their support in ICP-MS and Aaron Katz for this assistance in ALI studies.

Performing preliminary experiments and testing ideas is the beginning of all projects. Therefore, I would like to thank my students Rudolf Bittner and Tanja Vogt for her excellent work. It was a great pleasure for me to supervise you through my PhD time.

A great thanks goes to all my PhD colleagues. Especially the Nano-Boy office. We went through a lot of ups and downs. Therefore, I would like to thank you, Fabian Kriegel, Benjamin-Christoph Krause, Yves Hachenberger and Daniel Rosenkranz for your ongoing support during this time. It was pleasure to meet and work with you. On this way, I would also like to thank Henrik Herring for all the nice weekends we spent together in the cell culture. Always fun to work with you. I will certainly miss this time and wish you all the best for your future, personally and professionally.

At least the biggest thank goes to my family who supported me the entire time. In particular, my parents and my brother: You supported me from the beginning with all you got. Thank you for everything. It is more than I can enumerate here and can’t be taken for granted.

Table of contents

Summary

Animal experiments are still the gold standard to assess inhalation toxicology of nanomaterials (NMs). Due to financial and ethical reasons, it is of interest to create alternative methods based on human pulmonary *in vitro* models. There are accepted regulatory methods to investigate for example genotoxicity or sensitization like the Ames test, the micronucleus test, the Comet assay or the local lymph node assay. However, the toxicity of NMs also depends on the type of exposure.

In contrast to standard submerse cell culture; air liquid interface (ALI) systems closer represent the *in vivo* situation as they allow the exposure of an aerosol containing the substance of interest, which is considered a promising possibility as alternative method. Therefore, ALI exposure should be considered when assessing nanomaterial toxicity. Until today, there is no *in vitro* method based on ALI systems which is regulatory accepted. This is mainly due to the fact, that there are currently no standardized protocols for testing and evaluating nanomaterials in ALI application.

This thesis deals with the characterization of an ALI system to enhance data quality and reproducibility to further standardize ALI systems. Using a cause-and-effect (C&E) approach, several parameters like relative humidity, aerosol air temperature, flow rate and CO_2 concentration in the aerosol were identified to be critical for the viability of the used cells.

In addition to the type of exposure, the applied dose is also important for assessing toxicity. Since there is hardly any data on the concentration of CeO_2 NPs (nanoparticles) in air, previous investigations are do not include realistic concentrations as they occur in the environment.

For the first time, an intracellular delivery of CeO_2 NPs similar to *in vivo* conditions has been verified by using the characterized and optimized ALI system. The production of equal intracellular concentrations is a necessary starting point to compare *in vitro* and *in vivo* data, representing an important step in the development of an alternative testing method. It was demonstrated that the application of environmentally relevant and realistic CeO_2 NP concentrations can influence the composition of the cell membrane of the alveolar epithelium on a molecular level as a decrease in both phosphatidylcholines and lysophosphatidylcholines was detected. Since cell membrane lipids play an important role in the signaling cascade of proliferation and apoptosis, harmful effects like cancer development as a consequence of NP exposure cannot be excluded completely, even at such low NP concentrations. However, this needs further investigation. It is therefore important to conduct studies with very low doses in the future and include molecular level assessments.

Furthermore, the newly developed hAELVi and huAEC cell lines as well as the 3D alveolar cell model EpiAlveolar were investigated in detail. All cell systems showed a clear cell-cell contact formation and a barrier function comparable to *in vivo*. Additionally, both cell lines showed similar biological responses to CeO_2 NPs, comparable to the established but intact barrier function lacking cell model A549.

In conclusion, the goal of this submitted doctoral thesis of creating a reliable *in vitro* platform to assess and characterize the toxicity of CeO_2 NPs under realistic conditions with a commercially available ALI system was successful.

Zusammenfassung

Tierversuche sind bis heute der Goldstandard in der Inhalationstoxikologie von Nanomaterialien. Aus finanziellen und ethischen Gründen ist es jedoch von großem Interesse hierfür Alternativmethoden zu schaffen.

Zur Beurteilung von Endpunkten wie z.B. Genotoxizität oder Sensibilisierung existieren regulatorisch akzeptierte Alternativmethoden wie der Ames Test, der Mikrokerntest, der Comet Assay oder der Local lymph node assay.

Die Toxizität von Nanomaterialien hängt z.T. von der Art der Exposition ab. Air-liquid interface (ALI) Systeme bilden im Gegensatz zu klassischen submersen Expositionsmodellen die *in vivo* Situation besser ab. Daher sollte die Expositionsart ebenfalls bei der Beurteilung der Toxizität von Nanomaterialien Berücksichtigung finden. Gegenwärtig hat jedoch noch kein ALI basiertes *in vitro* Verfahren die regulatorische Akzeptanz erreicht. Grund dafür ist vor allem eine fehlende Standardisierung der Evaluationsmethoden zur Testung und Beurteilung der Toxizität von Nanomaterialien, obwohl ALI Methoden bereits lange als potenzielle Alternativmethode diskutiert wird.

Ein Ziel der vorgelegten Arbeit ist daher, die Datenqualität und Reproduzierbarkeit eines ALI Systems zu charakterisieren und zu optimieren. Hierzu wurde die Entwicklung eines neuen Ansatzes zur Datenauswertung mittels eines Bayesian Modells angewandt. Zudem wurde mit Hilfe einer cause–and-effect (C&E) Analyse verschiedene Parameter wie relative Feuchtigkeit, Lufttemperatur des Aerosols, Flussgeschwindigkeit und CO_2 Konzentration identifiziert, welche für die Viabilität der verwendeten Zellen essenziell sind.

Die Herstellung gleicher intrazellulärer Konzentrationen zwischen *in vivo* und *in vitro* ist ein notwendiger Ansatz, um *in vitro* und *in vivo* Daten miteinander vergleichen zu können und stellt daher einen wichtigen Schritt in der Entwicklung einer potenziellen Alternativmethode dar. Erstmals konnte gezeigt werden, dass die Applikation von CeO_2 Nanopartikeln mit dem beschrieben ALI System in der Lage ist, intrazelluläre CeO_2 Nanopartikelkonzentrationen zu generieren und somit einen Ansatz zur Vergleichbarkeit von *in vitro* und *in vivo* Daten schafft.

Zur Beurteilung der Toxizität ist neben der Expositionsart auch die applizierte Dosis relevant. Da es nur sehr wenige Daten zur Konzentration von CeO_2 Nanopartikeln in der Luft gibt, orientieren sich bisherige Bewertungen nicht an realistischen Konzentrationen wie sie in der Umwelt vorkommen. Die Exposition umgebungsrelevanter CeO_2 Nanopartikelkonzentrationen zeigte eine Verringerung der Phosphatidylcholine und Lysophosphatidylcholine in humanen Lungenepithelzellen. Dies zeigt deutlich, dass bereits sehr geringe Nanopartikelkonzentrationen einen signifikanten Einfluss auf die Zusammensetzung der Lipide der Zellmembran des alveolaren Epithels auf molekularer Ebene haben. Aufgrund der Beteiligung der Zellmembranlipide in den Signalkaskaden von Proliferation und Apoptose, ist es nicht auszuschließen, dass auch geringe Nanopartikelkonzentrationen schädliche Effekte wie z.B. die Entstehung von Krebs begünstigen könnten. Daher ist es wichtig künftig auch Untersuchungen mit sehr niedrigen Dosen durchzuführen und die molekulare Ebene mit in die Bewertungen einzubeziehen, um eventuelle Langzeitfolgen toxikologisch bewerten zu können.

In der vorliegenden Arbeit wurden die neu entwickelten Zelllinien hAELVi und huAEC sowie das 3D alveolare Zellmodell EpiAlveolar im Hinblick auf ihre Barrierefunktion detailliert untersucht. Beide Zelllinien zeigten ausgeprägte Zell-Zell-Kontakte sowie

vergleichbare biologische Antworten auf CeO_2 Nanopartikel, verglichen mit dem etablierten Zellmodell A549, welches jedoch keine intakte Barrierefunktion aufweist, was für die realistische Abbildung der Pharmakodynamik von Nanopartikeln nach Inhalationsexposition unter *in vivo* Bedingungen jedoch unerlässlich ist. Somit stellen die neu untersuchten Zellmodelle eine weitere Annäherung an die *in vivo* Situation dar, wodurch eine verbesserte Vergleichbarkeit zwischen *in vitro* und *in vivo* möglich wird.

Mit der erfolgreichen Charakterisierung des ALI Systems und der Verwendung neuartiger Zellsysteme wurde eine Plattform geschaffen, um die Toxizität von CeO_2 Nanopartikeln unter realistischen Bedingungen zu beurteilen.

Abbreviations

Ag	Silver
ALI	Air-liquid interface
Au	Gold
$BaSO_4$	Barium sulfate
C&E	Cause-and-effect
Ce	Cerium
CeO_2	Cerium dioxide
CO_2	Carbon dioxide
CPI	Consumer Products Inventory
DLS	Dynamic light scattering
DMEM	Dulbecco's Modified Eagle Medium
DNA	Desoxyribonucleic acid
EDTA	Ethylenediaminetetraacetic acid
EU	European Union
GBP	Granular biopersistent particle without known significant specific toxicity
h	Hour
hAELVi	Human Alveolar Epithelial Lentivirus immortalized
huAEC	Human Airway Epithelial Cells
ICP-MS	Inductively coupled plasma mass spectrometry
LDH	Lactatdehydrogenase
NM	Nanomaterial
NOAEL	No observed adverse effect level

NP	Nanoparticle
NTA	Nanoparticle tracking analysis
OECD	Organisation for Economic Co-operation and Development
OEL	Occupational exposure limit
PBS	Phosphate buffered saline
PCLS	Precision-cut lung slices
ppb	Parts per billion
PSLT	Poorly soluble low toxicity
REACH	Registration, Evaluation, Authorisation and Restriction of Chemicals
ROS	Reactive oxygen species
SMPS	Scanning mobility particle sizer
TEER	Transepithelial electrical resistance
TiO_2	Titanium dioxide
ToF-SIMS	Time of flight secondary ion mass spectrometry
WST	Water-soluble tetrazolium salt
ZnO	Zinc oxide
ZO-1	Zonula Occludens-1

1. Introduction

1.1 Nanomaterials: definition and general regulations

Nanotechnology is an emerging field and considered as a key innovation platform of the 21th century. The bases of this technology are materials with a size of 10^{-9} meter or 1 nanometer, so-called nanomaterials (NMs). In 2021, more than 1800 consumer products containing NMs were available on the European Union (EU) market based on the Consumer Products Inventory (CPI) [1].

To ensure the safety of these products, regulation is of great importance. Therefore, NMs were included into the REACH (Registration, Evaluation, Authorisation and Restriction of Chemicals) regulation [2,3]. Whereas a definition of the term NM was missing in this REACH regulation, the EU commission reported a recommendation in 2011, which is now used as a general definition [4]: *„Nanomaterial means a natural, incidental or manufactured material containing particles, in an unbound state or as an aggregate or as an agglomerate and where, for 50 % or more of the particles in the number size distribution, one or more external dimensions is in the size range 1 nm - 100 nm. In specific cases and where warranted by concerns for the environment, health, safety or competitiveness the number size distribution threshold of 50 % may be replaced by a threshold between 1 and 50 %."* [4].

An additional definition is adopted in the same recommendation that involves the surface area instead of size: *"A material should be considered as falling under the definition in point 2 where the specific surface area by volume of the material is greater than 60 m^2/cm^3. However, a material which, based on its number size*

distribution, is a nanomaterial should be considered as complying with the definition in point 2 even if the material has a specific surface area lower than 60 m^2/cm^3" [4]. Based on this definition NMs can be divided into three main groups: nanoparticles (NPs), nanofibers, and nanoplatelets where three dimensions, two dimensions or one dimension are in the range of 1-100 nm, respectively.

Besides REACH, specific EU regulations exist for NMs with specific provisions, using either the EU definition from 2011 or modified definitions. These specific provisions cover biocidal products [5], cosmetic products [6], food regulations and food contact materials [7-11], and medical devices [12,13].

1.2 History view of nanoparticles

Although nanotechnology is a relatively young term, nanotechnological applications have a long history. Certainly, the best known ”nano” effect is the lotus effect of plants where fluids are repelled from the surface of the leaves. This effect is mainly achieved by the microstructure plant surface in combination with wax, which minimizes the contact area between the leaf and the fluid avoid wetting of the surface [14].

Another well-known nanotechnological example can be found in the animal kingdom. Geckos run along different smooth and slippery walls like glass and they can even hang from ceilings. This extraordinary ability is caused by their feet which are covered with nano-sized hairs interacting with the surface via van-der-Waals forces to hold the gecko on the surface [15].

Without knowing it, people have already employed NMs for thousands of years.

More than 6500 years ago, people used asbestos nanofibers to reinforce ceramics [16]. Pigments and colors on NM basis have also been used centuries ago. For

example, the pigment Egyptian blue was the first nano based synthetic pigment containing cuprorivaite ($CaCuSi_4O_{10}$) nanosheets and nanoplates used by Egyptian people 3000 before Christ [17]. The pigment Maya blue, which consists of clay and metallic NPs, has been used to color artifacts and ceramics [18]. Already 2000 years ago, lead- sulfur nanocrystals were utilized as hair coloring agent in the Greco-Roman period [19]. One long tradition in nanotechnology is the use of metallic nanoparticles in coloring glass and ceramics. One example is the glassware from Satsuma. Its typical red color originates from incorporated copper NPs [20]. Other glassware shows yellow stain that originates from silver (Ag) NPs inside the glass [21]. One further famous example is the Lycurgus Cup from the 4th century, which is exposed in the British Museum in London. Depending on the location of illumination, the cup appears either green when it is illuminated from outside or red when it is illuminated from inside. This dichroism relies on the embedding of gold (Au) and silver NPs in a ratio of 3/7 inside the glass [22-24].

From an historical perspective, gold is one of the oldest known metals. For centuries gold NPs provides the red color of church windows [25]. In Europe, colloidal gold was applied by alchemists in the Middle Ages to treat various diseases [26]. Nowadays nano sized gold is an important part of many different biomedical applications such as contrast agent for CT examinations [27], conjugated to antibodies for specific targeting in cancer therapy [28] or as drug delivery systems [29].

1.3 Exposure and uptake routes of engineered nanomaterials

There is a wide range of NM applications covering biomedical fields like cancer therapy, [30-32] immunology [33] as well as a lot of different manufacturing areas, like the production of titanium dioxide (TiO_2) based solar cells [34,35]. In addition, nowadays, a lot of consumer products like textiles, [36] paints [37] or cosmetic products [38] contain NMs. So, for consumers an enhanced direct exposure risk might occur. Therefore, risk assessment is of major concern to ensure the safety of such products by identifying possible adverse short- and long-term health effects of users. For NMs, different exposure scenarios, like inhalation, dermal exposure, ingestion and intravenous injection have to be considered concerning suitable risk assessment processes.

Insoluble NPs like TiO_2 and zinc oxide (ZnO), which are part of sunscreens, have shown minor to no dermis penetration, suggesting the dermal exposure pathway is of rather minor concern [38-43].

Similarly, the ingestion of NMs is currently also considered to be of less importance [44-48].

In contrast, inhalation is considered as the main part of particle entrance into the human body [44,49-52].

1.4 Inhalation of engineered nanomaterials

1.4.1 Anatomy of the human lung

The lung is a highly specialized organ that is designed to perform gas exchange between air and blood stream to deliver oxygen to the body and remove carbon dioxide [53]. The human lung is divided into two lungs. The left lung consists of two lobes whereas the right lung possesses three lobes [54].

The human airway consists of two areas, the upper and the lower respiratory tract. After entering the upper respiratory tract, which consists of nose/mouth, paranasal sinuses, pharynx, and larynx, the air passes through the lower respiratory tract starting at the trachea (see figure 1). Distal from the trachea, the bronchial tree further divides dichotomy into the bronchioles and the terminal bronchioles. The terminal bronchioles then branch to form the respiratory bronchioles which passes into the alveolar ducts and finally into the alveoli (see figure 1) [55,56].

1.4.1.1 Anatomy of the alveolar region and the air-blood barrier

The human lung contains about 500 million alveoli [57]. These alveoli mainly consist of three cell types: The alveolar wall lining Type I and Type II pneumocytes and alveolar macrophages. Type I pneumocytes are terminally differentiated epithelia cells that cover 93% of the alveolar surface whereas the much smaller Type II pneumocytes cover about 7 % and act as progenitor stem cell [58-60]. In addition to that, one further important function of Type II cells is the secretion of surfactant, a mixture of phospholipids and proteins responsible for the reduction of surface tension in the alveolus during breathing [61-64].

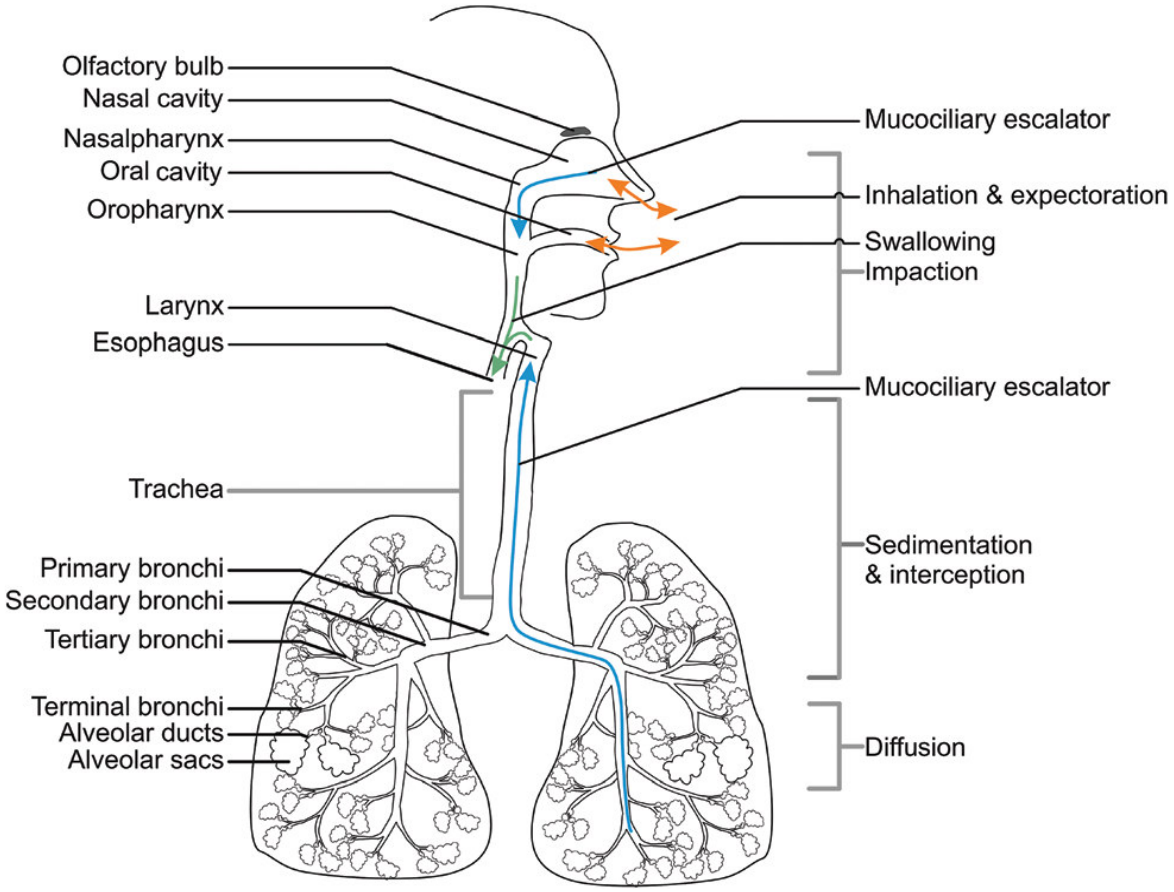

Figure 1: Schematic presentation shows the anatomy of the human lung on the left-hand side. Different particle deposition and clearing mechanisms are summarized on the right hand side (with permission from [55]).

The alveolar septa separate neighboring alveoli, thus creating the alveolar interstitium. Moreover, the alveolar septa provide the capillaries to the alveoli generating the air-blood barrier [65]. The whole air-blood barrier is about 2 µm thick and composed of the alveolar epithelium, the capillary endothelium and the alveolar interstitium [65,66]. In contrast, the air-blood diffusion barrier is formed by fusion of the basal membranes of endothelia and alveolar epithelia cells with a thickness of only 0.2 µm enables an improved gas exchange in the alveoli [65,66].

Considering the large alveolar surface of about 140 m^2 [65], the lung is exposed to many environmental factors and represents the main entrance for many pathogens and toxic substances like gases or particulate matter. For this, alveolar macrophages, the third type of alveolar cells, act as a defender of the alveolar environment maintaining the alveoli free of pathogens [67-69] and cleaning particulate matter and ultrafine particles from the lung [70-73].

1.4.2 Nanomaterials in the lung: pharmacodynamics and health risks

While respiring air, particulate matter and NMs can enter the lung where they deposit in different regions depending on their size [74-77]. Particular matter in the micrometer size range primarily deposit by impaction in the upper respiratory tract. Whereas particles in the nano size range can reach the bronchial and alveolar region where they deposit via sedimentation, interception or diffusion [55,75] (see figure 1). Due to the small size, NMs and especially NPs, mainly deposit in the alveolar region [70,76,77]. Once a NM has deposited onto the alveolar surface, it gets either internalized by the alveolar epithelium [78-80] or engulfed by an alveolar macrophage [70,81]. After phagocytizing a NM, alveolar macrophages move proximal to the bronchial region using the mucociliar escalator. The mucociliar escalator describes a clearing mechanism of the lung removing materials from the lower respiratory tract by cilia beating epithelia cells covered by a mucus layer. Material trapped in this mucus is then transported proximal by the cilia beating epithelium where it subsequently can be expired or swallowed to exclude it from the body [82,83]. The NM loaded alveolar macrophages utilize this mechanism to remove the engulfed NM mainly by swallowing the alveolar macrophages resulting in the NM exclusion from

the body via the gastrointestinal tract and feces [70,84,85]. Moreover, the mucociliar cleaning protects the epithelium from NPs reaching the underlying epithelium, representing an early-stage cleaning mechanism for NPs [86].

After passaging biological barriers like the air-blood barrier, further NP clearance takes place via the lymphatic system and blood [87-90]. These clearing mechanisms may lead to a NM translocation to extrapulmonary organs and tissues as demonstrated *in vivo* for different NPs like CeO_2 [70,91] or barium sulfate ($BaSO_4$) [92]. Depending on the particle, NP dissolution properties needs to be considered as well regarding particle clearance and retention. As shown in different *in vivo* studies, soluble NPs have a significant shorter half-life compared to insoluble NPs which are often referred as GBP (granular biopersistent particle without known significant specific toxicity) [70,93] or PSLT (poorly soluble low toxicity) particles [94,95]. For example, Gosens et al. reported a complete clearance of copper oxide NPs from rat lungs after one day, suggesting this may have been driven primarily by phagocytosis of alveolar macrophages leading to NP dissolution in the lysosome [96]. Similar results have been shown by Takenaka and colleagues who exposed rats to 15 nm silver NPs via inhalation. They could show that more than 95 % of the silver was cleared from the lung within seven days [97]. For soluble ZnO NPs a half-life of 28 days was observed in rats [98]. In contrast, for PSLT particles like CeO_2 or $BaSO_4$, much longer retention times were found with half-life times up of several months, depending on the initial lung burden [44,71,92]. However, human data suggests even longer retention times up to several decades. In a photoengraver that had not been exposed to rare earth elements for 17 years, cerium (Ce) particles could still be detected in the lung and the nails [99]. Another human case report revealed Ce in the respiratory tract of the patient after his latest occupational exposure 21 years ago

[100]. In a retrospective human study Ce retention times up to 29 years have been reported [101]. These prolonged retention times as well as the distribution to extrapulmonary organs and tissues might then cause adverse and pathophysiological such as lung fibrosis [102,103].

Soluble NMs like Ag and ZnO have been shown to induce cytotoxicity, oxidative stress and DNA damage due to their strong ion release [104-108]. For rather insoluble NMs, different results were found depending on the material. TiO_2 and CeO_2 NPs, for instance, are considered relatively low cytotoxic, but both are able to induce genotoxicity by DNA damage [109]. The production of oxidative stress in lung epithelium is also a quite common property for many NPs like Au [110], TiO_2 [111], CeO_2 [112,113] or ZnO [108]. Beside material properties, shape can also have an important impact on NM toxicity. It has been demonstrated that fibers like Ag nanowires showed a carcinogenic potential *in vitro* while Ag NPs did not [114]. Such carcinogenic potential is also well known for asbestos fibers. When asbestos fibers are longer than 10 µm, the alveolar macrophages cannot completely engulf the fiber leading to the process of frustrated phagocytosis where the fibers cannot be cleared and cause inflammation and even cancer [115,116].

As *in vitro* experiments are limited in assessing such systemically effects like cancer formation, *in vivo* testing is still the gold standard in pulmonary nanotoxicology [117-119].

For TiO_2 particles a 90 day exposure study displayed inflammation and lung fibrosis in rats [102]. Fibrotic effects were also reported for CeO_2 NPs by Ma and colleagues in a rat installation model [103]. Schwotzer et al. exposed rats in a subchronic inhalation study to CeO_2 and $BaSO_4$ NPs. They could show lung inflammation in the

lower respiratory tract mediated by CeO_2 NPs. However, $BaSO_4$ did not induce lung fibrosis [71].

Morphological characteristics can also have a significant impact on NM toxicity as mentioned early. As shown by Kasai et al. the exposure of rats to fibrous NMs like multi-walled carbon nanotubes caused inflammation, fibrosis and granulomatosis, even at low concentrations of 0.2 $\mu m/m^3$ [120]. Furthermore, fibrous NMs have also been associated with tumor formation and mesothelioma as published in a Japanese *in vivo* instillation study [121]. The group of Aalapati et al. reported inflammation, oxidative stress, fibrosis, necrosis and granuloma formation in mice after CeO_2 NP inhalation as well as degenerative structural changes of the kidneys which were related to CeO_2 NP translocation [122].

These toxicological evidence and the long retention time of some NMs clearly demonstrate the importance of an appropriate risk assessment to evaluate possible short and long-term health effects. Such toxicological and risk assessment evaluations require many laboratory animals. Based on the 3R principles from Russell and Burch in 1959 (the *reduction* of animals in experiments to a minimum, the *replacement* of *in vivo* test methods by *in vitro* methods, and the *refinement* which means the enhancement of animal welfare during the whole experiment the animal is used for) [123]. It is therefore highly desired to reduce the animal number to a minimum in inhalation nanotoxicology. With this goal in mind, different *in vitro* approaches have been developed during the last decades to better assess the toxicological effects of NMs and especially NPs.

1.5 *In vitro* exposure approaches in inhalation nanotoxicology

Engineered NMs cover a wide range of applications. As their production and use increase, the risks of human NM exposure also increase, especially considering aerosolization of NPs. To assess possible adverse health effects of those NPs, different *in vitro* exposure systems have been developed in the last decades.

On the one hand side there is the so-called ”submerse” approach where NPs are dispersed directly in culture medium and applied on top of the cellular test system. On the other hand, there are the so-called ”air-liquid-interface systems” (ALI systems). In ALI systems cells are cultured on a microporous membrane allowing the apical cell part to be in contact with air, while the basal side stays in contact with the culture medium to deliver nutrients to the cells (see figure 2). In ALI systems, the NPs are dispersed in a biological fluid and subsequently applied apically to the cellular test system as an aerosol [124]. Compared to submerse exposure, ALI exposure has several advantages like a closer resembling of the physiological environment by being exposed to air on the apical side, as it is also the case *in vivo*. Furthermore, cultivation of lunge epithelia cells on ALI closer mimics the transcriptional profile of pulmonary *in vivo* cells than submerse cultivation [125]. In addition, there are less variations of the physicochemical properties of the NPs due to a reduced interaction of the NPs with cell culture medium. Interaction with the medium that contains serum could otherwise lead to a protein corona that covers the surface of the NPs which might then influence particle properties [126] and uptake [127].

Therefore, ALI systems are considered as useful tool and possible an alternative method for animal experiments with the ultimate goal to replace them in the future.

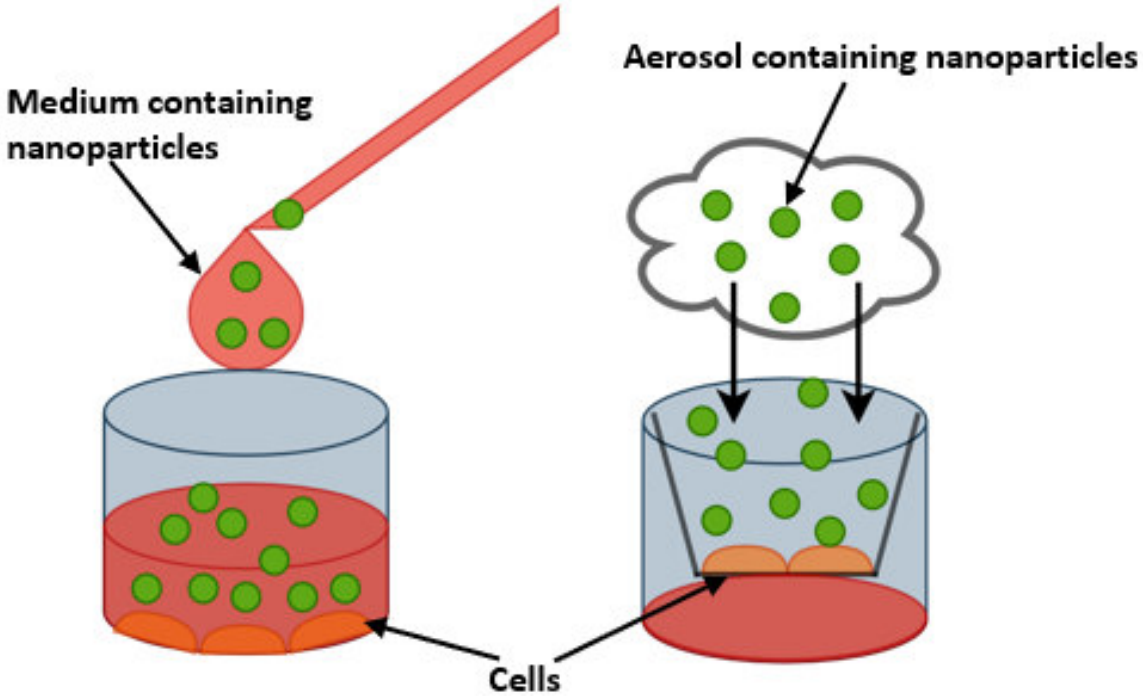

Figure 2: Principle of submerse (left) and ALI (right) exposure.

1.6 ALI systems

ALI systems have a wide range from those designed and used by individual research groups [128-131] to fully commercial available systems like Cultex® [56,132] or Vitrocell® [133,134]. There are also many different devices available based on the deposition mechanism. In this context, the two main types of ALI systems are cloud chamber systems [134,135] and flow-through systems [51,136] where the deposition is driven by sedimentation and diffusion, respectively.

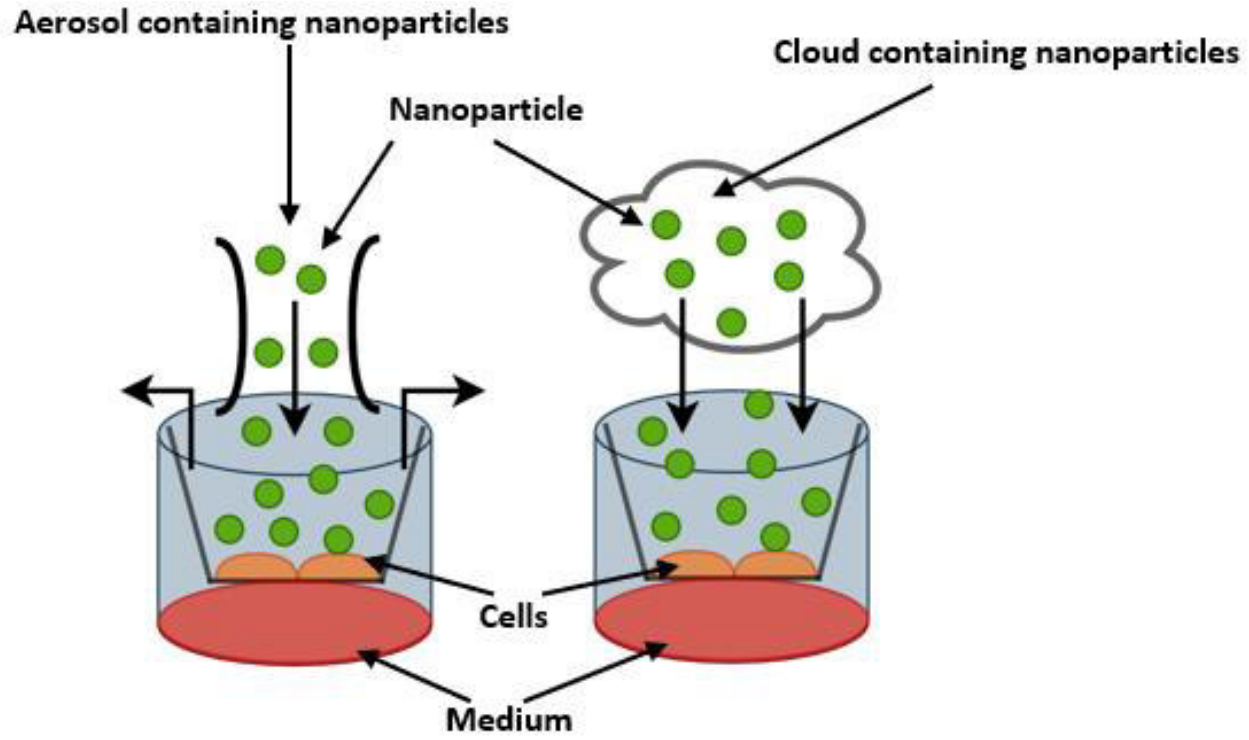

Figure 3: Exposure principle of flow-through (left) and cloud based (right) ALI devices.

1.6.1. Cloud chamber ALI

Cloud chamber systems are often used in inhalation nanotoxicity investigations as they represent an easy-to-use and fast application system [128,137,138]. Here, the NM is dispersed in a biological fluid or buffer and transferred into a nebulizer. The nebulizer subsequently atomizes the fluid to a cloud of droplets containing the NM, which then deposit onto the cells via sedimentation (see figure 3) [134,135]. This enables a fast and high exposure dose deposition in one application within minutes. Therefore, such devices are quite useful for investigating high doses, repeated exposures studies or worst-case scenarios. However, these systems do not allow an optimal representation of NP deposition in the alveolar lung as their deposition mechanism is primarily based on sedimentation instead of diffusion. To address this issue, flow-through systems can be used.

1.6.2 Flow-through ALI

One commonly used flow-through system is the commercially available Vitrocell® device. It has been used to study the effects of e-vapor gases and cigarette smoke [139,140] as well as NPs [141]. It can be equipped with a quarts microbalance sensor to determine the deposit particle mass directly during exposure [51]. Furthermore, electrostatic fields can be applied to enhance NP deposition [141].

The Vitrocell® device uses negative pressure to guide the aerosol that is produced in an aerosol generator (nebulizer or brush generator) into the exposure chamber where particle deposition takes place via diffusion/stagnation [142-144]. Compared to cloud-based ALI setups, flow-through ALI devices allow a close representation of the alveolar particle deposition *in vivo* making it an excellent tool to investigate toxicological effects of inhaled NMs and especially NPs. Therefore, such systems are considered preferable tools for developing alternative methods for animal testing.

1.6.3 ALI as possible *in vivo* alternative method

Different standardized guidelines exists on how to perform *in vivo* inhalation studies like the OECD test guidelines TG 412 [145], TG 413 or TG 453 [71] covering different scenarios like short term and long term exposure. These guidelines have already included animal welfare section, e.g., in terms of animal number used in the studies. Regarding genotoxicity of NMs, several alternatives are already accepted from the regulatory authority in inhalation toxicology, like the Ames test, the micronucleus test or the Comet test [146]. The type of exposure can also affect the toxicity of NMs. Hence, besides endpoint measurements, the type of exposure should also be considered when NMs toxicity testing is conducted. Nevertheless, an *in vitro*

alternative test method to assess inhalation toxicity considering the exposure method itself would be a further step to animal free test systems and reliable results.

ALI systems are considered to be promising tools to close this gap as they resemble the *in vivo* situation much closer than standard submerse exposure scenarios [147-149]. Until today, there is no ALI based alternative exposure method for inhalation toxicity accepted by the regulatory authority even ALI systems have been used in research for years. This is for several reasons: One aspect is that there are many different ALI systems and protocols, but no standardized guidelines are available on how *in vitro* inhalation toxicological tests should be carried out in general. This makes it difficult to compare the obtained *in vitro* data. In addition, comparisons between *in vitro* and *in vivo* studies are rather rare so far because of missing *in vivo* data (like intracellular or organ concentrations are not routinely measured), different endpoints that have been addressed or different concentrations that are used [150,151].

The literature describes the assessment of NP toxicity by comparing ALI and submerse exposure as well as submerse exposure to *in vivo*. For example, Loret and colleagues showed that ALI exposure of TiO_2 and CeO_2 NPs resulted in a higher toxicity than submerse exposure using equal dosages [51]. Teeguarden et al investigated the effect of iron oxide NPs *in vivo* on mice, as well as on alveolar macrophages and epithelia cells under submerse exposure conditions. Regarding inflammation, they found good *in vivo – in vitro* comparability for macrophages but not for epithelia cells. In addition, the authors mentioned that similar concentrations are needed in *in vivo* and *in vitro* experiments to make them more comparable [152]. A more realistic *in vitro* to *in vivo* comparison have been recently conducted by Jing and coworkers based on ALI experiments using similar doses of copper oxide NPs. They found good

agreement between mice and A549 cells exposed at ALI for low-density lipoprotein and interleukin release [153].

When mice and ALI cultured A549 cells were exposed to diesel using similar doses it was shown that the oxidative stress protein HO-1 increased in both systems to an equal extent indicating good accordance between *in vitro* (ALI) and *in vivo* models [132].

These results demonstrate that ALI systems can be a useful tool to compare *in vitro* and *in vivo* exposure when similar doses are used. However, from a regulatory or risk assessment point of view, realistic environmental NP concentrations should be considered in such studies. Unfortunately, data about realistic concentration of NPs are rare and exist only for a few NMs like carbon nanotubes, Ag, or TiO_2 mainly based on occupational concentrations [154,155]. Studies quantitatively describing realistic environmental concentrations for example for CeO_2, which is a NP that is frequently used as catalyst in diesel additive and released in the atmosphere via combustion engine exhausts [156], are quite rare. Park et al. monitored Ce air content in the UK and reported a concentration up to 0.6 $\mu g/m^3$ [157]. In addition, the authors calculated the Ce air concentration to be 5-25 mg/m^3 on the highway and 20-80 ng/m^3 in a street canyon [157]. Similar results were predicted by Erdakos and colleagues with a Ce air concentration range of 0.5-20 ng/m^3 for the US [158]. A modeled CeO_2 ambient air concentration more than 12 ng/m^3 was mentioned by Giese and coworkers [159]. Recently, the group of Liu et al. predicted a CeO_2 ambient air concentration of about 0.05 ng/m^3 [160]. In 2014, Gantt et al. measured a Ce air concentration of 0.3 ng/m^3 [161]. Thus, quantitative measured data on realistic environmental concentrations are rare and often missing for a lot NMs which makes

it difficult to investigate NM-related effects under realistic *in vivo* and *in vitro* conditions.

Besides data availability, little standardization and missing guidelines for ALI studies makes it tough to reliably reproduce the complex microenvironment of the alveoli with *in vitro* models.

1.7 *In vitro* models in inhalation nanotoxicity

Optimizing the predictive power of *in vitro* models in inhalation nanotoxicology, mimicking the *in vivo* environment more closely, has been addressed extensively in recent years ranging from simple 2D cell systems to sophisticated multi cultured cell models. Typical 2D mono-cultured cell systems for NP toxicity testing are the alveolar type II cell line A549 [109] and the bronchial cell line Calu-3 [162]. Co-culture models based on lung epithelia cells and immune cells have recently been used to investigate inflammatory effects of CeO_2 NPs under submerse and ALI conditions suggesting higher sensitivity for co-culture systems compared to mono-cultured cells [51]. Rothen-Rutishauser et al. generated a triple co-culture model to investigate micro- and nanoparticle cell interactions based on A549 cells, macrophages and dendritic cells [137,163]. Mimicking the blood air barrier, a co-culture of four different cell types (A549 lung epithelia cells, EA.hy 926 endothelia cells, HMC-1 mast cells, and THP-1 macrophages) has been developed to assess the uptake of silicon dioxide NPs [164]. In addition to the self-generated models, there are also commercial cell systems available like MucilAir™, EpiAirway™ [133,165] or EpiAlveolar™ [166] that are produced from different donors, which can subsequently be used to test NP toxicity. With the advantage of a primary phenotype, they represent the *in vivo*

situation closer than cell lines. Additionally, these models are also applied to study NP effects under specific pathological conditions like asthma [128].

Furthermore, highly sophisticated organ-on-a-chip systems have opened the research field of particle translocation under more physiological conditions as they allow dynamic culture by stretching the epithelial cell layer mimicking inhalation and exhalation [167,168]. *Ex vivo* models like precision-cut lung slices (PCLS) represent an interesting tool to study NP toxicity as they mimic the anatomical *in vivo* structure of the lung as close as possible [169,170]. Nevertheless, animals have to be sacrificed to generate PCLS. Therefore, their use as possible alternative method is questionable. Neither PCLS nor lung-on-the-chip systems have made it into mainstream testing yet, as they represent complex and costly approaches. Therefore, most nanotoxicological studies are still conducted with 2D cell cultures. In these experiments, either bronchial cells are usually used to represent functional barrier models [112,162] or A549 cells to represent the alveolar compartment [171]. As nanoparticles mainly deposit in the alveolar region, alveolar cells should be considered as most relevant target region in inhalation nanotoxicology [70,76,77]. A549 cells are type II alveolar epithelia cells [171] incapable to express functional tight junctions [162,172,173]. Thus, they do not reflect a proper *in vitro* model for inhalation toxicity studies, especially when more sophisticated questions like particle translocation are addressed. Nevertheless, A549 cells were used for a long period of time in inhalation toxicology because there was no alternative cell model with functional tight junctions available; except primary cells [172]. This changed in 2016 when Kuehn et al (2016) introduced a new alveolar type I cell model called hAELVi (human Alveolar Epithelial Lentivirus immortalized) which were able to build a dense tight junction network [174]. As type I cells cover more than 90 % of the alveolar surface, they are the main cell type that comes in contact

with inhaled particles in the alveolar region [174,175]. Therefore, hAELVi cells represent a promising tool to further improve *in vitro* systems and help generating data mimicking the *in vivo* situation closer. However, since little is known about this cell system to date, its value for inhalation nanotoxicology needs to be further validated, especially with respect to other well established cell models.

2. Objective

During the last decades, the use of NMs has drastically increased in consumer products and technological applications [1]. Accompanied by that, a higher exposure of the consumer to NMs is likely. This raises questions regarding adverse health effects and possible regulations. Toxicity testing of chemicals including their nanoforms is still mainly conducted *in vivo*. Reducing animal studies to a minimum is therefore of big relevance. To reach this goal, ALI systems are considered useful tools as they allow NP exposure mechanisms under *in viv*o like terms. Even though intensive *in vitro* investigations have been conducted, no ALI based alternative method has reached the level of a validated or regulatory accepted procedure so far allowing the evaluation of inhalation toxicity of NPs *in vitro* [176]. However, as different *in vivo* studies have extensively shown, NP translocate from the lung to secondary organs and tissues after inhalation, a proper risk assessment is required. The reason for that gap is a missing standardization of ALI exposure studies as well as the used cellular *in vitro* models which reflects the *in vivo* situation only to a limited extent avoiding complex investigations, which are however addressed *in vivo*. Moreover, studies comparing *in vit*ro to *in vivo* are quite rare. In addition, different doses are used when comparing *in vitro* to *in viv*o which makes it very difficult to compare the data and responses.

Therefore, the first objective of this work was to establish and characterize an ALI interface system in order to provide a first step of standardization. Afterwards, the obtained *in vitro* data were compared to *in vivo* results to prove that this ALI system is able to deliver intracellular CeO_2 NPs concentrations similar to *in vivo* exposure. The second objective covers the developed of two new cell lines concerning their

ability to express tight junctions under ALI NP exposure to further enhance the comparability between *in vitro* to *in vivo*.

With this, a standardized ALI procedure was established allowing optimal *in vitro* test conditions similar to *in vivo*.

The results obtained during this thesis will help in the standardization of ALI exposure systems using *in vivo* relevant cell culture models for NP inhalation toxicity with the long-term goal of establishing an alternative method for *in vivo* inhalation studies.

In the following section, the results of my work are presented.

3. Results:

Publications are displayed in a non-chronological order to ease understanding.

3.1. Objective 1: Parametric Optimization of an Air–Liquid Interface System for Flow-Through Inhalation Exposure to Nanoparticles Assessing Dosimetry and Intracellular Uptake of CeO_2 Nanoparticles

Lars B. Leibrock, Harald Jungnickel, Jutta Tentschert, Aaron Katz, Blaza Toman, Elijah J. Petersen, Frank S. Bierkandt, Ajay Vikram Singh, Peter Laux and Andreas Luch

This chapter was published online on 28.11.2020 in:
Nanomaterials **2020**, *10(12)*, 2369 by MDPI
https://doi.org/10.3390/nano10122369

Involvement of the author within this publication: Project planning (75 %), project execution (90 %), data analysis (70 %), manuscript writing (85 %).

Supplementary materials for this publication are shown in Annex I.

nanomaterials

MDPI

Article

Parametric Optimization of an Air–Liquid Interface System for Flow-Through Inhalation Exposure to Nanoparticles: Assessing Dosimetry and Intracellular Uptake of CeO_2 Nanoparticles

Lars B. Leibrock [1,*], Harald Jungnickel [1], Jutta Tentschert [1], Aaron Katz [1], Blaza Toman [2], Elijah J. Petersen [3], Frank S. Bierkandt [1], Ajay Vikram Singh [1], Peter Laux [1] and Andreas Luch [1]

1 German Federal Institute for Risk Assessment (BfR), Department of Chemical and Product Safety, Max-Dohrn-Strasse 8-10, 10589 Berlin, Germany; harald.jungnickel@bfr.bund.de (H.J.); jutta.tentschert@bfr.bund.de (J.T.); aaron.katz@bfr.bund.de (A.K.); frank.bierkandt@bfr.bund.de (F.S.B.); ajay-vikram.singh@bfr.bund.de (A.V.S.); peter.laux@bfr.bund.de (P.L.); andreas.luch@bfr.bund.de (A.L.)

2 Information Technology Laboratory, National Institute of Standards and Technology, 100 Bureau Drive, Gaitherburg, MD 20899-8311, USA; blaza.toman@nist.gov

3 Materials Measurement Laboratory, National Institute of Standards and Technology, 100 Bureau Drive, Gaitherburg, MD 20899-8311, USA; elijah.petersen@nist.gov

* Correspondence: lars.leibrock@bfr.bund.de; Tel.: +49-151-16985009

Received: 3 November 2020; Accepted: 27 November 2020; Published: 28 November 2020

Abstract: Air–liquid interface (ALI) systems have been widely used in recent years to investigate the inhalation toxicity of many gaseous compounds, chemicals, and nanomaterials and represent an emerging and promising *in vitro* method to supplement *in vivo* studies. ALI exposure reflects the physiological conditions of the deep lung more closely to subacute *in vivo* inhalation scenarios compared to submerged exposure. The comparability of the toxicological results obtained from *in vivo* and *in vitro* inhalation data is still challenging. The robustness of ALI exposure scenarios is not yet well understood, but critical for the potential standardization of these methods. We report a cause-and-effect (C&E) analysis of a flow through ALI exposure system. The influence of five different instrumental and physiological parameters affecting cell viability and exposure parameters of a human lung cell line *in vitro* (exposure duration, relative humidity, temperature, CO_2 concentration and flow rate) was investigated. After exposing lung epithelia cells to a CeO_2 nanoparticle (NP) aerosol, intracellular CeO_2 concentrations reached values similar to those found in a recent subacute rat inhalation study *in vivo*. This is the first study showing that the NP concentration reached *in vitro* using a flow through ALI system were the same as those in an *in vivo* study.

Keywords: air–liquid interface system; inhalation toxicology; nanoparticles; CeO_2; standardization; cause-and-effect analysis

1. Introduction

During the last two decades, engineered nanomaterials (ENMs) have received widespread attention due to their broad range of applications including industry, [1–7] medicine [8–10] and consumer products [11–13]. During the manufacturing process and consumer usage of these products, there is the potential for an increased risk of inhalation exposure [14–17].

Currently, evaluation of the potential health hazards from inhalation exposure is predominantly conducted using animal models [18–24]. For governmental and regulatory purposes as well as

based on the 3R principle ("replace, reduce, refine"), the development of alternative non-animal test methods represents a pressing issue [25]. Typically, *in vitro* nanotoxicological studies are performed under "submerged" conditions where the cells are exposed to particles dispersed in the overlying cell culture medium containing a mixture of proteins and other biological compounds [23,25,26]. However, dispersing nanoparticles (NPs) in cell culture media might alter their physical and chemical properties such as their agglomeration status and the adsorption of serum proteins onto the particles, which subsequently might impact the resulting toxicological data [27,28]. In contrast, for aerosol exposure using air–liquid interface (ALI) systems the NPs can be dispersed in water. Only after aerosolization and deposition on cells will the NPs come in contact with the cell microenvironment such as mucus or epithelia lining fluid [29].

Overall, ALI approaches can mimic *in vivo* inhalation experiments of airborne nanomaterials more closely than *in vitro* studies using submerged conditions [29]. In recent years, different ALI systems have been developed for nanomaterial testing *in vitro* [30–34]. The Vitrocell exposure system is one of the most commonly used commercially available ALI exposure systems for inhalation toxicity testing [29]. It has been successfully used to examine the effects of cigarette smoke [35–37], NPs [38–41], and diesel exhaust [30,42,43]. However, despite the increasing use of ALI systems, there is no standard operation procedure (SOP) on how NP exposure should be performed to ensure robust and reproducible results among different laboratories [29,30,39,40,42,44]. Furthermore, there are few comprehensive studies on the technical challenges of such systems (e.g., deposition efficiency, exposure time), and how to identify or overcome them. In the current literature, generally only a minimal description of the exact setup (e.g., relative humidity, temperature of the aerosol flow, or the distance between air inlet and cells) is given and a description of experimental challenges encountered is rarely provided [37,40–42,44,45]. This hampers the comparison among *in vitro* results achieved with such systems and with *in vivo* data [46–48].

A primary aim of this study was to evaluate parameters expected to influence cell viability during cell exposure using an ALI flow through system. Therefore, the human alveolar epithelia cell line A549, which was derived from a human adenocarcinoma in 1973 [49], was exposed to clean filtered air, and five parameters (relative humidity, flow rate, aerosol temperature, exposure duration, and CO_2 supply) were varied to evaluate the impact of these parameters on the cell viability from the air exposure itself. Although A549 cells are not a primary cell line, their use here is appropriate as the main focus is to assess the robustness of the ALI system itself [41]. Using conditions that avoided a decrease in cell viability, cells were then exposed to CeO_2 NPs. The deposition and intracellular particle uptake were characterized using inductively coupled plasma-mass spectrometry (ICP-MS) and time of flight-secondary ion mass spectrometry (ToF-SIMS) and then compared with previously obtained *in vivo* data.

2. Materials and Methods

2.1. Cell Culture

A549 cells (obtained from ATCC; catalog number: CCL-185) were cultured in Dulbecco's Modified Eagle Medium (DMEM) supplemented with 10% fetal bovine serum (FBS) (PAN-Biotech GmbH, Aidenbach, Germany), 1% penicillin/streptomycin (PAN-Biotech GmbH, Aidenbach, Germany) and 1% L-glutamine (PAN-Biotech GmbH, Aidenbach, Germany). Cells were passaged two times per week. *In vitro* experiments were conducted with the passages 19–79. Mycoplasma contamination was tested regularly and was always negative; details about this method are described in Supplementary Materials Tables S1 and S2.

2.2. Cause-And-Effect Analysis

A cause-and-effect (C&E) analysis was performed on a cell viability assay for NP exposure using the ALI flow through exposure system to reveal the expected key sources of variability in the protocol.

C&E analysis is a conceptual process that can help guide robustness testing and determine process control measurements that should be included in a protocol to support control charting of important sources of variability. This approach has been recently used to support the development and evaluation of several nanotoxicity assays: a cell viability assay using a submerged exposure system with A549 cells [50,51], a suite of four *in vitro* nanobioassays that measure endpoints that can be impacted in cells through oxidative stress [52], and the use of an International Standardization Organization (ISO) *Caenorhabditis elegans* assay with ENMs [53,54].

2.3. Characterization of the Vitrocell Exposure System (12/3 CF Module): Determination of Relative Humidity and Temperature Inside the Exposure Chamber

To assess the relative humidity in the exposure gas (clean filtered air or aerosol) an ALMEMO 2590-2A system with a FHAD 46-C0 sensor (Ahlborn GmbH, Holzkirchen, Germany) was used. The sensor was directly placed into the aerosol flow between the exposure chamber and the aerosol delivery system above the chamber by cutting a small hole in the tubing and sealing the sensor inside the tube. To understand the environmental conditions for the cells inside the exposure chamber, a second sensor (type K thermocouple PeakTech® TF-56, PeakTech Prüf- und Messtechnik GmbH, Ahrensburg, Germany) was used to assess the aerosol flow temperature inside the exposure chamber using a multimeter (digital multimeter, DM01M, TACKLIFE). The sensor was placed into the tube as described above for the relative humidity measurements and then moved further into the exposure chamber. Due to its small size, the sensor could be placed slightly above the insert membrane inside the exposure chamber. To avoid a bias in the measurements from contact with medium, the sensor was not placed in direct contact with the transwell membrane which overlays the medium.

2.4. Parameter Optimization to Improve Cell Viability and Exposure Time

Five different parameters (exposure duration, relative humidity, temperature, CO_2 concentration, and flow rate) were identified by the C&E analysis as factors that may impact cell viability during ALI exposure in the flow through system and experimentally evaluated. To isolate the impact on the parameter adjusted, the cells were only exposed against clean filtered air (exposure system air negative control). The following protocol settings were used unless otherwise stated: a water bath connected to the exposure chamber and the chamber lid with a temperature of 38 °C, an exposure duration of 1 h, a total flow rate within the aerosol guiding system of 150 mL/min, and a flow rate of 5 mL/min on each insert. The air flow was guided through a glass pipe featuring three outlets on the bottom where the exposure chambers were connected (Figure 1). The flow rate was controlled by a mass flow meter (Aalborg, Orangeburg, New York, NY, USA) at the end of the pipe. A vacuum pump was used to generate the insert flow and the individual insert flow rates were adjusted using needle valves and a mass flow meter (Aalborg, Orangeburg, New York, NY, USA). The distance between the cellular monolayer and the air inlet was measured and set to 4 mm based on a spacer delivered by Vitrocell. To maintain a stable pH in the absence of 5% CO_2, the cell culture medium (using the same composition as described before for cell culture) was supplemented with 2% (*v*/*v*) Hepes (PAN- Biotech GmbH, Aidenbach, Germany). Cell viability was compared to the incubator control for which the cells were added to the inserts at the same time and with the same cell concentration as those exposed in the ALI system.

The relative humidity was monitored and ranged from below 10% up to ≥90% depending on the setup. The relative humidity was adjusted by guiding the air through a humidifier (Gasmet Technologies GmbH, Karlsruhe, Germany) before introducing it into the glass pipe and the exposure chamber. The lid temperature was set to room temperature.

When the effect of the temperature of the exposure chamber lid was analyzed, the temperatures tested were room temperature (21 °C), 38 °C and 45 °C, while the relative humidity was set to <10%. To control the lid temperature, a second water bath was connected to the lid and set at different temperatures. As the exposure chamber is not include in a headed box, room temperature on the outer

side of the chamber and tubes resulted in a condense moisture in the tubes guiding the air from the chamber exit to the exhaust. As the chamber is not transparent, condensation conditions inside the chamber (at the air inlet exit) cannot be evaluated.

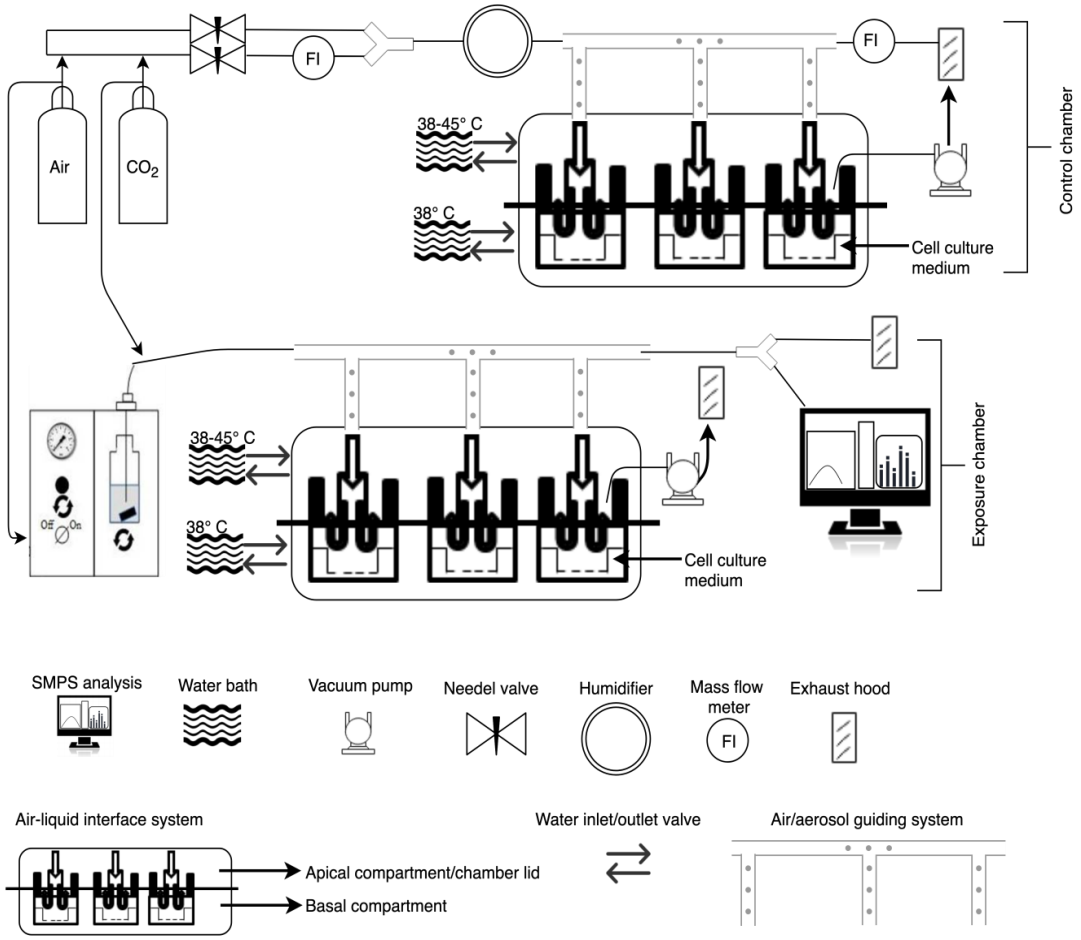

Figure 1. Schematic diagram of the different components of the air-liquid interface setup, aerosol mixtures, and temperature flow units.

To assess the impact of the flow rate on cell viability, different flow rates (1 mL/min, 5 mL/min, or 10 mL/min) were investigated. For these experiments, the relative humidity was set to >90% and the lid temperature was set to 38 °C.

The impact of the CO_2 concentration was tested by supplementing the clean air with 5% CO_2. Adding CO_2 to the clean air flow was conducted in front of the humidifier and was monitored by a mass flow meter (Aalborg, Orangeburg, New York, NY, USA) (7.5 mL/min CO_2 and ≈140 mL/min air). To ensure a 5% CO_2 supply, the final flow rate was monitored at the exhaust of the glass pipe with a second mass flow meter (Aalborg, Orangeburg, New York, NY, USA). Needle valves were used to adjust the flow rates for each gas. For investigating the impact of adding CO_2, the relative humidity was set to >90%, the lid temperature was set to 38 °C, and a flow rate of 5 mL/min was used.

After optimizing the aforementioned parameters, the exposure time was varied between 1 h, 2 h, 4 h and 8 h to determine the maximal exposure time during which no significant loss in cell viability was induced by clean air exposure. ALI setup conditions were set to relative humidity >90%, 5 mL/min flow rate, 38 °C lid temperature and 5% CO_2. Overall, as described in more detail in the discussion section, an exposure of A549 cells with a flow rate of 5 mL/min, a lid temperature of 38 °C, a relative humidity of >90% and 5% CO_2 supply were found to represent the optimal exposure conditions among those tested in this study.

In addition to the negative controls (incubator control, clean air control), a positive control was tested to confirm the dynamic range of the WST-1 (water soluble tetrazolium-1) assay. The basal compartment was filled with the culture medium spiked with Triton -X 100. Afterwards the cells were placed inside the exposure chamber and exposed to a water-based aerosol (without NPs, relative humidity >90%, 5 mL/min flow rate, 38 °C lid temperature and 5 % CO_2).

2.5. Cell Viability

To evaluate the viability of the A549 cells using the exposure conditions described in the preceding section, a WST-1 assay was conducted to assess the metabolic activity of the cells. The principle of this assay is based on the stable tetrazolium salt WST-1 which is cleaved into a soluble formazan dye by cellular mechanisms including NAD(P)H-dependent oxidoreductases and dehydrogenases. Thus, the amount of formazan dye formed, directly correlates with the number of metabolically active cells in the culture [55]. A549 cell number per 12 well insert (cat. number 353180, Corning B.V., Amsterdam, Netherland; 0.4 µm pore size, 1.12 cm^2 diameter) was 50 000. After ALI exposure of cells to air or an ENM aerosol, cells were rinsed once with 500 µL phosphate buffered saline solution (PBS) (PAN-Biotech GmbH, Aidenbach, Germany), and 300 µL fresh cell culture medium (without phenol red) containing 10 % (*v*/*v*) WST-1 reagent (4-[3-(4-iodophenyl)-2-(4-nitrophenyl)-2H-5-tetrazolio]-1,3-benzene disulfonate) (Roche Diagnostics GmbH, Mannheim, Germany) was added. After 30 min incubation at 37 °C, three technical replicates (each 50 µL) of the supernatant per insert were transferred into individual wells in a new 96 well plate and the absorbance was measured with a Tecan (GENios) plate reader (Tecan Deutschland GmbH, Crailsheim, Germany) at a wavelength of 450 nm. The absorption was also measured at a second wavelength of 562 nm, a wavelength outside the spectrum of the WST-1 probe, to evaluate for potential interferences such as bubbles. Cell viability was compared to the incubator negative control using the following equation:

$$Percentage\ viability = \frac{(test\ parameter\ -\ medium\ blank\ control)}{(negative\ control\ -\ medium\ blank\ control)} \times 100\% \quad (1)$$

where test parameter is the absorbance value of the parameter tested. Medium blank control represents the absorbance value of the test media (reagents but without cells), and the negative control represents the absorbance value for the cells in the incubator and not exposed to the ALI system.

2.6. Nanoparticle Dispersion and Characterization

NM-212 NPs were purchased from Joint Research Center (JRC) (JRC, Ispra, Italy). The Ce content in this material is about 81.6% [56] and the oxidative state of the CeO ion is 93.1% and 6.9% for CeO^{4+} and CeO^{3+}, respectively [56]. Further details about the composition of NM-212 can be found in the JRC report [56]. The particle dispersion was prepared in accordance with the protocol of the NANOGENOTOX SOP with slight modification [57]. In summary, the following protocol was used. NM-212 were weighed and the particles were prewetted in 50 µL of 99% ethanol before being dispersed in MilliQ water to a final stock concentration of 2.5 mg/mL (10 mL final volume). Subsequently, the particle dispersion was sonicated for 5 min and 9 s (Sonoplus HD 220/UW 2200, Bandelin, Germany) to avoid particle aggregation as described in the NANOGENOTOX dispersion protocol [57]. This sonication duration allowed for a specified amount of power to be applied NM containing dispersion. For all experiments, particle dispersions were freshly prepared. Particle characterization (transmission electron microscopy, nanoparticle tracking analysis, dynamic light scattering, zeta potential and selected area electron diffraction (SAED)) of particle dispersions prepared with this method were conducted. The analytical methodology was described in detail previously [58,59]. SAED data were obtained by a JEM-2100HR transmission electron microscopy (JEOL, Tokio, Japan).

2.7. Particle Exposure to A549 Cells

A customized VITROCELL 12/3 CF module (Vitrocell GmbH, Waldkirch, Germany) was used to expose A549 cells to CeO_2 NPs (NM-212) (Figure 1). A Palas VAGF 2.0 aerosol generator (Palas GmbH, Karlsruhe, Germany) operated at 1 bar inlet pressure was used to produce the particle aerosol. Cells were exposed for 1 h, 2 h or 4 h. Exposure was performed under the following conditions: a flow rate of 5 mL/min. Basal and apical compartments of the exposure chamber were heated to 38 °C. The relative humidity was >90%. The inlet distance to the cells was 4 mm. The nominal particle concentration of the aerosolized samples was 250 µg/mL. The medium volume under the insert was 3.175 mL.

2.8. Aerosol Characterization

A scanning mobility particle sizer (SMPS, TSI Model 3083, CPC Model No. 3775, TSI Incorporated, Shoreview, MN, USA) was used to analyze the particle size distribution and the particle mass concentration in the aerosol. Due to their electrical mobility, particles are divided in different fractions which then can be counted. Based on this information (particle number and size fraction), the particle size distribution is determined. The particle mass can be calculated based on the particle size distribution and particle number concentration.

The instrument was running with an aerosol flow to sheath flow ratio of 1/10. Operating mode was set to "low" which uses an aerosol flow of 0.3 L/min. CeO_2 NP density was assumed to be 7.3 g/cm^3 [18]. The inlet pressure of the aerosol generator in terms of the CeO_2 aerosol particle size distribution was examined by adjusting the inlet pressure directly on the generator (Figure 1).

2.9. Determination of Intracellular Uptake of NM-212

For the determination of the particle deposition as well as the intracellular particle uptake, inductively coupled plasma mass spectrometry (ICP-MS) was used. 50 000 A549 cells were seeded per 12 well insert (cat. number 353180, Corning B.V., Amsterdam, Netherland; 0.4 µm pore size, 1.12 cm^2 diameter). After 48 h, the basolateral medium was changed, cells were washed once with PBS, transferred onto ALI conditions, and cultured for 24 h. Subsequently, cells were used for the ALI exposure experiments.

A549 cells were exposed to a CeO_2 NP aerosol for 1 h, 2 h or 4 h, and placed back in the incubator for 24 h (post exposure time). Subsequently, cells were washed two times with PBS (each 0.5 mL). The wash solution as well as the basolateral medium was collected and subsequently microwave digested as described in the following section.

2.10. Microwave Digestion and ICP-MS Analysis

Microwave digestion was conducted as described previously [60]. In brief, the membranes from the cells exposed to CeO_2 NPs and the incubator negative control were separated from insert using a scalpel and transferred into a digestion tube. 2 mL MilliQ water, 2.5 mL HNO_3 (69% *v*/*v*) (VWR, Darmstadt, Germany) and 1 mL H_2O_2 (30% *v*/*v*) (Merk, Darmstadt, Germany) were added to this tube. For the washing solution and the basal medium, 1 mL MilliQ water was added to 1 mL wash solution or 1 mL basal medium, respectively, before adding HNO_3 and H_2O_2. The collected samples were digested in a microwave (MLS ultraCLAVE 2; MLS GmbH, Leutkirch, Germany).

To analyze the Ce amount using ICP-MS, we used an in house validated method based on a Ce reference material (BCR 667) [60]. ^{140}Ce was quantified using a respective Ce calibration based on an ionic Ce standard solution (VWR International LTD, Leicestershire, England). ^{103}Rh was used as internal standard. The recovery of this method was within the range of 86% to 120% [61]. The limit of detection (LOD) and limit of quantification (LOQ) were calculated as 3 and 10 times the standard deviation of the blank samples, respectively. Background levels of Ce were determined by blank

measurements (see Table S3 for details). All cerium samples were blank-corrected by subtracting the average value of six blank samples from the measured sample concentration.

ICP-MS measurements were conducted with an iCaP-Q (ThermoFisher GmbH, Dreieich, Germany) or a Thermo Scientific XSERIES II, (Thermo Fisher Scientific, Waltham, MA, USA). For ICP-MS calibrations, LOQ's and LOD's are shown in Figure S6 and Table S3, respectively. Particle deposition rates were calculated by adding the ICP-MS concentration measured intracellularly and the concentrations in the washing solution and the basal medium.

2.11. Calculation of Deposition Efficiency

The deposition efficiency was calculated from the SMPS data and ICP-MS results. Here, the obtained particle aerosol concentration was converted to mass per surface area and the maximum deposition was determined by using Equation (2).

$$Maximum\ Deposition = \frac{aerosol\ concentration \times flow\ rate \times exposure\ time}{insert\ surface\ area} \quad (2)$$

The measured deposition was determined using the following Equation:

$$Measured\ Deposition = \frac{Deposited\ CeO_2\ concentration}{insert\ surface\ area} \quad (3)$$

The deposition efficiency was calculated by Equation (4).

$$Deposition\ efficiency = \frac{Measured\ Deposition}{Maximum\ Deposition} \times 100\% \quad (4)$$

2.12. Time of Flight-Secondary Ion Mass Spectrometry (ToF-SIMS)

To confirm the intracellular uptake of CeO_2 NPs into A549 cells, ToF-SIMS measurements were carried out. Cells were exposed to the CeO_2 NPs containing aerosol for 1 h or 4 h under optimized exposure conditions as described in the section above. After exposure, the cells were placed back in the incubator for 24 h. Subsequently the cells were rinsed twice with 0.5 mL PBS and fast frozen in liquid propane using a cryoplunger device (EMS-002, Electron Microscopy Sciences, Hatfield, PA, USA).

ToF-SIMS depth profiles were acquired using a ToF-SIMS V instrument (ION-TOF GmbH, Münster, Germany) with a 30 keV nano-bismuth primary cluster ion beam source $(Bi)_x^{(y+)-}$ with a Bi_{Mn} emitter [62]. The ion currents were 0.5 pA at 5 kHz using a Faraday cup. A pulse of 0.7 ns from the bunching system resulted in a mass resolution that usually exceeded 9000 (full width at half-maximum) at m/z < 500 in positive ion mode. The primary ion dose was controlled below 10^{12} ions × cm^{-2} to ensure static SIMS conditions. Charge compensation on the sample was obtained by a pulsed electron flood gun with 20 eV. The primary ion gun scanned a field of view of 200 µm by 200 µm applying a 512 pixel by 512 pixel measurement raster. Once the primary ion gun was aligned, a ToF-SIMS mass spectrum was generated by summing the detected secondary ion intensities and plotting them against the mass channels. The analytical methodology was described in detail elsewhere [63–67]. All depth profiles were performed in dual beam mode on the ToF-SIMS V instrument of the reflectron-type, equipped with a 30 keV bismuth liquid metal ion gun (LMIG) as primary ion source, a 20 keV argon gas cluster ion source both mounted at 45° with respect to the sample surface and an electron flood gun. Bi^{3+} was selected as primary ion by appropriate mass filter settings. Primary and sputter ion currents were directly determined at 200 µs cycle time (i.e., a repetition rate of 5.0 kHz) using a Faraday cup located on a grounded sample holder. The scanning area for analysis was 200 µm by 200 µm with 512 by 512 pixels. The sputter area for each measurement was 1000 µm by 1000 µm. Surface charging was compensated by flooding with low energy electrons. ToF-SIMS depth profiles were acquired in positive ion mode. The mass scale was internally calibrated using a number of well-defined and

easily assignable secondary ions ($C_2H_5^+$, $C_3H_7^+$ and $C_4H_9^+$) keeping the error in calibration for all spectra below 5 µg/mL. The data were evaluated using the Surface Lab software (ION-TOF GmbH, Münster, Germany).

2.13. Statistical Analysis

Statistical calculations were performed using a Markov Chain Monte Carlo Bayesian analysis to evaluate if the percentage viability was less than 100% and if the different treatment conditions were statistically equal (the null hypotheses). A Bayesian model [68,69] was applied using Markov Chain Monte Carlo programmed in OpenBUGS [70]. All measurements were assumed to be Gaussian. We used the usual Gaussian prior distributions for all the means, and Half Cauchy distributions for all the unknown variances [69]. We calculated the percentage viability with 95% uncertainty bounds for each treatment condition and plate and for the consensus values among the three plates; an example of the R code used is provided in the Supporting Information. Data was not available for the solvent system for one of the three plates for two conditions. Given the relatively small variability among the plates for the solvent system values compared to that for negative control and test condition values, the solvent system data for another plate for the same tested conditions was used for the statistical analyses for these two plates. If the MCMC of some of the posterior distributions did not converge when evaluating the consensus values, as occurred for one condition, the NIST consensus builder program (https://consensus.nist.gov/app/nicob) was used instead using the mean and standard uncertainty values calculated for each plate.

Statistical analysis of the ToF-SIMS data was performed as described in detail elsewhere [63–67]. In brief, the acquired data were binned to 1 mass unit (u). Data processing was carried out with the statistical package SPSS + (version 21) (IBM Deutschland GmbH, Ehningen, Germany) using the mass range between 200 mass units and 1200 mass units to detect significant differences between treated and untreated cells. Ions lower than 200 mass units were excluded from the study to avoid contaminating ions from salts, system contaminants, and other medium components; ions from the CeO_2 particles are much larger than this range and would not be expected to impact these results. Each acquired spectrum was then normalized, setting the peak sum to 100%. A Principal Component Analysis (PCA) was performed using all ions. To show that data sets could be separated with a supervised model from each other, a Fisher's discriminant analysis was performed (n = 6) (Figure S5). The performance of the discriminant model was verified by applying the cross-validation procedure based on the "leave-one-out" cross-validation formalism. * = $p > 0.05$ was considered as significant.

3. Results

3.1. Cause-And-Effect Analysis

The C&E analysis revealed six main branches (Figure 2): cell maintenance and seeding, instrument performance, plate reader, positive control, WST-1 assay, and engineered nanomaterial dispersion and handling. These sources of variability were similar for branch 1 (cell maintenance and seeding), branch 3 (plate reader), branch 4 (positive control), branch 5 (WST-1 assay) and branch 6 (engineered nanomaterial dispersion and handling) to previous C&E diagrams prepared for the 3-(4,5-dimethylthiazol-2-yl)-5-(3-carboxymethoxyphenyl)-2-(4-sulfophenyl)-2H-tetrazolium (MTS) nanocytotoxicity assay with A549 cells [50–52]. Important sources of variability in branch 1 (cell maintenance and seeding) revealed during analysis of the MTS nanocytotoxicity assay were the cell number and the cell identity as some of the culture were composed of cells missing an allele and had a different toxicity to the positive chemical control [50]. Branch 3 relates to the performance of the plate reader, and therefore factors that determine the plate reader performance such as its calibration and evaluating the homogeneity across the test plate to avoid systematic biases are critical. The positive chemical control (branch 4) can serve multiple functions such as evaluating the assay sensitivity and its dynamic range. Thus, it is important to choose a positive chemical control that fulfills the measurement

assurance functions for the positive chemical control for each particular assay. The important factors for branch 5 (WST-1) relate to the performance of the WST-1 assay reagents similar to those for the MTS assay. These sources of variability can be evaluated using two in-process control measurements: the blank control (medium + WST-1 assay reagents only) and the absorbance data for the incubator negative control, and can be plotted using control charts to monitor their performance across time. One key source of variability in branch 6 (engineered nanomaterial dispersion and characterization) is the dispersion procedure and NP characterization. It is known that reproducible sample dispersion methods are critical as is thorough characterization using orthogonal methods of the dispersion to confirm that the dispersion has the expected characteristics [51]. The sole branch for the WST-1 assay using exposure with the ALI system that is substantially different from those for the MTS assay was branch 2 (exposure system). Compared to the simpler exposure approach, namely pipetting, in the MTS assay which tested nanomaterial toxicity using submerged culture conditions, branch 2 is substantially more complex for the flow through ALI exposure system. A different set of process control measurements and robustness evaluation are needed for this system. This difference is the main reason why the robustness testing performed in this manuscript focused predominately on the sources of variability in branch 2. An overview of the different in-process control measurements used and evaluated in this assay is provided in Table 1.

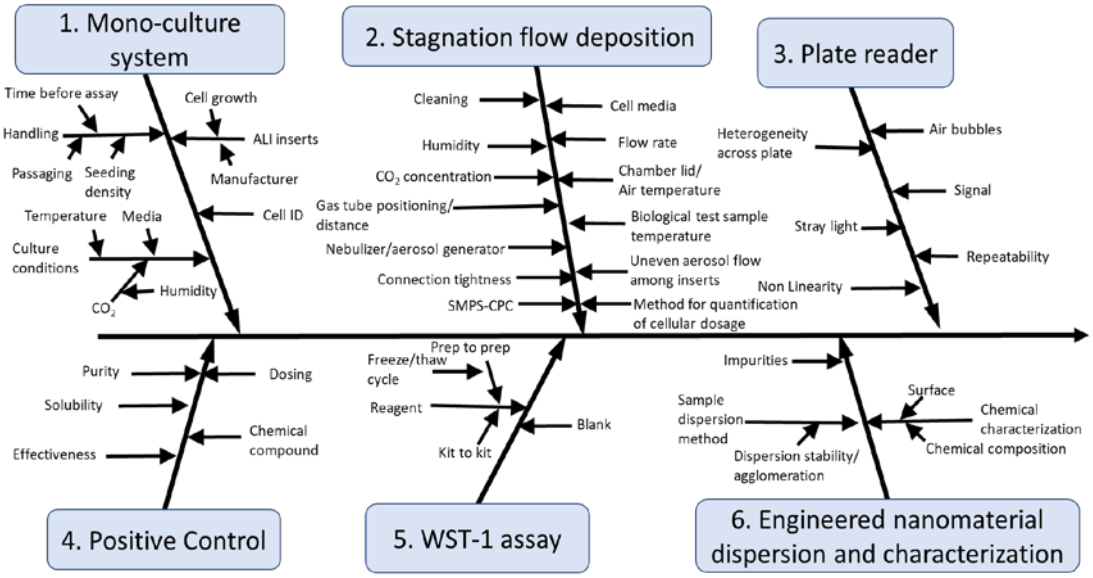

Figure 2. Cause-and-effect (C&E) diagram for WST-1 assay.

Table 1. Different in-process control measurements for the WST-1 ALI exposure assay.

Control Measurement	C&E Diagram Branch(es)	Procedure	Purpose
Medium blank control	Branches 3, 5	Measure the signal in wells without cells but with the WST-1 reagents	Evaluate the plate reader performance, & signals for the WST-1 reagents
Cell dosage	Branch 2	Quantify the test substance (in this case, CeO_2 NPs) associated with the cells to evaluate the deposited dose and the intracellular concentration	Evaluate the amount of the test substance that comes into contact with the cells and is internalized; evaluate the homogeneity in the dosage among inserts

Table 1. *Cont.*

Control Measurement	C&E Diagram Branch(es)	Procedure	Purpose
Positive control	Branches 1, 4, 5	Expose cells to air flow only (no aerosolized chemicals or particles) in the ALI system after adding a 0.2% *v/v* concentration of Triton-X 100 to the basal medium	Evaluate the dynamic range of the assay
Exposure system negative control	Branches 1, 2	Expose cells in the exposure system to air flow only (no aerosolized chemicals or particles) and then evaluated with the WST-1 assay	Evaluate the potential for a decrease in viability compared to the air flow only
Incubator negative control	Branches 1, 5	Evaluate the number of cells in wells not exposed to chemicals and kept in the incubator	Evaluate if a consistent number of cells have been added to the inserts, evaluate the performance of the WST-1 reagent
Relative humidity	Branch 2	A humidity sensor was used to monitor the gas prior to reaching the cells	To evaluate the impact of humidity on the exposure system negative control
SMPS-CPC	Branches 2, 6	Analyze the aerosol generated using SMPS and CPC	Characterize the NP size distribution, number concentration and mass concentration in the produced aerosol
Temperature sensor (air)	Branch 2	Use a thermocouple to measure the air temperature prior to reaching the cells	Evaluate the impact of air temperature on cell viability for the exposure system negative control
Temperature sensor (lid)	Branch 2	Use a thermocouple to measure the temperature on the insert where the cells are located	Evaluate the impact of the temperature on the insert on the cell viability for the exposure system negative control
Interference control reading	Branch 3	Measure the signal in wells at a second wavelength (562 nm) which is outside of the absorption spectrum of the WST-1 reagent	Evaluate each well for potential interferences (e.g., bubbles)

3.2. CeO_2 NP Dispersion Characterization

Given the importance of characterization of the nanomaterial dispersion (branch 6), the hydrodynamic diameter of the CeO_2 dispersion was analyzed using two different methods, nanoparticle tracking analysis and dynamic light scattering, which revealed a hydrodynamic diameter of 180 nm ± 8.1 nm and 220 nm ± 16.6 nm after three measurements of the same suspension (values are mean ± standard deviation), respectively. The dispersed CeO_2 NPs had a positive surface charge of 13 mV ± 1.1 mV. Further details of the nanomaterial characterization such as TEM analysis can be found in Figure S1 or here [58].

3.3. Evaluation of the Impact of Different Parameters in the ALI Exposure System on Cell Viability

To better understand the factors that influence the cell viability using this exposure system (branch 2), five parameters were evaluated (Figure 3). Changing the relative humidity from <10% to >90% resulted in a significant increase in cell viability from 35% up to 90% (Figure 3A); data for

the relative humidity under various exposure conditions are shown in Figure S3A. Heating the lid to 38 °C resulted in a cell viability of 75% compared to about 1% at room temperature (Figure 3B). A further temperature increase in the lid temperature up to 45 °C showed no significant difference in cell viability compared to 38 °C (corresponding air flow temperature data are shown in Figure S3B); however, the data at 45 °C among the three different plates was more consistently close to 100% viability than that for 38 °C (Figure S7B). An increase in the flow rate from 1 mL/min to 5 mL/min or 10 mL/min led to a decrease in cell viability from 97% to 86% or 39%, respectively (Figure 3C). It was decided to set the flow rate to 5 mL/min in the optimal exposure conditions, because a higher flow rate is expected to yield a higher deposition concentration even though there was a statistically significant decrease in the percentage viability compared to the incubator negative control. To emulate the *in vivo* conditions even closer and mimic the gas conditions in the alveoli, 5% CO_2 was added to the exposure gas, which showed no decrease in the cell viability compared to the incubator negative control during a 1 h exposure duration (Figure 3D). However, for longer exposure periods, it is expected that the buffering effects of CO_2 would have a greater impact.

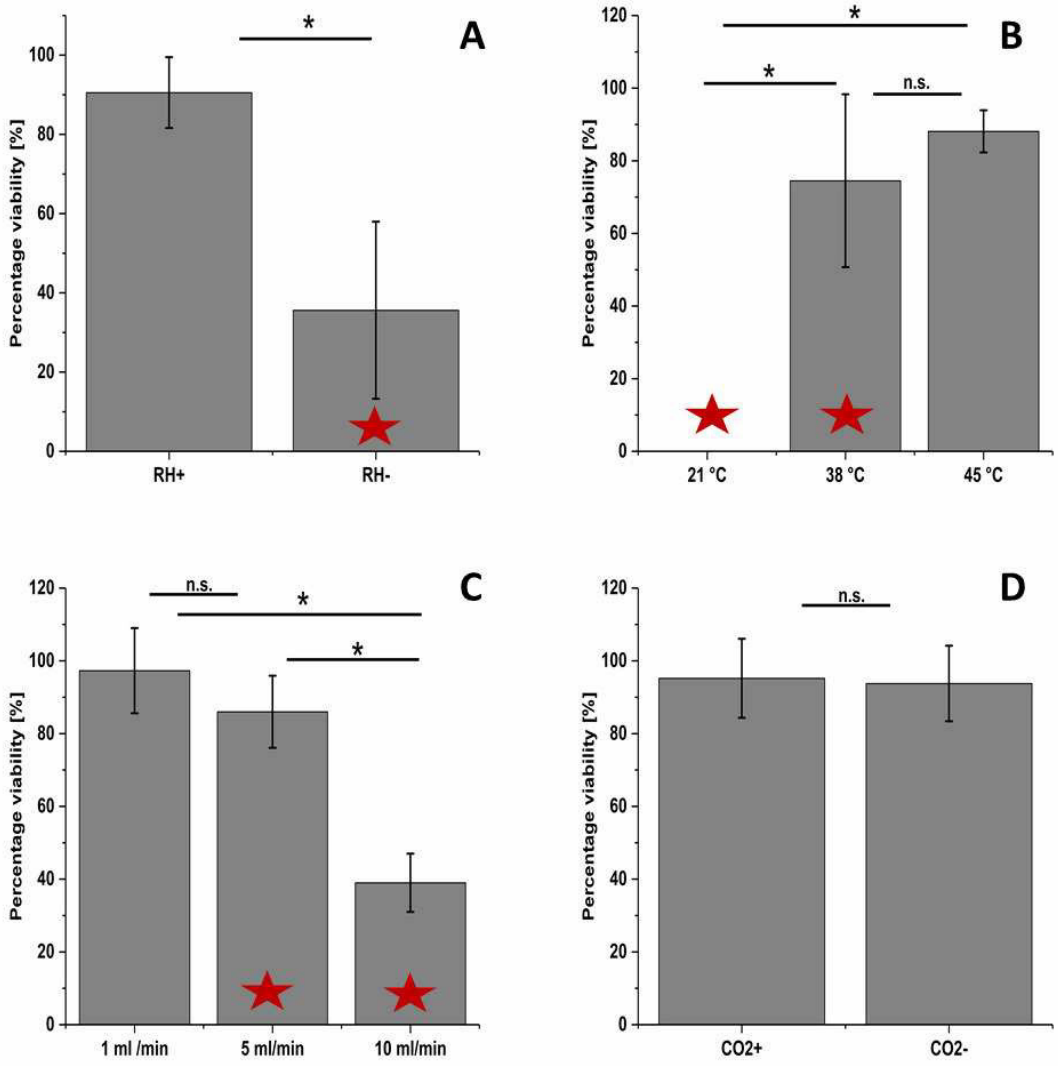

Figure 3. Parametric optimization of the Vitrocell exposure 12/3 CF module. Parameters affecting cell viability after 1 h clean air exposure: Relative humidity (**A**), lid temperature (**B**), flow rates (**C**) and 5% CO_2 supply (**D**). Percentage viability values are the consensus values calculated for all three plates using the Bayesian modeling. The values are the means, and the error bars the standard deviations. n.s. = not significant. * = $p > 0.05$. Red asterisks indicate that the consensus value is significantly less than the incubator control with a 95% likelihood using the Bayesian modeling.

An exposure of A549 cells with a flow rate of 5 mL/min, a lid temperature of 38 °C, a relative humidity of >90% and 5% CO_2 supply were found to represent the optimal exposure conditions among those tested in this study. Using these optimized parameters, the impact of exposure time up to 8 h on cell viability was investigated (Figure 4A). The results show stable cell viability over a period of up to 4 h. For exposure for 8 h, there was no statistically significant drop in viability (76% viability) among the treatment conditions for the consensus value, but two of the three plates did have values significantly less than the incubator negative control. Exposing the A549 cells to aerosolized MilliQ water for 4 h (ALI exposure system negative control) caused a significant decrease compared to the incubator negative control for the exposure without CO_2 but was not observed when CO_2 gas was added (Figure 4B). During these analyses, multiple experimental challenges were encountered that required troubleshooting of the exposure system to resolve. These pitfalls and suggested solutions are listed in the Table S4. In addition, results are provided for each of the three plates to show the day-to-day variability when performing the assay (Figures S7 and S8).

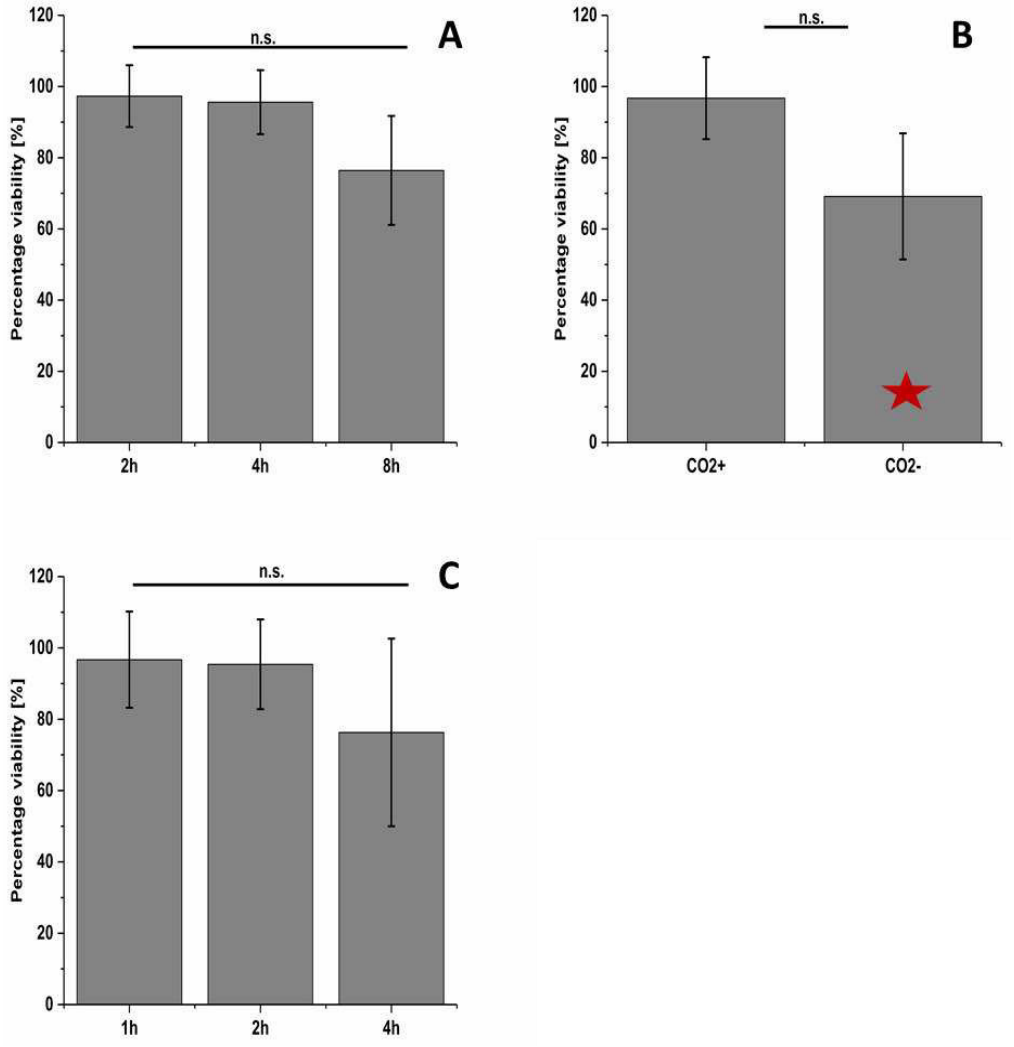

Figure 4. (**A**) Time-dependent cell viability for MilliQ water aerosol exposure (without ENM) using the optimized Vitrocell setup. (**B**) shows the effect of 5% CO_2 supply to the air on the cell viability after 4 h MilliQ water aerosol exposure using the optimized Vitrocell exposure setup. (**C**) exhibits a time-dependent NM-212 exposure compared to MilliQ water aerosol (without NP) exposed cells. Percentage viability values are the consensus values calculated for all three plates using the Bayesian modeling. The values are the means and the error bars the standard deviations. n.s. = not significant. Red asterisks indicate that the consensus value is significantly less than the incubator control with a 95% likelihood using the Bayesian modeling.

Afterwards, lung epithelia cells (A549) were exposed to CeO_2 NPs (NM-212) using the optimal exposure conditions identified in this study. No decrease in cell viability was detected after NM-212 exposure for 1, 2 or 4 h for the consensus values (Figure 4C), but a significant decrease was observed for one of the plates for the 4 h exposure (Figure S8C).

Two incubator in-process control measurements were consistently measured to evaluate the assay performance: the incubator negative control (branches 1, 3, and 5) and blank control (branch 5). An exposure system positive chemical control was performed using 0.2% Triton X-100 to evaluate the dynamic range of the assay. A decrease in cell viability down to about 6% after exposure for 1 h to 1% after 2 and 4 h exposure was observed. This data was not significantly different than the medium blank indicating a complete loss of cell viability and that the full dynamic range of the assay could be consistently achieved.

Control charts were made to investigate the consistency of the WST-1 assay performance for the incubator negative control and the blank control (Figure 5). The mean absorbance value for the medium blank control was approximately 3% of that of the incubator negative control. Plotting the coefficient of variation (COV) values shows the range of variabilities among individual experiments. The mean value for the COV for the incubator negative control cells was approximately 12% (Figure 5C), while the mean value for the COV for the medium blank control was 7.5% (Figure 5D), suggesting that pipetting cells is more variable than pipetting just the medium.

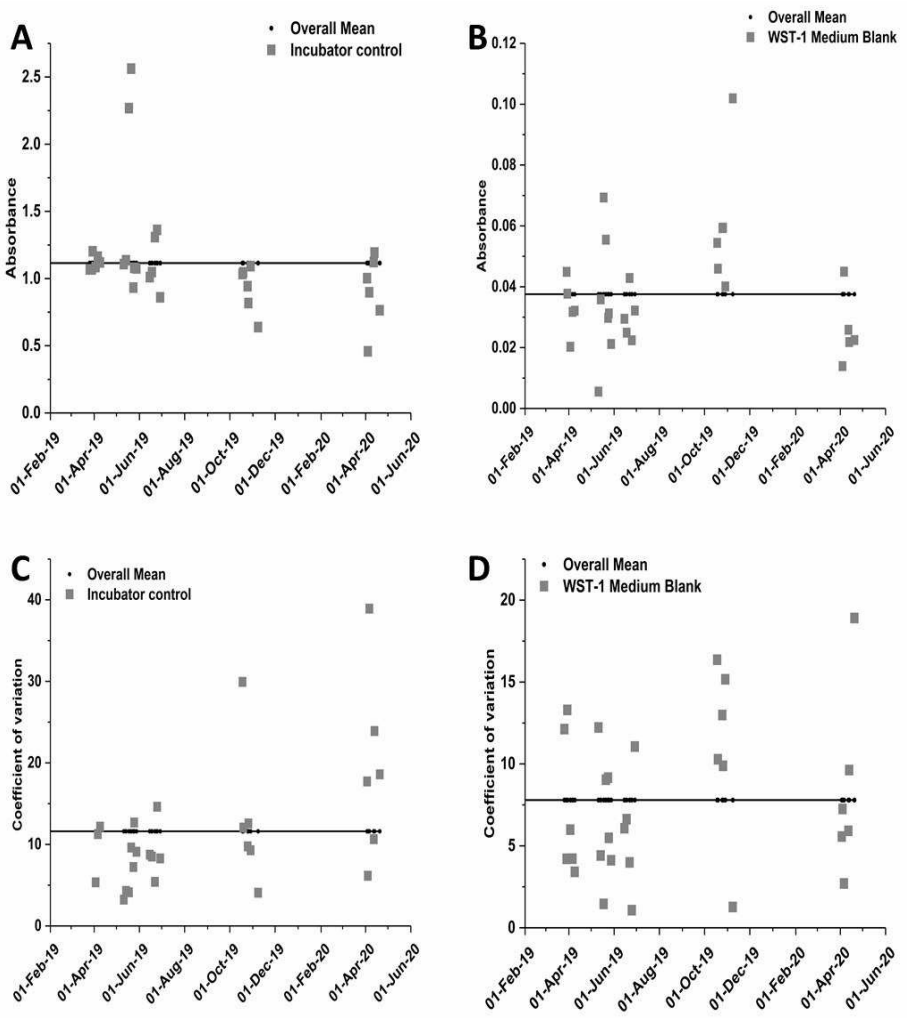

Figure 5. Control charting data for the WST-1 assay for the negative incubator control (**A**) and the medium blank control (**B**). (**C**,**D**) represents the coefficient of variation for all experiments depending on the date they were performed for the incubator control and the medium blank control, respectively.

3.4. Characterization of the CeO_2 NP Aerosol

One of the key factors for branch 2 (exposure system) is characterization of the aerosolized CeO_2 dispersion with different instrument settings. For example, the effect of the inlet pressure of the aerosol generator on the particle size distribution of a 250 µg/mL CeO_2 NP solution was examined. From 1.0 bar to 1.5 bar inlet pressure, an increase in particle number was observed. However, no further increase in particle number was detected at a higher inlet of 1.8 bar (Figure S4). To avoid cell damage by static pressure into the ALI chamber, 1 bar was used for all cell exposure experiments (pressure was measured by a flow meter which is part of aerosol generator). Furthermore, the particle size distribution of NM-212 at 1 bar showed a bimodal pattern with a first maximum at approximately 20 nm and a second maximum at about 90 nm (Figure 6A). Measuring only MilliQ water showed a peak at about 25 nm that extended to up to approximately 50 nm. Additionally, a strong variability of the MilliQ size distribution was observed when measuring MilliQ solutions on different days. Therefore, a background subtraction was challenging and data under 50 nm were excluded.

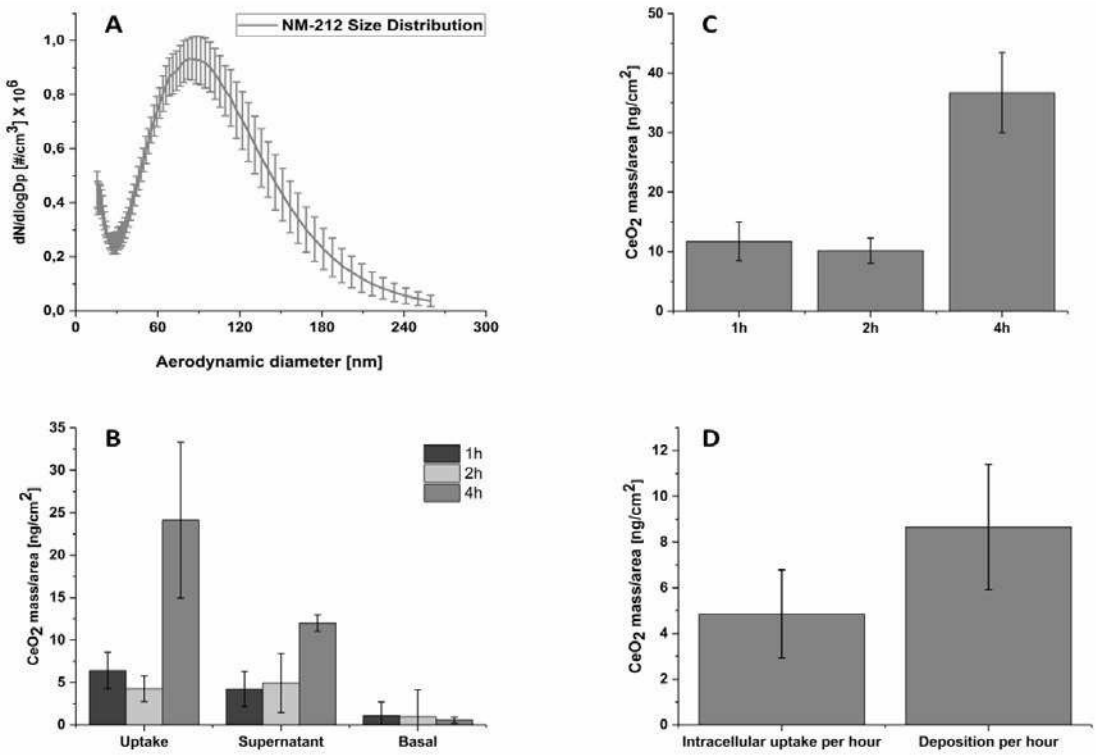

Figure 6. Inductively coupled plasma mass spectrometry (ICP-MS) analyses: The particle size distribution of NM-212 at 1 bar (n = 9). Three independent experiments with 3 data points each. Data are combined and shown as mean ± SD in (**A**). NM-212 particle uptake (**B**) and deposition (**C**) of A549 cells after air-liquid interface exposure at different time points revealed a time dependent behavior. (**D**) displays the mean intracellular uptake and mean deposition for A549 cells per h × cm^2 after air-liquid interface exposure. (n = 9 = three independent experiments with 3 wells for each data point).

3.5. Intracellular Uptake and Localization of CeO_2

After characterization of the aerosol, the particle deposition and the intracellular particle uptake were analyzed by ICP-MS after exposing A549 cells to a CeO_2 NP containing aerosol (generated using a 250 µg/mL dispersion and a pressure in the aerosol generator of 1 bar) for 1 h, 2 h or 4 h. There was an increase in particle deposition and uptake over time (Figure 6B,C). A mean intracellular CeO_2 content of 4.85 ng × cm^{-2} × h^{-1} ± 1.93 ng × cm^{-2} × h^{-1} and a CeO_2 deposition of 8.66 ± 2.74 ng/cm^2 × h^{-1} were detected (Figure 6D). Furthermore, about 50% of the deposited particles were found to be intracellular.

Given that dead cells might also internalize particles, the cells were washed twice with PBS to remove dead cells and particles that are weakly membrane bound.

To determine the complete particle deposition, this washing solution was also analyzed, and these results are shown in Figure 6B for the supernatant (washing solution + surfactant). The overall particle deposition includes particle deposition from dead and living cells whereas the uptake shows only the deposition and internalization by living cells. SMPS data revealed a mean aerosol concentration of 1.07 ± 0.34 mg/m^3 for the whole size distribution and 1.03 ± 0.35 mg/m^3 for the size distribution containing only particles bigger than 50 nm. A 100% particle deposition (5 mL/min flow rate) would therefore correspond to a theoretical, maximum aerosol deposition rate of approximately 0.29 µg/cm^2 × h^{-1} for the whole size distribution or 0.28 µg/cm^2 × h^{-1} for the size distribution of particles only bigger than 50 nm. Using Equation (4), a deposition efficiency of 2.98% for the whole size distribution or 3.09% for the size distribution of particles only bigger than 50 nm was achieved.

ToF-SIMS 3D depth profiles for 1 h and 4 h exposure were generated to evaluate cellular uptake using an orthogonal method. Both time points show a strong CeO^+ peak in the corresponding acquired mass spectra indicating the presence of CeO_2 NPs within the cells (Figure 7C). Moreover, a significant increase of particle uptake from 1 h exposure (ca. 0.9 × 10^3 ion counts) to 4 h (ca. 1.4 × 10^3 ion counts) was observed. The reconstructed 3D ion images of the ToF-SIMS data reveal CeO_2 agglomerates within the tissue section (Figure 7A,B, red arrows). No membrane associated CeO_2 agglomerates could be found, thus suggesting intracellular localization of the CeO_2 particle agglomerates in A549 cells after ALI exposure.

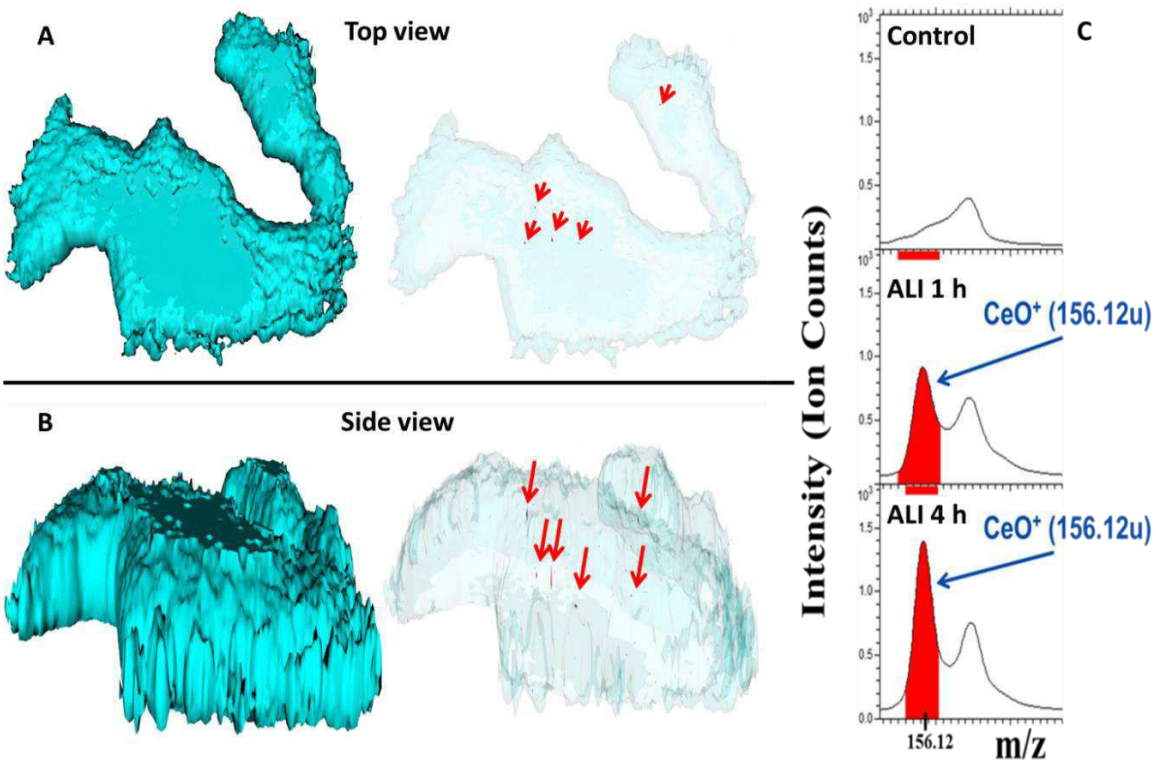

Figure 7. Reconstructed 3D ion images of A549 cells indicate CeO_2 agglomerates after 4 h of air-liquid interface exposure within the tissue section (200 µm by 200 µm). The blue cell outline represents the cell membrane based on the $C_3H_8N^+$ signal. (**A**) shows the top view while (**B**) represents the side view. (**C**) shows ToF-SIMS mass spectra (positive mode) of A549 cells exposed for 1 h or 4 h in the air-liquid interface system, showing the CeO^+ peak in red color at m/z 156.12u. The upper spectrum shows unexposed control cells (clean air exposure). The x-axis shows the molecular weight; the y-axis the ion intensities for the peaks (n = 6).

In addition to NP uptake, distribution and metabolic effects, we assessed molecular alterations of the cell membrane constituents by ToF-SIMS analysis that have been caused during ALI exposure of A549 cells to CeO_2 NPs. Unexposed A549 cells were used as controls (clean filtered air ALI exposure). The results indicate a significant reduction of the lipid phosphatidylcholine biosynthesis. Down regulation of the lysophosphatidylcholine series C18:1, C20:1, C22:1 and C24:1 (Figure 8, bottom) has been detected already after 1 h of exposure. By contrast, significant downregulation of the biosynthesis of phosphatidylethanolamine and its precursor, i.e., phosphatidylcholine, was only visible in A549 cells exposed for 4 h (Figure 8, top). All the following ion assignments were done tentatively, since certified reference materials were not available. Ion m/z 791 was attributed to phosphatidylcholine PC (C36:0), ion m/z 813 to phosphatidylcholine PC (C38:3). Ion m/z 777 was matched to the applicable library spectrum of phosphatidylethanolamine PE (C38:0). Additionally, the downregulation of the ceramide biosynthesis (ion m/z 625) after 4 h of exposure could be correlated to ceramide (d40:0).

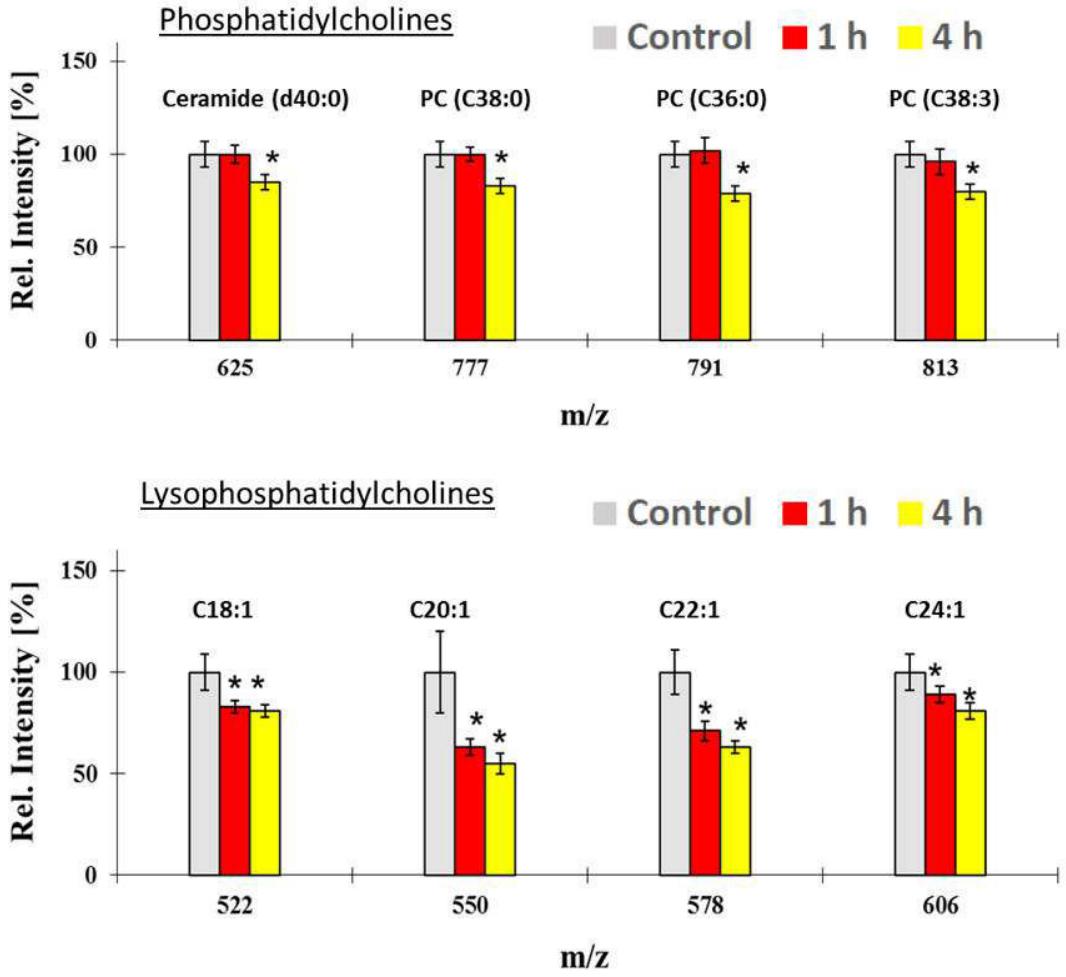

Figure 8. TOF-SIMS analysis of cell membranes composition changes of A549 cells after air-liquid interface exposure to CeO_2 NPs for 1 h and 4 h. The histograms show comparisons of ion yields for characteristic cell membrane lipids for the different exposure times. For the relative intensity, the mean of the control group (clean air) of unexposed A549 cells was taken as 100% in all cases. *: $p \leq 0.05$. Data represent the mean and error bars the standard deviation values ($n = 6$).

4. Discussion

This study provides a conceptual evaluation of key sources of variability that were identified using C&E analysis (Figure 2) of a cell viability assay with an ALI flow through exposure system. This analysis then guided the in-process control measurements used in the protocol (Table 1) and

the robustness testing performed. Our first experiments with a Vitrocell 12/3 CF module and A549 cells revealed a cell viability of about 45% after 1 h of clean air exposure (Figure S2B). Such a high decrease in viability in the air negative control system would severely limit the ability of this exposure system to evaluate potential toxicological impacts from aerosol exposure to substances such as ENMs. By systematically evaluating five potential sources of variability in the ALI exposure system (branch 2), experimental settings were determined which enabled longer exposure duration for the A549 cells (more than 4 h) while maintaining >85% cell viability when compared to the incubator negative control. Our results suggest that the relative humidity, lid temperature, flow rate, CO_2 concentration and exposure duration are crucial parameters for an ALI flow through exposure system given their impact on the cell viability (Figures 3 and 4). Controlling only the cell medium temperature below the cells was not sufficient to create an adequate environment for the cells. Instead, the lid temperature also had to be controlled. These findings are in accordance to a previous study that also found that the relative humidity and aerosol flow temperature impacted the exposure system negative control cells [71]. Given the impact that these factors were shown to have an impact on the exposure system negative control cells, it is strongly recommended for other researchers to report these parameters in the methods section of papers to enable comparability of results.

Overall, nine in-process control measurements were tested to carefully evaluate key sources of variability in the assay each time it was performed to increase confidence in the measurement results (Table 1). Several of these in-process control measurements were performed in the exposure chamber while others were performed in the incubator. The positive control, which tested cells using 0.2% Triton X-100 spiked to the medium and exposed to a MilliQ aerosol, was evaluated to confirm the dynamic range of the assay. One consideration for future development of the positive control would be to test a broader range of Triton X-100 concentrations to yield a dose-response curve that could be used to ensure the consistency of the assay sensitivity, or to identify a positive control that can be nebulized and then exposed to cells using the aerosol generated. To further optimize this control measurement, a highly toxic ENM like ZnO NPs [72,73] could be used and exposed to the cells under ALI conditions to generate an "positive control". Incubator negative control cells and the medium blank controls were also evaluated to assess the reproducibility of the WST-1 assay and of the cell pipetting on the inserts.

Using the optimal exposure setup, an exposure time up to 8 h could be achieved without a statistically significant decrease in cell viability for the consensus values (Figure 4A). Nevertheless, a trend to lower cell viability can be seen when exposing the cells longer than 4 h. Moreover, an evaluation of all three plates individually for the 8 h exposure condition revealed two of the three to be statistically less than the incubator negative control (Figure S8A). In future experiments, a 6 h time point should be evaluated to better assess the maximum exposure duration without a decrease in the viability for an individual plate. When examining the consensus values for the NM-212, there was a trend for a decrease in cell viability for the longest exposure time (4 h) even though the consensus value did not have a statistically significant decrease. There were differing results among the three plates (Figure S8C) and testing a greater number of plates would be needed to clarify if there is a real trend. Repeating experiments more than once provides more robust data, which is an important aspect in method validation [40,41,63,71,74].

To evaluate assay performance and day-to-day variability of the process control measurements, control charts were plotted (Figure S7). The mean value for COV of the incubator negative control (12%) is similar to the median average deviation values, which were typically less than 10%, obtained in a previous interlaboratory study with the MTS assay using submerged exposure conditions and A549 cells [50]. This suggests that the variability from pipetting cells is similar regardless of whether they are cultured in submerged conditions or on an ALI insert. This type of analysis helps to reveal the consistency of the data over time and should be considered when developing assay specifications that indicate the assay is preforming as expected. Combining the results from assays performed on different days, for this study from three different days, helps to account for day-to-day variability and leads to more robust statistical evaluations. Additional statistical analysis can help reveal the extent to

which increasing the number of incubator negative control wells or blank control wells would improve the assay's precision.

The particle size distribution measured by SMPS showed a bimodal shape for the CeO_2 aerosol. When evaluating the aerosolized MilliQ water, only the first peak was detectable which is probably from residuals like salts [75–77]. However, NM-212 NPs have a broad size distribution ranging from below 10 nm to more than 100 nm [56]. Thus, it might be that NM-212 NPs size distribution partly contributes to the first peak. Moreover, a strong variability in the residual peak in terms of particle number concentration was seen during different experiments which caused a high background. Therefore, two calculations were performed to avoid a possible particle mass underestimation. First, the residual peak was not subtracted from the whole size distribution when determining the deposited dose. For a second more conservative approach, particles measured for the aerosolized CeO_2 NP dispersion below 50 nm were not included when calculating the amount of deposition, because it was not possible to distinguish between the particle concentration contribution from the NPs and that from the MilliQ water. There was only a reduction of about 3% in total aerosol mass using the second approach compared to the first approach; this result is understandable because the smallest particles only had a minimal contribution to the total mass. In this particular setup of the ALI system, online measuring of the particle size distribution during the exposure experiments was not possible due to different tubing sizes of the ALI system and the SMPS system. To characterize the aerosol, the tubing was adjusted by guiding the aerosol through a glass tube. For cell experiments, the original steel tubing system from Vitrocell was used to ensure optimal performance (avoiding particle interactions with the glass wall). Another option is to measure the particle size distribution before and after the exposure. This could reveal if there was a change in the exposure concentration or particle size concentration during the course of the experiment, which may occur since NPs are known to agglomerate. Nevertheless, the deposition efficiency in this study was approximately 3%, which is in good agreement with the literature where the deposition efficiency for similar ALI systems has been reported to be between 1% to 2% [30,74,78,79].

To assess the toxicity of ENMs, quantification of the intracellular concentration is needed to facilitate the comparison between different *in vivo* or *in vitro* ENM exposure scenarios. An *in vivo* rat inhalation exposure study using CeO_2 NPs (NM-212) revealed that the particles were exclusively found to be intracellular located [80]. This is in agreement with our ToF-SIMS data where CeO_2 NPs were detected exclusively intracellular in A549 cells after ALI exposure and were not membrane associated (Figure 7). Thus, the washing protocol was sufficient to remove NPs which were solely present on top of the cells, or alternatively, the cells fully internalized the NPs prior to the washing procedure. ICP-MS analysis showed that of the deposited dose only half of the NPs could actually be found in the exposed A549 cells. The other half of the NPs were either located on the cell surface or in cells, such as dead cells, that were removed by the washing procedure. Exposing the human alveolar cell line A549 to a CeO_2 NP containing aerosol (1.07 ± 0.34 mg/m^3) an intracellular uptake rate of $4.85\ \text{ng} \times \text{cm}^{-2} \times \text{h}^{-1} \pm 1.93\ \text{ng} \times \text{cm}^{-2} \times \text{h}^{-1}$ was achieved. This is similar to the subacute whole body rat *in vivo* inhalation study from Keller et al. (2014) [22] where $4.76\ \text{ng/cm}^{-2} \times \text{h}^{-1}$ was found (authors reported a lung deposition of 2620 µg NM-212/rat lung for a dose of 25 mg/m^3; assuming a mean alveolar surface area of 50 d to 100 d old rats with 4584 cm^2 [81] and an exposure time of 120 h) [22]. Due to their higher deposition rates compared to flow through systems, cloud chamber systems can be considered for experiments where higher deposited masses of NPs are needed than can be obtained using flow through systems [31,82]. Furthermore, more sophisticated 3D cell models amenable to longer exposure periods than systems with a single adherent cell type can help to investigate long-term effects via repeated exposure under low dose and high dose conditions [37,83].

The potential toxicological effects of NP exposure were tested using the WST-1 assay and also a ToF-SIMS metabolic interactions assay. A reduction in cell viability was not found after CeO_2 treatment in WST-1 assay. As this assay represents an overall mean value of the metabolic activity of a cell population, its sensitivity to detect minimal adverse effects coming from low dose exposure might be

limited. Thus, TOF-SIMS investigations were conducted to enhance the sensitivity of metabolic analysis to detect possible adverse effects on a molecular level [84]. With this, a reduction in phospholipids composition within the bilayer was found (Figure 8). Since the CeO_2 NPs tested are positively charged, it is possible that washing of particles which could lead to a loss of lipids because of lipid attachment onto the particles, but this will likely be a minor effect since the fraction of the cell surface area that is covered by particles (approximately 8×10^{-4}) is much smaller than the change in the lipid composition. In addition, other recent studies of human macrophages exposed to silver NPs have also reported changes in the phospholipid pattern [67]. Both studies show that different lipids can be affected differently after ENM exposure similar to what was observed in this study. At the moment, the exact mechanism(s) how NPs affect the cell membrane lipid bilayer composition is yet not fully understood. Therefore, more studies are needed to fully provide mechanistic explanations of the lipid changes in general as well as for single lipids. Moreover, as the A549 cell line resembles a carcinogenic phenotype, the toxicological response might be different compared to primary cells [41]. Therefore, further studies should also consider using primary cells to more closely mimic the *in vivo* environment.

To the best of our knowledge, this is the first report describing the use of an ALI system with a flow through exposure system to generate an intracellular NP concentration comparable to those observed *in vivo*. This is an important step in the development of complementary methods for inhalation studies using flow through systems. A valuable next step for future work would be to use this assay to further establish physiological relevance by evaluating a broader range of nanomaterials, especially those known to cause toxicity at lower concentrations, and compare those results to *in vivo* data for the same materials. The performance with this assay could also be evaluated with different adherent cell lines or 3D cell constructs.

5. Conclusions

ALI systems are considered to be a promising exposure system to study toxicological effects of airborne nanomaterials instead of *in vivo* inhalation studies and have been widely used to assess the toxicology of nanomaterials in recent years. However, the robustness of these methods is not yet well understood. Here we reported a C&E analysis of a commonly used flow through ALI exposure system. This led to a systematic evaluation of key parameters of a frequently used ALI system that could influence cell viability results and the incorporation of nine in-process control measurements into the measurement protocol. Furthermore, this ALI case study provides a robust setup to standardized ALI approaches which can be useful for regulatory context where standardized and validated *in vitro* methods are needed. Furthermore, we showed that this ALI system is able to deposit concentrations to human lung epithelia cells that result in an intracellular NP uptake similar in quantity to uptake rates observed in an *in vivo* rat study [22]. These results support the potential standardization of ALI-based exposure methods. The general procedure reported here may help to improve the standardization of the ALI *in vitro* exposure approach better enabling comparability between experiments.

Supplementary Materials: The following are available online at http://www.mdpi.com/2079-4991/10/12/2369/s1. Figure S1: Nanoparticle size characterization. (A) TEM image shows the size and shape of CeO2 NPs. (B) Selected area electron diffraction (SAED) of CeO2 NPs. (C) Dynamic light scattering (DLS) analysis of the particle diameter calculated via size distribution by numbers. (n = 3 = three independent experiments, each experiment was performed in triplicates). Out of three, two of them were overlapping and the 3rd one covered the purple one. Figure S2: A549 cell viability. (A) shows cell viability under ALI and submerged (LL) culture conditions (no ALI exposure) compared to ALI cultured cells. (B) exhibits the cell viability after 1 h ALI clean air exposure compared to the incubator control without any optimization of the ALI system (start conditions). Percentage viability values are the consensus values calculated for each of the three plates using the Bayesian modeling. The values are the means and the error bars the standard deviation. Figure S3: Characterization of the Vitrocell exposure 12/3 CF module. The relative humidity of the exposure air with and without humidification of the clean air, or a water droplet aerosol (MilliQ aerosol), which was used for particle exposure, is shown in (A). Heating the lid temperature to a certain degree does not necessarily mean that the aerosol flow temperature is equal to the lid temperature. Therefore, the relationship between the temperature of the air flow and the water bath temperature, which was used to heat the lid, is shown in part (B) for the particle exposure module and the control module (clean air only). n = 3 independent experiments with 1 technical replicate each. Figure S4: The particle size distribution of NM-212

as a function of the inlet pressure of the aerosol generator (n = 9 = three independent experiments with 3 data points each. Data from each experiment are combined and shown as mean ± SD). Figure S5: Fisher's linear discriminant of ToF-SIMS analysis (n = 6). Different groups show distinct differences. Figure S6: ICP-MS calibration curves of the three different measurements. The solid lines indicate a linear regression fit to the data. Figure S7: Plate to plate analysis of consensus values for the different parameters affecting cell viability: Relative humidity (A), lid temperature (B), flow rates (C) and 5% CO_2 supply (D). Percentage viability values are the consensus values calculated for each of the three plates using the Bayesian modeling. The values are the means and the error bars the standard deviation. Black asterisks indicate that the consensus value is significantly less than the incubator control with a 95% likelihood using the Bayesian modeling. Figure S8: Plate to plate analysis of consensus values for the different parameters affecting cell viability: (A) Time-dependent cell viability for MilliQ water aerosol exposure (without ENM) using the optimized Vitrocell setup. (B) Effect of 5% CO_2 supply to the air on the cell viability after 4 h MilliQ water aerosol exposure using the optimized Vitrocell exposure setup. (C) A time-dependent NM-212 exposure compared to MilliQ water aerosol (without NP) exposed cells. Percentage viability values are the consensus values calculated for each of the three plates using the Bayesian modeling. The values are the means and the error bars the standard deviation. Black asterisks indicate that the consensus value is significantly less than the incubator control with a 95% likelihood using the Bayesian modeling. Table S1: Mycoplasma test, PCR compounds. Table S2: Mycoplasma test, PCR conditions and protocol. Table S3: ICP-MS LOD/LOQ levels of the three different measurements. Table S4: Possible pitfalls during an ALI exposure experiment.

Author Contributions: Conceptualization, L.B.L., J.T. and E.J.P.; data curation, L.B.L., H.J. and E.J.P.; formal analysis, H.J., B.T. and E.J.P.; funding acquisition, A.L.; investigation, L.B.L., H.J. and A.K.; methodology, L.B.L. and A.V.S.; project administration, F.S.B.; software, B.T.; supervision, J.T., P.L. and A.L.; validation, L.B.L. and E.J.P.; writing—original draft, L.B.L., H.J. and E.J.P.; writing—review and editing, J.T., A.K., F.S.B., A.V.S., P.L. and A.L. All authors have read and agreed to the published version of the manuscript.

Funding: This research was funded by the German Federal Institute for Risk Assessment (BfR), grant number SFP 1322-594 for L.B.L., A.K., F.S.B., A.V.S., J.T., H.J., P.L. and A.L.

Acknowledgments: We thank Max Planck institute for solid state research for transmission electron microscopy images. We also thank Tobias Krebs from VITROCELL Systems GmbH and all partners from the ERA-NET SIINN project NANOaers for fruitful discussions. The authors also thank Philipp Reichardt for ToF-SIMS imaging. Certain commercial products or equipment are described in this paper in order to specify adequately the experimental procedure. In no case does such identification imply recommendation or endorsement by the National Institute of Standards and Technology, nor does it imply that it is necessarily the best available for the purpose.

Conflicts of Interest: The authors declare no conflict of interest.

References

1. Ren, G.G.; Hu, D.W.; Cheng, E.W.C.; Vargas-Reus, M.A.; Reip, P.; Allaker, R.P. Characterisation of copper oxide nanoparticles for antimicrobial applications. *Int. J. Antimicrob. Agents* **2009**, *33*, 587–590. [CrossRef] [PubMed]
2. Kaur, R.; Giordano, C.; Gradzielski, M.; Mehta, S.K. Synthesis of Highly Stable, Water-Dispersible Copper Nanoparticles as Catalysts for Nitrobenzene Reduction. *Chem. Asian J.* **2014**, *9*, 189–198. [CrossRef] [PubMed]
3. Izu, N.; Shin, W.; Matsubara, I.; Murayama, N. Development of resistive oxygen sensors based on cerium oxide thick film. *J. Electroceram.* **2004**, *13*, 703–706. [CrossRef]
4. Patil, S.; Kuiry, S.C.; Seal, S.; Vanfleet, R. Synthesis of nanocrystalline ceria particles for high temperature oxidation resistant coating. *J. Nanoparticle Res.* **2002**, *4*, 433–438. [CrossRef]
5. Corma, A.; Atienzar, P.; Garcia, H.; Chane-Ching, J.Y. Hierarchically mesostructured doped CeO_2 with potential for solar-cell use. *Nat. Mater.* **2004**, *3*, 394–397. [CrossRef]
6. Murray, E.P.; Tsai, T.; Barnett, S.A. A direct-methane fuel cell with a ceria-based anode. *Nature* **1999**, *400*, 649–651. [CrossRef]
7. Zheng, X.C.; Zhang, X.L.; Wang, X.Y.; Wang, S.R.; Wu, S.H. Preparation and characterization of CuO/CeO_2 catalysts and their applications in low-temperature CO oxidation. *Appl. Catal. A Gen.* **2005**, *295*, 142–149. [CrossRef]
8. Mainali, M.; Ngwa, W.; Cifter, G.; Celli, J. Potential of Using Cerium Oxide Nanoparticles (CONP) for Protecting Healthy Tissue During Accelerated Partial Breast Irradiation (APBI). *Med. Phys.* **2015**, *42*, 3643. [CrossRef]

9. Neuhaus, V.; Chichester, J.A.; Ebensen, T.; Schwarz, K.; Hartman, C.E.; Shoji, Y.; Guzman, C.A.; Yusibov, V.; Sewald, K.; Braun, A. A new adjuvanted nanoparticle-based H1N1 influenza vaccine induced antigen-specific local mucosal and systemic immune responses after administration into the lung. *Vaccine* **2014**, *32*, 3216–3222. [CrossRef]
10. Sun, J.; Petersen, E.J.; Watson, S.S.; Sims, C.M.; Kassman, A.; Frukhtbeyn, S.; Skrtic, D.; Ok, M.T.; Jacobs, D.S.; Reipa, V.; et al. Biophysical characterization of functionalized titania nanoparticles and their application in dental adhesives. *Acta Biomater.* **2017**, *53*, 585–597. [CrossRef]
11. Hsu, P.C.; Song, A.Y.; Catrysse, P.B.; Liu, C.; Peng, Y.C.; Xie, J.; Fan, S.H.; Cui, Y. Radiative human body cooling by nanoporous polyethylene textile. *Science* **2016**, *353*, 1019–1023. [CrossRef] [PubMed]
12. Graczyk, H.; Lewinski, N.; Zhao, J.Y.; Sauvain, J.J.; Suarez, G.; Wild, P.; Danuser, B.; Riediker, M. Increase in oxidative stress levels following welding fume inhalation: A controlled human exposure study. *Part. Fibre Toxicol.* **2016**, *13*. [CrossRef] [PubMed]
13. Smulders, S.; Luyts, K.; Brabants, G.; Golanski, L.; Martens, J.; Vanoirbeek, J.; Hoet, P.H.M. Toxicity of nanoparticles embedded in paints compared to pristine nanoparticles, in vitro study. *Toxicol. Lett.* **2015**, *232*, 333–339. [CrossRef] [PubMed]
14. Kuijpers, E.; Bekker, C.; Fransman, W.; Brouwer, D.; Tromp, P.; Vlaanderen, J.; Godderis, L.; Hoet, P.; Lan, Q.; Silverman, D.; et al. Occupational Exposure to Multi-Walled Carbon Nanotubes During Commercial Production Synthesis and Handling. *Ann. Occup. Hyg.* **2016**, *60*, 305–317. [CrossRef]
15. Brouwer, D. Exposure to manufactured nanoparticles in different workplaces. *Toxicology* **2010**, *269*, 120–127. [CrossRef]
16. Schulte, P.; Geraci, C.; Zumwalde, R.; Hoover, M.; Kuempel, E. Occupational risk management of engineered nanoparticles. *J. Occup. Environ. Hyg.* **2008**, *5*, 239–249. [CrossRef]
17. Birch, M.E.; Ku, B.K.; Evans, D.E.; Ruda-Eberenz, T.A. Exposure and Emissions Monitoring during Carbon Nanofiber Production-Part I: Elemental Carbon and Iron-Soot Aerosols. *Ann. Occup. Hyg.* **2011**, *55*, 1016–1036. [CrossRef]
18. Morimoto, Y.; Izumi, H.; Yoshiura, Y.; Tomonaga, T.; Oyabu, T.; Myojo, T.; Kawai, K.; Yatera, K.; Shimada, M.; Kubo, M.; et al. Pulmonary toxicity of well-dispersed cerium oxide nanoparticles following intratracheal instillation and inhalation. *J. Nanoparticle Res.* **2015**, *17*. [CrossRef]
19. Schwotzer, D.; Ernst, H.; Schaudien, D.; Kock, H.; Pohlmann, G.; Dasenbrock, C.; Creutzenberg, O. Effects from a 90-day inhalation toxicity study with cerium oxide and barium sulfate nanoparticles in rats. *Part. Fibre Toxicol.* **2017**, *14*, 23. [CrossRef]
20. Demokritou, P.; Gass, S.; Pyrgiotakis, G.; Cohen, J.M.; Goldsmith, W.; McKinney, W.; Frazer, D.; Ma, J.; Schwegler-Berry, D.; Brain, J.; et al. An in vivo and in vitro toxicological characterisation of realistic nanoscale CeO_2 inhalation exposures. *Nanotoxicology* **2013**, *7*, 1338–1350. [CrossRef]
21. Konduru, N.V.; Murdaugh, K.M.; Swami, A.; Jimenez, R.J.; Donaghey, T.C.; Demokritou, P.; Brain, J.D.; Molina, R.M. Surface modification of zinc oxide nanoparticles with amorphous silica alters their fate in the circulation. *Nanotoxicology* **2016**, *10*, 720–727. [CrossRef] [PubMed]
22. Keller, J.; Wohlleben, W.; Ma-Hock, L.; Strauss, V.; Groters, S.; Kuttler, K.; Wiench, K.; Herden, C.; Oberdorster, G.; van Ravenzwaay, B.; et al. Time course of lung retention and toxicity of inhaled particles: Short-term exposure to nano-Ceria. *Arch. Toxicol.* **2014**, *88*, 2033–2059. [CrossRef] [PubMed]
23. Teeguarden, J.G.; Mikheev, V.B.; Minard, K.R.; Forsythe, W.C.; Wang, W.; Sharma, G.; Karin, N.; Tilton, S.C.; Waters, K.M.; Asgharian, B.; et al. Comparative iron oxide nanoparticle cellular dosimetry and response in mice by the inhalation and liquid cell culture exposure routes. *Part. Fibre Toxicol.* **2014**, *11*. [CrossRef] [PubMed]
24. Kreyling, W.G.; Hirn, S.; Moller, W.; Schleh, C.; Wenk, A.; Celik, G.; Lipka, J.; Schaffler, M.; Haberl, N.; Johnston, B.D.; et al. Air-Blood Barrier Translocation of Tracheally Instilled Gold Nanoparticles Inversely Depends on Particle Size. *ACS Nano* **2014**, *8*, 222–233. [CrossRef]
25. Wiemann, M.; Vennemann, A.; Sauer, U.G.; Wiench, K.; Ma-Hock, L.; Landsiedel, R. An in vitro alveolar macrophage assay for predicting the short-term inhalation toxicity of nanomaterials. *J. Nanobiotechnol.* **2016**, *14*. [CrossRef]
26. L'Azou, B.; Jorly, J.; On, D.; Sellier, E.; Moisan, F.; Fleury-Feith, J.; Cambar, J.; Brochard, P.; Ohayon-Courtes, C. In vitro effects of nanoparticles on renal cells. *Part Fibre Toxicol.* **2008**, *5*. [CrossRef]

27. Cohen, J.; DeLoid, G.; Pyrgiotakis, G.; Demokritou, P. Interactions of engineered nanomaterials in physiological media and implications for in vitro dosimetry. *Nanotoxicology* **2013**, *7*, 417–431. [CrossRef]
28. Morimoto, Y.; Horie, M.; Kobayashi, N.; Shinohara, N.; Shimada, M. Inhalation Toxicity Assessment of Carbon-Based Nanoparticles. *Acc. Chem. Res.* **2013**, *46*, 770–781. [CrossRef]
29. Lacroix, G.; Koch, W.; Ritter, D.; Gutleb, A.C.; Larsen, S.T.; Loret, T.; Zanetti, F.; Constant, S.; Chortarea, S.; Rothen-Rutishauser, B.; et al. Air-Liquid Interface In Vitro Models for Respiratory Toxicology Research: Consensus Workshop and Recommendations. *Appl. Vitr. Toxicol.* **2018**, *4*, 91–106. [CrossRef]
30. Mülhopt, S.; Dilger, M.; Diabate, S.; Schlager, C.; Krebs, T.; Zimmermann, R.; Buters, J.; Oeder, S.; Wascher, T.; Weiss, C.; et al. Toxicity testing of combustion aerosols at the air-liquid interface with a self-contained and easy-to-use exposure system. *J. Aerosol. Sci.* **2016**, *96*, 38–55. [CrossRef]
31. Lenz, A.G.; Karg, E.; Lentner, B.; Dittrich, V.; Brandenberger, C.; Rothen-Rutishauser, B.; Schulz, H.; Ferron, G.A.; Schmid, O. A dose-controlled system for air-liquid interface cell exposure and application to zinc oxide nanoparticles. *Part. Fibre Toxicol.* **2009**, *6*. [CrossRef] [PubMed]
32. Seagrave, J.; McDonald, J.D.; Mauderly, J.L. In vitro versus in vivo exposure to combustion emissions. *Exp. Toxicol. Pathol.* **2005**, *57*, 233–238. [CrossRef] [PubMed]
33. Ji, J.; Hedelin, A.; Malmlof, M.; Kessler, V.; Seisenbaeva, G.; Gerde, P.; Palmberg, L. Development of Combining of Human Bronchial Mucosa Models with XposeALI (R) for Exposure of Air Pollution Nanoparticles. *PLoS ONE* **2017**, *12*. [CrossRef] [PubMed]
34. Svensson, C.R.; Ameer, S.S.; Ludvigsson, L.; Ali, N.; Alhamdow, A.; Messing, M.E.; Pagels, J.; Gudmundsson, A.; Bohgard, M.; Sanfins, E.; et al. Validation of an air-liquid interface toxicological set-up using Cu, Pd, and Ag well-characterized nanostructured aggregates and spheres. *J. Nanopart Res.* **2016**, *18*. [CrossRef] [PubMed]
35. Fields, W.; Maione, A.; Keyser, B.; Bombick, B. Characterization and Application of the VITROCELL VC1 Smoke Exposure System and 3D EpiAirway Models for Toxicological and e-Cigarette Evaluations. *Appl. Vitr. Toxicol.* **2017**, *3*, 68–83. [CrossRef]
36. Thorne, D.; Larard, S.; Baxter, A.; Meredith, C.; Gaca, M. The comparative in vitro assessment of e-cigarette and cigarette smoke aerosols using the gamma H2AX assay and applied dose measurements. *Toxicol. Lett.* **2017**, *265*, 170–178. [CrossRef]
37. Ishikawa, S.; Matsumura, K.; Kitamura, N.; Ishimori, K.; Takanami, Y.; Ito, S. Application of a direct aerosol exposure system for the assessment of biological effects of cigarette smoke and novel tobacco product vapor on human bronchial epithelial cultures. *Regul. Toxicol. Pharm.* **2018**, *96*, 85–93. [CrossRef]
38. Lucci, F.; Castro, N.D.; Rostami, A.A.; Oldham, M.J.; Hoeng, J.; Pithawalla, Y.B.; Kuczaj, A.K. Characterization and modeling of aerosol deposition in Vitrocell (R) exposure systems—Exposure well chamber deposition efficiency. *J. Aerosol. Sci.* **2018**, *123*, 141–160. [CrossRef]
39. Loret, T.; Peyret, E.; Dubreuil, M.; Aguerre-Chariol, O.; Bressot, C.; le Bihan, O.; Amodeo, T.; Trouiller, B.; Braun, A.; Egles, C.; et al. Air-liquid interface exposure to aerosols of poorly soluble nanomaterials induces different biological activation levels compared to exposure to suspensions. *Part. Fibre Toxicol.* **2016**, *13*, 58. [CrossRef]
40. Kim, J.S.; Peters, T.M.; O'Shaughnessy, P.T.; Adamcakova-Dodd, A.; Thorne, P.S. Validation of an in vitro exposure system for toxicity assessment of air-delivered nanomaterials. *Toxicol. In Vitro* **2013**, *27*, 164–173. [CrossRef]
41. Jing, X.F.; Park, J.H.; Peters, T.M.; Thorne, P.S. Toxicity of copper oxide nanoparticles in lung epithelial cells exposed at the air-liquid interface compared with in vivo assessment. *Toxicol. In Vitro* **2015**, *29*, 502–511. [CrossRef] [PubMed]
42. Klein, S.G.; Cambier, S.; Hennen, J.; Legay, S.; Serchi, T.; Nelissen, I.; Chary, A.; Moschini, E.; Krein, A.; Blomeke, B.; et al. Endothelial responses of the alveolar barrier in vitro in a dose-controlled exposure to diesel exhaust particulate matter. *Part. Fibre Toxicol.* **2017**, *14*. [CrossRef] [PubMed]
43. Oeder, S.; Kanashova, T.; Sippula, O.; Sapcariu, S.C.; Streibel, T.; Arteaga-Salas, J.M.; Passig, J.; Dilger, M.; Paur, H.R.; Schlager, C.; et al. Particulate Matter from Both Heavy Fuel Oil and Diesel Fuel Shipping Emissions Show Strong Biological Effects on Human Lung Cells at Realistic and Comparable In Vitro Exposure Conditions. *PLoS ONE* **2015**, *10*. [CrossRef] [PubMed]

44. Frohlich, E.; Bonstingl, G.; Hofler, A.; Meindl, C.; Leitinger, G.; Pieber, T.R.; Roblegg, E. Comparison of two in vitro systems to assess cellular effects of nanoparticles-containing aerosols. *Toxicol. In Vitro* **2013**, *27*, 409–417. [CrossRef]
45. Klein, S.G.; Serchi, T.; Hoffmann, L.; Blomeke, B.; Gutleb, A.C. An improved 3D tetraculture system mimicking the cellular organisation at the alveolar barrier to study the potential toxic effects of particles on the lung. *Part. Fibre Toxicol.* **2013**, *10*, 31. [CrossRef]
46. Bohmer, N.; Rippl, A.; May, S.; Walter, A.; Heo, M.B.; Kwak, M.; Roesslein, M.; Song, N.W.; Wick, P.; Hirsch, C. Interference of engineered nanomaterials in flow cytometry: A case study. *Colloids Surf. B Biointerfaces* **2018**, *172*, 635–645. [CrossRef]
47. Nelson, B.C.; Petersen, E.J.; Marquis, B.J.; Atha, D.H.; Elliott, J.T.; Cleveland, D.; Watson, S.S.; Tseng, I.-H.; Dillon, A.; Theodore, M.; et al. NIST gold nanoparticle reference materials do not induce oxidative DNA damage. *Nanotoxicology* **2013**, *7*, 21–29. [CrossRef]
48. Romeo, D.; Salieri, B.; Hischier, R.; Nowack, B.; Wick, P. An integrated pathway based on in vitro data for the human hazard assessment of nanomaterials. *Environ. Int.* **2020**, *137*, 105505. [CrossRef]
49. Giard, D.J.; Aaronson, S.A.; Todaro, G.J.; Arnstein, P.; Kersey, J.H.; Dosik, H.; Parks, W.P. In vitro cultivation of human tumors: Establishment of cell lines derived from a series of solid tumors. *J. Natl. Cancer Inst.* **1973**, *51*, 1417–1423. [CrossRef]
50. Elliott, J.T.; Rosslein, M.; Song, N.W.; Toman, B.; Kinsner-Ovaskainen, A.; Maniratanachote, R.; Salit, M.L.; Petersen, E.J.; Sequeira, F.; Romsos, E.L.; et al. Toward achieving harmonization in a nano-cytotoxicity assay measurement through an interlaboratory comparison study. *ALTEX* **2017**, *34*, 201–218. [CrossRef]
51. Rosslein, M.; Elliott, J.T.; Salit, M.; Petersen, E.J.; Hirsch, C.; Krug, H.F.; Wick, P. Use of Cause-and-Effect Analysis to Design a High-Quality Nanocytotoxicology Assay. *Chem. Res. Toxicol.* **2015**, *28*, 21–30. [CrossRef] [PubMed]
52. Petersen, E.J.; Hirsch, C.; Elliott, J.T.; Krug, H.F.; Aengenheister, L.; Arif, A.T.; Bogni, A.; Kinsner-Ovaskainen, A.; May, S.; Walser, T.; et al. Cause-and-effect analysis as a tool to improve the reproducibility of nanobioassays: Four case studies. *Chem. Res. Toxicol.* **2020**, *33*, 1039–1054. [CrossRef] [PubMed]
53. Hanna, S.K.; Cooksey, G.A.; Dong, S.; Nelson, B.C.; Mao, L.; Elliott, J.T.; Petersen, E.J. Feasibility of using a standardized Caenorhabditis elegans toxicity test to assess nanomaterial toxicity. *Environ. Sci. Nano* **2016**, *3*, 1080–1089. [CrossRef]
54. Shannon, K.H.; Bustos, A.M.; Peterson, A.W.; Reipa, V.; Scanlan, L.D.; Coskun, S.H.; Cho, T.J.; Johnson, M.E.; Hackley, V.A.; Nelson, B.C.; et al. Agglomeration of Escherichia coli with positively charged nanoparticles can lead to artifacts in a standard Caenorhabditis elegans toxicity assay. *Environ. Sci. Technol.* **2018**, *52*, 5968–5978. [CrossRef]
55. Berridge, M.V.; Herst, P.M.; Tan, A.S. Tetrazolium dyes as tools in cell biology: New insights into their cellular reduction. *Biotechnol. Annu. Rev.* **2005**, *11*, 127–152. [CrossRef] [PubMed]
56. Singh, C.; Friedrichs, S.; Ceccone, G.; Gibson, N.; Jensen, K.A.; Levin, M.; Infante, H.G.; Carlander, D.; Rasmussen, K. *Cerium Dioxide, NM-211, NM-212, NM-213. Characterisation and Test Item Preparation*; European Commission, Joint Research Centre. Available online: http://publications.jrc.ec.europa.eu/repository/bitstream/JRC89825/lbna26649enn.pdf,2014 (accessed on 2 November 2020).
57. Hartmann, N.B.; Jensen, K.A.; Baun, A.; Rasmussen, K.; Rauscher, H.; Tantra, R.; Cupi, D.; Gilliland, D.; Pianella, F.; Riego Sintes, J.M. Techniques and Protocols for Dispersing Nanoparticle Powders in Aqueous Media-Is there a Rationale for Harmonization? *J. Toxicol. Environ. Health B Crit. Rev.* **2015**, *18*, 299–326. [CrossRef]
58. Leibrock, L.; Wagener, S.; Singh, A.V.; Laux, P.; Luch, A. Nanoparticle induced barrier function assessment at liquid–liquid and air–liquid interface in novel human lung epithelia cell lines. *Toxicol. Res.* **2019**. [CrossRef]
59. Singh, A.V.; Jahnke, T.; Wang, S.; Xiao, Y.; Alapan, Y.; Kharratian, S.; Onbasli, M.C.; Kozielski, K.; David, H.; Richter, G.; et al. Anisotropic Gold Nanostructures: Optimization via in Silico Modeling for Hyperthermia. *ACS Appl. Nano Mater.* **2018**, *1*, 6205–6216. [CrossRef]
60. Tentschert, J.; Laux, P.; Jungnickel, H.; Brunner, J.; Estrela-Lopis, I.; Merker, C.; Meijer, J.; Ernst, H.; Ma-Hock, L.; Keller, J.; et al. Organ burden of inhaled nanoceria in a 2-year low-dose exposure study: Dump or depot? *Nanotoxicology* **2020**, *14*, 554–576. [CrossRef]

61. Hachenberger, Y.U.; Rosenkranz, D.; Kriegel, F.L.; Krause, B.; Matschass, R.; Reichardt, P.; Tentschert, J.; Laux, P.; Jakubowski, N.; Panne, U.; et al. Tackling Complex Analytical Tasks: An ISO/TS-Based Validation Approach for Hydrodynamic Chromatography Single Particle Inductively Coupled Plasma Mass Spectrometry. *Materials* **2020**, *13*, 1447. [CrossRef]
62. Krause, B.; Meyer, T.; Sieg, H.; Kastner, C.; Reichardt, P.; Tentschert, J.; Jungnickel, H.; Estrela-Lopis, I.; Burel, A.; Chevance, S.; et al. Characterization of aluminum, aluminum oxide and titanium dioxide nanomaterials using a combination of methods for particle surface and size analysis. *RSC Adv.* **2018**, *8*, 14377–14388. [CrossRef]
63. Sieg, H.; Braeuning, C.; Kunz, B.M.; Daher, H.; Kastner, C.; Krause, B.C.; Meyer, T.; Jalili, P.; Hogeveen, K.; Bohmert, L.; et al. Uptake and molecular impact of aluminum-containing nanomaterials on human intestinal caco-2 cells. *Nanotoxicology* **2018**, *12*, 992–1013. [CrossRef] [PubMed]
64. Haase, A.; Arlinghaus, H.F.; Tentschert, J.; Jungnickel, H.; Graf, P.; Mantion, A.; Draude, F.; Galla, S.; Plendl, J.; Goetz, M.E.; et al. Application of Laser Postionization Secondary Neutral Mass Spectrometry/Time-of-Flight Secondary Ion Mass Spectrometry in Nanotoxicology: Visualization of Nanosilver in Human Macrophages and Cellular Responses. *ACS Nano* **2011**, *5*, 3059–3068. [CrossRef] [PubMed]
65. Jungnickel, H.; Jones, E.A.; Lockyer, N.P.; Oliver, S.G.; Stephens, G.M.; Vickerman, J.C. Application of TOF-SIMS with chemometrics to discriminate between four different yeast strains from the species Candida glabrata and Saccharomyces cerevisiae. *Anal. Chem.* **2005**, *77*, 1740–1745. [CrossRef] [PubMed]
66. Booth, A.; Storseth, T.; Altin, D.; Fornara, A.; Ahniyaz, A.; Jungnickel, H.; Laux, P.; Luch, A.; Sorensen, L. Freshwater dispersion stability of PAA-stabilised-cerium-oxide nanoparticles and toxicity towards Pseudokirchneriella subcapitata. *Sci. Total Environ.* **2015**, *505*, 596–605. [CrossRef] [PubMed]
67. Tentschert, J.; Draude, F.; Jungnickel, H.; Haase, A.; Mantion, A.; Galla, S.; Thunemann, A.F.; Taubert, A.; Luch, A.; Arlinghaus, H.F. TOF-SIMS analysis of cell membrane changes in functional impaired human macrophages upon nanosilver treatment. *Surf. Interface Anal.* **2013**, *45*, 483–485. [CrossRef]
68. Possolo, A.; Toman, B. Tutorial for Metrologists on the Probabilistic and Statistical Apparatus Underlying the GUM and Related Documents. National Institute of Standards and Technology, Gaithersburg, MD, November 2011. Available online: www.itl.nist.gov/div898/possolo/TutorialWEBServer/TutorialMetrologists2011Nov09.xht (accessed on 2 November 2020). [CrossRef]
69. Gelman, A.; Carlin, J.; Stern, H.; Rubin, D. *Bayesian Data Analysis*, 2nd ed.; Chapman & Hall: London, UK, 2008.
70. David, L.; David, S.; Andrew, T.; Nicky, B. The BUGS project: Evolution, critique and future directions. *Stat. Med.* **2009**, *28*, 3049–3067. [CrossRef]
71. Zavala, J.; Greenan, R.; Krantz, Q.T.; DeMarini, D.M.; Higuchi, M.; Gilmour, M.I.; White, P.A. Regulating temperature and relative humidity in air-liquid interface in vitro systems eliminates cytotoxicity resulting from control air exposures. *Toxicol. Res.* **2017**, *6*, 448–459. [CrossRef]
72. Heng, B.C.; Zhao, X.; Xiong, S.; Ng, K.W.; Boey, F.Y.; Loo, J.S. Toxicity of zinc oxide (ZnO) nanoparticles on human bronchial epithelial cells (BEAS-2B) is accentuated by oxidative stress. *Food Chem. Toxicol.* **2010**, *48*, 1762–1766. [CrossRef]
73. Annangi, B.; Rubio, L.; Alaraby, M.; Bach, J.; Marcos, R.; Hernandez, A. Acute and long-term in vitro effects of zinc oxide nanoparticles. *Arch. Toxicol.* **2016**, *90*, 2201–2213. [CrossRef]
74. Bitterle, E.; Karg, E.; Schroeppel, A.; Kreyling, W.G.; Tippe, A.; Ferron, G.A.; Schmid, O.; Heyder, J.; Maier, K.L.; Hofer, T. Dose-controlled exposure of A549 epithelial cells at the air-liquid interface to airborne ultrafine carbonaceous particles. *Chemosphere* **2006**, *65*, 1784–1790. [CrossRef] [PubMed]
75. Fissan, H.; Ristig, S.; Kaminski, H.; Asbach, C.; Epple, M. Comparison of different characterization methods for nanoparticle dispersions before and after aerosolization. *Anal. Methods UK* **2014**, *6*, 7324–7334. [CrossRef]
76. Krames, J.; Buttner, H.; Ebert, F. Submicron Particle Generation by Evaporation of Water Droplets. *J. Aerosol. Sci.* **1991**, *22*, S15–S18. [CrossRef]
77. Whitby, K.T.; Liu, B.Y.H. Polystyrene Aerosols—Electrical Charge and Residue Size Distribution. *Atmos. Environ.* **1968**, *2*, 103–116. [CrossRef]
78. Kooter, I.M.; Gröllers-Mulderij, M.; Steenhof, M.; Duistermaat, E.; van Acker, F.A.A.; Staal, Y.C.M.; Tromp, P.C.; Schoen, E.; Kuper, C.F.; van Someren, E. Cellular Effects in an In Vitro Human 3D Cellular Airway Model and A549/BEAS-2B In Vitro Cell Cultures Following Air Exposure to Cerium Oxide Particles at an Air–Liquid Interface. *Appl. In Vitro Toxicol.* **2016**, *2*, 56–66. [CrossRef]

79. Lenz, A.G.; Karg, E.; Brendel, E.; Hinze-Heyn, H.; Maier, K.L.; Eickelberg, O.; Stoeger, T.; Schmid, O. Inflammatory and oxidative stress responses of an alveolar epithelial cell line to airborne zinc oxide nanoparticles at the air-liquid interface: A comparison with conventional, submerged cell-culture conditions. *Biomed. Res. Int.* **2013**, *2013*, 652632. [CrossRef]
80. Brunner, J.; Tentschert, J.; Jungnickel, H.; Laux, P.; Estrela-Lopis, I. NANoREG Deliverable D4.04 Organ. Burden and Particle Detection Pattern in Other Organs after Subacute Exposure. 2014. Available online: https://www.rivm.nl/en/documenten/nanoreg-d4-04-dr-organ-burden-and-particle-detection-pattern-in-other-organs-after (accessed on 2 November 2020).
81. Ohashi, T.; Pinkerton, K.; Ikegami, M.; Jobe, A.H. Changes in Alveolar Surface-Area, Surfactant Protein-a, and Saturated Phosphatidylcholine with Postnatal Rat Lung Growth. *Pediatr. Res.* **1994**, *35*, 685–689. [CrossRef]
82. Herzog, F.; Clift, M.J.; Piccapietra, F.; Behra, R.; Schmid, O.; Petri-Fink, A.; Rothen-Rutishauser, B. Exposure of silver-nanoparticles and silver-ions to lung cells in vitro at the air-liquid interface. *Part. Fibre Toxicol.* **2013**, *10*, 11. [CrossRef]
83. Huang, S.; Wiszniewski, L.; Constant, S.; Roggen, E. Potential of in vitro reconstituted 3D human airway epithelia (MucilAir (TM)) to assess respiratory sensitizers. *Toxicol. In Vitro* **2013**, *27*, 1151–1156. [CrossRef]
84. Kriegel, F.L.; Reichardt, P.; Krause, B.C.; Singh, A.V.; Tentschert, J.; Laux, P.; Jungnickel, H.; Luch, A. The Vitamin A and D Exposure of Cells Affects the Intracellular Uptake of Aluminum Nanomaterials and its Agglomeration Behavior: A Chemo-Analytic Investigation. *Int. J. Mol. Sci.* **2020**, *21*, 1278. [CrossRef]

3.2 Objective 2: Nanoparticle induced barrier function assessment at liquid–liquid and air–liquid interface in novel human lung epithelia cell lines

Lars Leibrock, Sandra Wagener, Ajay Vikram Singh, Peter Laux, and Andreas Luch

This chapter was published online on 19.11.2019 in:

Toxicology Research, 2019, **8**, 1016-1027 by Oxford University Press

https://doi.org/10.1039/C9TX00179D

Involvement of the author within this publication: Project planning (75 %), project execution (90 %), data analysis (85 %), manuscript writing (90 %).

Supplementary materials for this publication are shown in Annex II.

Toxicology Research

PAPER

Cite this: *Toxicol. Res.*, 2019, **8**, 1016

Nanoparticle induced barrier function assessment at liquid–liquid and air–liquid interface in novel human lung epithelia cell lines†

Lars Leibrock,* Sandra Wagener, Ajay Vikram Singh, Peter Laux and Andreas Luch

Inhalation is the most relevant entry point for nanoparticles (NPs) into the human body. To date, toxicity testing of nanomaterials in respect to oral, dermal and inhalative application is mainly based on animal experiments. The development of alternative test methods is the subject of current research. *In vitro* models can help to investigate mechanistic aspects, as *e.g.* cellular uptake or genotoxicity and might help to reduce *in vivo* testing. Lung cell lines are proper *in vitro* tools to assess NP toxicity. In respect to this, various cell models have been developed during the recent years, but often lack in a proper intact barrier function. However, besides other important *in vivo* criteria which are still missing like *e.g.* circulation, this is one basic prerequisite to come closer to the *in vivo* situation in certain mechanistic aspects such as particle translocation which is an important task for risk assessment of nanomaterials. Novel developed *in vitro* models may help to investigate the translocation of nanomaterials from the lung. We investigated the barrier function of the recently developed human lung cell lines CI-hAELVi and CI-huAEC. The cells were further exposed to CeO_2 NPs and ZnO NPs, and their suitability as *in vitro* models for toxicological investigations was proven. The obtained data were compared with data generated with the A549 cell line. Measurement of transepithelial resistance and immunohistochemical examination of tight junctions confirmed the formation of a functional barrier for both cell lines for submerged and air–liquid cultivation. For particle exposure, hAELVi and huAEC cells showed comparable results to A549 cells without losing the barrier function. CeO_2 NP exposure revealed no toxicity for all cell lines. In contrast, ZnO NPs was toxic for all cell lines at a concentration between 10–50 μg ml^{-1}. Due to the comparable results to A549 cells CI-hAELVi and CI-huAEC offer new opportunities to investigate nanoparticle cell interactions more realistic than recent 2D cell models.

Received 12th July 2019,
Accepted 14th October 2019

DOI: 10.1039/c9tx00179d

rsc.li/toxicology-research

Introduction

Due to the increased use of nanomaterials in consumer products, investigations into their safety and potential risks are key tasks.[1] Despite interspecies variations,[2–4] understanding any potential implications of nanoparticles (NPs) to human health are normally conducted in animal models.[5–13] However, based on the 3R (refine, reduce and replace) principle, the development of alternative testing methods is an important task.[14] For this, *in vitro* models can be helpful to answer mechanistic issues like *e.g.* cellular uptake[15] or genotoxicity.[16] Due to their small diameter NPs deposit deep into the lung.[17] Therefore, NPs are mainly taken up *via* inhalation[18] followed by a presumed deposition in the lower regions of the lung. Here, they come in contact with bronchial epithelia cells and pneumocyte type I & II cells. There are several human *in vitro* systems reported to assess adverse effects of NP cell-interactions in the lung. This includes bronchial cell lines, alveolar cell lines, different co-culture models as well as 3D models.[15,19–24] For instance, an increased oxidative stress and apoptosis of BEAS-2B cells after cerium dioxide (CeO_2) NPs exposure has been previously reported.[25] Another group used the BEAS-2B cells line as well as the bronchial 3D system MucilAir™ to investigate the toxicity of CeO_2 NPs. They found that the 3D model is more resistant to oxidative stress and DNA damage than simple cell cultures.[23] In contrast, there are also reports demonstrating protective functions of CeO_2 NPs which could be attributed to their antioxidant properties as studied in details in many published work.[14,26–29] For the alveolar region, A549 is the most frequently used cell line to study particle cell interactions. These cells are used either as a single monolayer or as co-culture in combination with other

German Federal Institute for Risk Assessment (BfR), Department of Chemical and Product Safety, Max-Dohrn-Straße 8-10, 10589 Berlin, Germany.
E-mail: lars.leibrock@bfr.bund.de

†Electronic supplementary information (ESI) available. See DOI: 10.1039/c9tx00179d

cell lines. For example, cytotoxicity of gold NPs in A549 cells was recently reported by inducing cell cycle arrest, oxidative stress and apoptosis.[30] A549 cells were also used to determine the toxicity of copper oxide NPs,[31] CeO_2 NPs[21] and zinc oxide (ZnO) NPs.[32] In addition to single cell lines that allow investigation of mechanistic aspects only, there are approaches to improve the used cell models to closely mimic the *in vivo* situation by using more sophisticated cell models such as co-cultures or 3D cell models. *E.g.* a co-culture system of A549, alveolar macrophages and dendritic cells was used to investigate the uptake of polystyrene particles. Most of the particles were found in macrophages but A549 and dendritic cells were also able to take up polystyrene particles.[33] Another conducted study even went one step further and developed a 3D co-culture model composed of A549, THP-1, mast cells (HMC-1) and endothelia cells (EA·hy 926). This tetraculture model was subsequently exposed to 50 nm SiO_2 rhodamin labeled NPs. SiO_2 NPs were only found in the macrophage like THP-1 cell line but not in A549 cells.[34] Despite the improved complexity of these models, a decisive disadvantage about barrier function still remains. The epithelial cells used in all alveolar models were A549 cells, a cell line which do not possess an intact barrier function.[35–37] Thus, they are not fully suited for studying the translocation of NPs. The NP translocation from the lung to secondary organs and tissues was previously described in the literature.[11,18,38] There are hints that NPs reach extrapulmonary structures *via* the blood stream circulation.[13,39] In 2006 rats were exposed to gold NPs. An uptake into epithelia cells and a translocation into the circulation occurred. However, an uptake by the endothelium has not been reported.[40] This raises the question how the NPs reached the blood stream. A translocation of NPs loaded macrophages into the lymph nodes was recently shown which could be one further mechanism.[8,41] In 2010 real-time intraoperative near-infrared fluorescence imaging was used to show that both mechanisms mentioned above may take place simultaneously.[42] However, the exact mechanism is not yet fully understood and subject of current research. Human alveolar *in vitro* models with intact barrier function would allow a closer estimation of the *in vivo* situation in terms of translocation of NPs. Hence, the aim of this work is to determine a cell model that reflects the *in vivo* situation more realistic than current used models and allows studying the translocation of NP under more realistic conditions. For this purpose, we investigated the recently developed human alveolar type I cell line CI-hAELVi (human Alveolar Epithelial Lentivirus immortalized) hereinafter stated as hAELVi.[43] hAELVi cells were characterized regarding their barrier function and the influence of CeO_2 NPs and ZnO NPs. Furthermore, the recently developed airway epithelia cell line CI-huAEC (human Airway Epithelial Cells),[44] a model of the lower respiratory tract, was examined for the same endpoints. The CI-huAEC cell line is hereinafter stated as huAEC. In addition, we evaluated the alveolar 3D model EpiAlveolar in terms of barrier function. The obtained data were compared to results achieved with A549 cells.

Experimental

Cell culture

A549 cells (ATCC cat. no.: CCL-185) were cultured in Dulbecco's Modified Eagle Medium (DMEM) supplemented with 10% fetal calf serum (FCS) (PAN-Biotech GmbH, Germany), 1% penicillin/streptomycin (PAN-Biotech GmbH, Germany) and 1% L-glutamine (PAN-Biotech GmbH, Germany). Cells were passaged two times per week.

CI-hAELVi (cat. no.: INS-CI-1015) and CI-huAEC (cat. no.: INS-CI-1011) cells were purchased from InSCREENeX GmbH (InSCREENeX GmbH, Germany). Both cell lines were cultured in CI-huAEC media supplemented with 1% penicillin/streptomycin (PAN-Biotech GmbH, Germany) and the CI-huAEC basal supplement provided by the manufacture (InSCREENeX GmbH, Germany). Cells were passaged two times per week.

EpiAlveolar. EpiAlveolar is a three dimensional human alveolar model and consists of lung epithelia cells, fibroblasts and endothelia cells.[45] EpiAlveolar was purchased from MatTek (MatTek Corporation, USA). Cultivation was conducted in accordance to the manufacturer's protocol. The medium was supplemented with 1% penicillin/streptomycin (PAN-Biotech GmbH, Germany).

Air–liquid cultivation. For trans-epithelial electrical resistance measurements, cells were seeded on transwell membranes and cultured for two days in submerse culture conditions (cat. no. 353180, Coring B.V., Netherland; 0.4 μm pore size, 1.12 cm^2) prior transferring them to the air–liquid phase. Therefore, the apical medium was removed and cells were washed once with PBS. Basal medium was changed every two days.

Trans-epithelial electrical resistance (TEER)

To determine the barrier properties of all lung models we conducted TEER measurements. Cell lines were seeded onto transwell membranes and cultured for two days under submerse conditions. Subsequently, the cells were divided in two groups and cultured for further 15 days: five membranes were further cultivated under submerge conditions (LL = liquid–liquid), six under air–liquid conditions (ALI). One insert without cells was used as background control. The background control was subtracted from the measured data. TEER measurements were performed each day with a Millicell-ERS system (Merk, Darmstadt, Germany) (STX2 electrode). Before measuring, cells were washed once with PBS. 1 ml fresh medium was added into the apical compartment and the cells were placed in the incubator for 1 h before measuring. In order to prevent the electrode being in contact with the plate wall, the membranes were transferred into a 6 well plate before starting the measurement. The 6-well plate was filled with 5 ml PBS per well. After measuring, apical medium was removed from ALI cultured inserts. The basolateral medium was changed every two days. For huAEC and hAELVi cells, membranes were coated with huAEC coating solution three hours before seeding. For A549, medium was added in the apical part of the membranes three hours before seeding. For EpiAlveolar, TEER

measurement was performed as mentioned above. Due to the shortened life span of EpiAlveolar, TEER was only monitored for eight days.

ZO-1 staining

For the optical characterization of tight junctions cells were grown on microscopic dishes (cat. no. D35-20-1-N, IBL Baustoff + Labor GmbH, Austria) or on transwell membranes (cat. no. 353180, Coring B.V., Netherland; 0.4 μm pore size). Seeding density was 50 000 cells. ZO-1 staining was performed after 14 days as described below. Cells were washed three times with PBS and fixed with 4% paraformaldehyde for 15 minutes at room temperature (RT). Afterwards, the samples were permeabilized with 0.2% Triton X-100 (Merck, KGaA, Darmstadt, Germany) for 10 minutes at RT. Subsequently, a blocking step with PBS containing 10% FCS was performed. The primary anti-ZO-1 antibody (cat. no. 402200, Fisher Scientific, Germany) was diluted 1 : 200 in PBS containing 1% FCS and incubated at 4 °C overnight. The secondary antibody (rabbit IgG, Alexa 488, cat. no. A-11034, Fisher Scientific, Germany) was diluted 1 : 400 in PBS containing 1% FCS and incubated for 1 h at RT. Then cells were washed with PBS three times and counterstained with Hoechst or DAPI (1 μg ml^{-1}). Samples were analyzed by a confocal laser scanning microscopy (LSM 700, Zeiss).

Growth curve and population doubling time

To assess the growth behavior of the different lung cells, 50 000 cells per well were seeded into a 6 well plate. Cells were harvested by trypsinization and counted in a haemocytometer by trypan blue dye exclusion after 24 h, 48 h, 72 h and 96 h. For each time point three wells were counted. The population doubling (PDT) time was determined based on the following equation:

$$\mathrm{PDT} = t/((\mathrm{Log}\ (\mathrm{C1}) - \mathrm{Log}(\mathrm{C2})/\mathrm{Log}(2))$$

With PDT = population doubling time (h), t = time point of harvesting (h), Log = 10 based Log, C1 = 1 cell number counted at harvesting time point, C2 = cell number initially seeded. PDT was calculated from the exponential growth phase (harvesting time points: 48, 72 and 96 h).

Particle characterization

Transmission electron microscope (TEM). *In situ* TEM observation of NPs was performed by a JEM-2100HR transmission electron microscopy (JEOL, Japan) operated at 100 kV equipped with an energy-dispersive X-ray (EDX) spectrum. For TEM analysis, the sample solution was drop coated on TEM copper grids (Agar Scientific, United Kingdom) from a 10 μg ml^{-1} particle solution and allowed to dry overnight under RT.

Dynamic light scattering (DLS)/zeta potential. Determination of the hydrodynamic diameter and the zeta potential were performed with a Zetasizer Nano ZS from Malvern (Malvern Inc., UK) in MilliQ water and in both cell culture media. For analysis, particle concentration for both materials was set to 50 μg ml^{-1}.

Nanoparticle tracking analysis (NTA). NTA was performed with a NanoSight LM20 (NanoSight, Amesbury, UK), equipped with a 632 nm laser, in MilliQ water and in both cell culture media. For analysis, particle concentration was set to 250 ng ml^{-1} and 10 μg ml^{-1} for CeO_2 and ZnO NPs, respectively. All measurements were performed at RT. The software used for recording and analyzing the data was NTA 2.3. All samples were measured for 60 seconds at five positions.

Particle toxicity

CeO_2 NPs (NM-212) was chosen as a well characterized granular biopersistent particle (GBP).[46] As zinc oxide is known as cytotoxic, it was chosen as positive particle control as well as soluble particle model. To determine adverse effects after submerged NP exposure, A549, huAEC and hAELVi cells were exposed to CeO_2 NPs and ZnO NPs for 24 h. CeO_2 NPs (JRC) and ZnO NPs were weighed and the particles were dispersed in MilliQ water to a final stock concentration of 2.5 mg ml^{-1}. Subsequently, the particle dispersion was sonicated for 5 minutes and 9 seconds (Sonoplus HD 220/UW 2200, Bandelin, Germany) to avoid particle aggregation. For all experiments, particles were freshly prepared. For cell exposure, particles were diluted in media to reach the final concentration. After exposure, cell viability, cytotoxicity and ROS production was determined using a WST-1 (water soluble tetrazolium-1), a lactatdehydrogenase (LDH) assay and a 2′,7′-dichlorofluorescin diacetate (DCFDA) assay, respectively.

Cell viability. After particle exposure, the supernatant was transferred in a new 96 well plate and subsequently used for LDH analysis (see below). Cells were rinsed with PBS and fresh medium containing 10% WST-1 reagent (Roche Diagnostics GmbH, Germany) was added into the well (100 μl). After 1 h incubation at 37 °C, 90 μl was transferred in a new 96 well plate and the absorbance was measured with a Tecan plate reader using wavelengths of 450 nm and 562 nm (reference wavelength). Six technical replicates were performed.

Cytotoxicity. After particle exposure a LDH assay was conducted to check for membrane damage after particle exposure. The assay was performed according to the manufactures instructions (Roche Diagnostics GmbH, Germany). In brief, LDH reagent was added to the supernatant and incubated for 15 minutes in dark at RT. Afterwards the absorbance was measured with a Tecan plate reader at 450 nm. Six technical replicates were performed.

Reactive oxygen species. The level of intracellular reactive oxygen species (ROS) generation was determined by using a DCFDA assay. After particle exposure, the cells were rinsed with PBS and DCFDA (80 μM in Medium) (Merck KGaA, Darmstadt, Germany) was added to the cells and incubated for 45 minutes at 37 °C. Afterwards, DCFDA was aspirated and the cells were rinsed again once with PBS. New medium and the positive control (*tert*-butyl hydroperoxide (TBHP 1/20 000 from stock solution), Merck KGaA, Darmstadt, Germany) was added to the cells and further incubated for 2 h. Subsequently, DCFDA fluorescence intensity was measured within a plate reader (Biotek Synergy™ HTX multi detection reader, BioTek

Instruments, Inc., Winooski, USA) at excitation and emission wavelengths of 485 and 528 nm, respectively. Three technical replicates were performed.

Statistical analysis

Data are shown as mean ± standard deviation. If not stated otherwise data represents three independent experiments. For statistical analysis a Mann–Whitney-*U*-Test was performed using Origin 9.1 software. $*P > 0.05$ was considered as significant; $**P > 0.01$; $***P > 0.001$.

Results and discussion

Most studies investigating the interactions of NPs and airway epithelia were carried out with bronchial and alveolar cells.[5,20,22,23,35,47,48] Unfortunately, the most commonly used alveolar model, the A549 cell line, possess a carcinogenic phenotype[49] and lacks in a proper barrier function.[35–37] Due to the regulation of paracellular substance transport, the barrier function is important for the systemic distribution of inhaled NPs.[50] Therefore, we investigated the recently developed cell line hAELVi, a model for type I pneumocytes,[43] as well as the new developed bronchial cell line huAEC[44] in respect of their capability to form an intact and functional cell–cell-barrier. In addition, we also analyzed the more complex 3D human alveolar model EpiAlveolar in respect of ongoing experiments regarding particle uptake and location/translocation. All received data were compared to the frequently used alveolar cell line A549.

Particle characterization

Compared to the widely used NANOGENOTOX protocol, we slightly modified the particle generation procedure (no bovine serum albumin, 10 ml dispersion volume instead of 6 ml and final concentration of 2.5 mg ml^{-1} instead of 2.56 mg ml^{-1}). Therefore, the NPs were again thoroughly characterized.[51] The particle size of CeO_2 and ZnO NPs were characterized using TEM, NTA and DLS measurements. In addition the zeta potential was determined. Particle size distributions can be found in ESI.† As shown in Table 1, both particle types exhibit a comparable size and zeta potential. As depicted in Fig. 1, ZnO particles were spherical whereas CeO_2 particles displayed a rather platelet shape. Furthermore, CeO_2 NPs showed strong agglomeration behavior compared to ZnO NPs. DLS and NTA were used to determine the hydrodynamic diameter of both materials. For CeO_2 NPs DLS revealed a slightly higher hydrodynamic diameter as NTA. This is mainly due to the fact that during the DLS measurements large particles contribute more to the diameter determination as NTA analysis. Nevertheless, our DLS results are consistent with data published by the manufacture JRC.[52] For ZnO NPs, DLS and NTA analysis displayed a similar size of about 250 nm. Electron microscopy analysis revealed no agglomeration for ZnO NPs whereas CeO_2 NPs showed a strong agglomeration behavior. Taken this into account, this explains the differences between the DLS and NTA data for CeO_2 NPs.

Table 1 NPs characterization of CeO_2 and ZnO

	NTA [nm]	DLS [nm]	Zeta potential [mV]
CeO_2 in MilliQ	164.1 ± 33.4	212.9 ± 20.6	22.6 ± 0.9
ZnO in MilliQ	265.6 ± 78.7	244.5 ± 4.6	25.5 ± 1.6
CeO_2 in DMEM	86.0 ± 43.7	1550.8 ± 157.1	−11.3 ± 0.8
ZnO in DMEM	227.9 ± 41.8	189.6 ± 10.3	−10.8 ± 0.6
CeO_2 in huAEC	146.5 ± 72.4	2159.7 ± 104.5	−10.8 ± 0.7
ZnO in huAEC	231.3 ± 57.0	337.1 ± 28.7	−9.5. ± 0.7

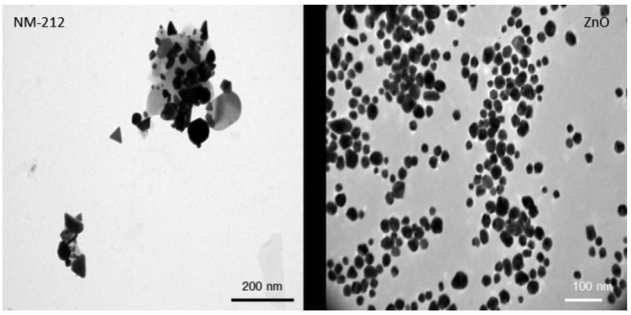

Fig. 1 NP characterization: Representative TEM pictures of CeO_2 (left) and ZnO (right) NPs. ZnO NPs show a spherical morphology and less agglomeration whereas CeO_2 NPs were more clustered and displayed a rather platelet like shape.

Characterization of lung cells: growth behavior

A549 cells are a well-established cell line in particle toxicity studies, whereas hAELVi and huAEC are relatively new cell lines. To the best of our knowledge, there are no data for huAEC cells published so far except the technique used to create them.[44] Therefore, we firstly investigated the growth behavior of the different cell lines to basically understand their growth behavior. Fig. 2 illustrates the growth curve of all lung epithelia cell lines we used. As expected, all of them showed an exponential growth pattern.[43,53] The population doubling time for all cell lines was 28 hours and is in accordance with previous A549 studies[53,54] indicating a similar growth behavior than standard cell lines used in this field.

Characterization of barrier function: transepithelial resistance measurement and tight junction staining

To characterize the barrier function of the different lung epithelia models, we performed TEER measurements and immunohistochemical analysis of the tight junction protein zonula occludens-1 (ZO-1).[55] Air–liquid cultivation resembles the *in vivo* situation closer than standard liquid–liquid cultivation.[56] Therefore, daily TEER experiments were performed under both culture conditions. As shown in Fig. 3 A hAELVi cells reached stable TEER values of about 1200–1500 Ω cm^2. A549 showed no barrier formation with resistance values between 30–50 Ω cm^2 which was expected as this cell line is known to lack functional tight junctions.[35–37] TEER data of the novel cell lines revealed a distinct difference between huAEC

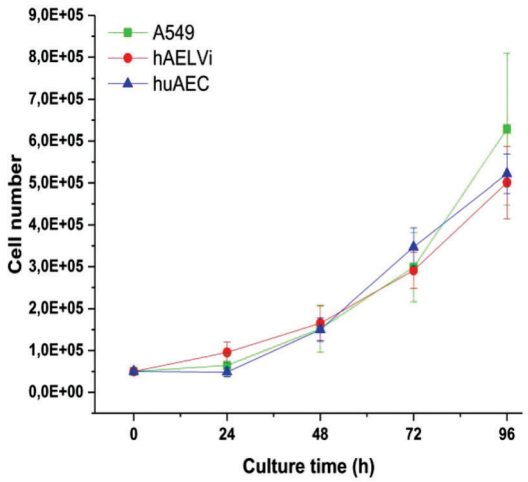

Fig. 2 Characterization of growth behavior: Growth curves of A549, hAELVi and huAEC cells show similar growth behavior for all cell types.

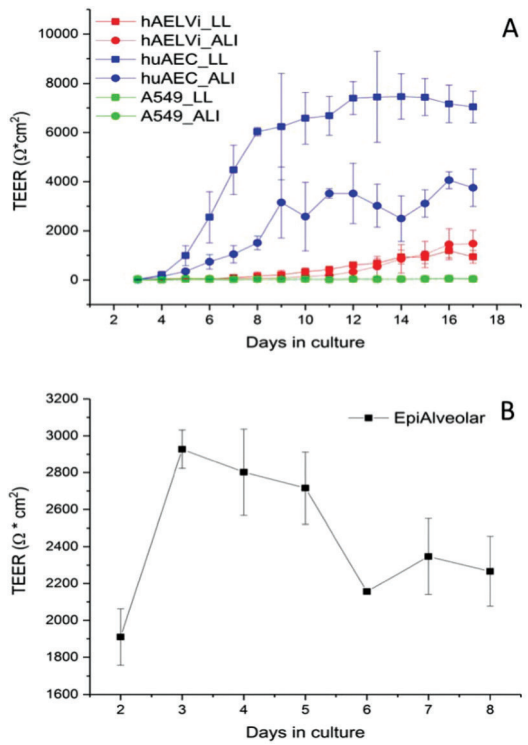

Fig. 3 Barrier function assessment of different lung epithelia cells *via* TEER measurement. (A) Evolution of TEER has been measured under liquid–liquid (LL) and air liquid (ALI) conditions in different cell models; n = 3. (B) Barrier function in the 3D model EpiAlveolar, n = 1 with 3 technical replicates. Data are shown as mean ± SD.

and hAELVi. hAELVi cells evolved a resistance of about 1500 Ω cm^2 which is slightly less as previously described.[43] This might be due to the fact that Kuehn and co-workers used corning transwell membranes and SAGM medium instead of huAEC medium and falcon transwell membranes.[36,43] In contrast to hAELVi cells, huAEC cells reached TEER values up to 3000–7000 Ω cm^2, dependent on the culture conditions. An influence of the culture conditions on the barrier function of hAELVi and A549 cells was not observed. Notably, huAEC cells developed barrier properties two fold higher in submerged culture compared with air–liquid interface, which we assume on account of enormous nutrient resource available in submerged culture.[57] Aside from the differences in the resistance values, the time to achieve high TEER values was also different between huAEC and hAELVi. For huAEC cells a strong barrier formation was detected at about day six to day eight, whereas hAELVi cell starts do display a tight barrier at about day 12. This is in consistent with the findings from Kuehn *et al.*[43] where hAELVi cells start to develop TEER values of approximately 1000 Ω cm^2 at day 12. While performing manually TEER measurements with an EVOM the position of the electrode is of crucial importance for the resistance value. This is one reason which may explain the large standard deviation for all cell lines achieved in our experiments. A study recently reported a lung on the chip system with integrated electrodes to investigate the resistance of primary humane airway epithelia cells for more than 60 days.[58] Using such devices might help to overcome such kind of handling issues. Furthermore with a chip design a direct influence of NPs on the barrier function could be studied over a long period of time. In addition to the 2D models the 3D model EpiAlveolar was analyzed over eight days (Fig. 3B). During this time, a strong increase in TEER data was observed during the first two days. Subsequently, a daily decrease in TEER values was seen. This behavior fits with the short life span of primary cells.[43] The achieved standard deviation was clearly smaller compared with the cell lines, which suggests good cell homogeneity in the model. Taken together, the measured TEER values of the new developed models are similar to primary bronchial and primary alveolar cells.[36] Thus, hAELVi, huAEC as well as EpiAlveolar resembles the *in vivo* situation vastly better than the common used A549 cell line regarding a functional cell barrier as well as a potential *in vitro* model to investigate particle translocation. hAELVi cells are known to express the tight junction protein ZO-1.[43,59] Due to the minimal amount of data about hAELVi, we decided to characterize them again in terms of growth and cell–cell-connections. Immunohistochemical staining of the tight junction protein ZO-1 was performed after 14 days. For huAEC cells there were no data reported so far about the barrier formation (TEER and tight junctions). To close this gap we analyzed huAEC cells concerning their barrier properties. As indicated on the TEER values we expected a ZO-1 expression in this cell line as well. hAELVi and huAEC cells developed a complete tight junction network (see Fig. 4). As already shown in the TEER data above, our immunofluorescence staining of ZO-1 confirmed the data of Kuehn *et al.*[43] ZO-1 staining for A549 cells as comparison was negative as diffused signal can be viewed in Fig. 4 and verified the absence of a barrier function in this cell line as it was found in the resistance measurement which is in agreement with the literature.[35–37] Unfortunately, direct ZO-1 staining of EpiAlveolar was not successful due to strong backscattering

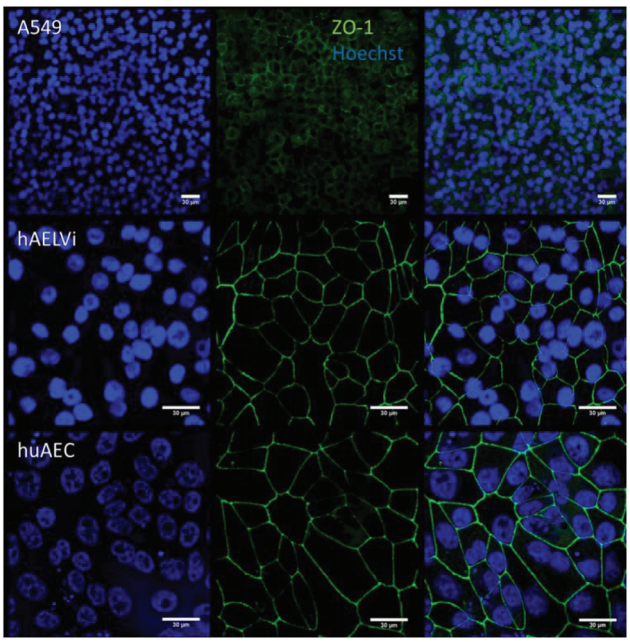

Fig. 4 Representative images of ZO-1 staining of lung cells after 14 days in culture. The first line represents nuclei staining in blue, 2nd line shows the tight junction protein ZO-1 in green and 3rd line displays the overlay of ZO-1 and nuclei.

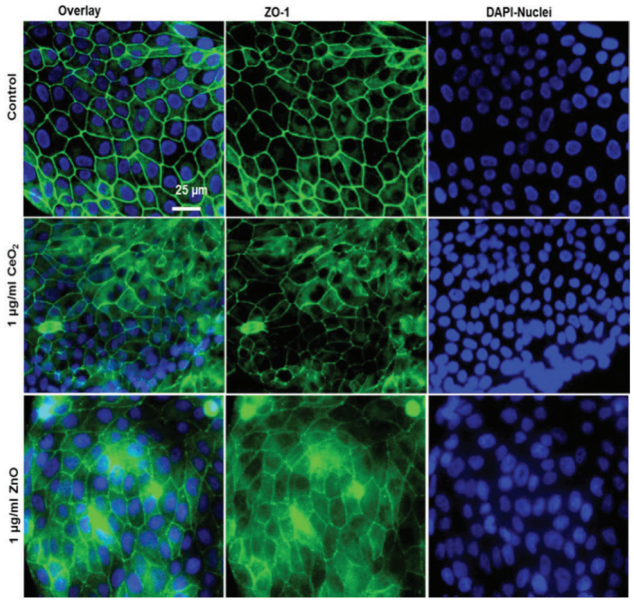

Fig. 5 Tight junction staining reveals no major effect of NPs exposure at submerged conditions to huAEC cells. The control group shown in upper row contains the overlay image of fluorescently labelled tight junction protein ZO-1 in green and nuclei in blue (DAPI) as first image, 2nd and 3rd images show ZO-1 and nuclei staining respectively. The middle row displays the overlay of ZO-1 in green and nuclei in blue after 24 h exposure to 1 µg ml^{-1} CeO_2 NPs as first image, 2nd and 3rd images show ZO-1 and nuclei staining respectively. The lower row shows the overlay of ZO-1 in green and nuclei in blue after 24 h exposure to 1 µg ml^{-1} ZnO NPs as first image, 2nd and 3rd images show ZO-1 and nuclei staining respectively.

from the membrane. However the exact mechanism of particle translocation is still not fully understand. In 2005 a possible mechanism was published by Rothen-Rutishauser and colleagues.[33] The authors exposed a co-culture model of A549 cells, macrophages and dendritic to polystyrene particles. The particles were added on top of the cell model without having contact to the dendritic cell layer. Particle localization revealed an uptake in all cell types, even in dendritic cells which have never been in direct contact to the particles. Further investigations showed particle localization in the pseudopods of the A549 cells. This might suggests a particle transfer between A549 and dendritic cells *via* the pseudopodia as possible translocation mechanism *in vitro*.[33] Nevertheless other mechanisms, for example an influence on the tight junction formation are also conceivable, as has been recently reported for some materials *e.g.* CeO_2 [60] or multi-walled carbon nanotubes.[48] Despite the increased permeability, a cytotoxic effect has not been observed for these materials.[48,60] This suggests that the absence of cytotoxicity is not an indication of an intact barrier function. In respect to particle translocation and a possible altered permeability, we next stained huAEC cells for ZO-1 expression in routine culture exposed to CeO_2 and ZnO NPs, under LL and ALI to ensure no damage on the tight junctions during particle exposure. As shown in Fig. 5 and 6, we did not observe any significant change in ZO-1 expression profile irrespective of exposure conditions. This means that the exposure conditions we used did not lead to an alteration of the tight junction barrier.

This allows for future investigations to deepen the understanding of the exact mechanism of particle translocation. Taken together, all new developed cell models we investigated showed a distinct barrier formation. Therefore, all examined models exhibit the potential to examine NP translocation *in vitro* more realistically than current models.

Particle toxicity and metabolic activity analysis

After characterization of the barrier properties, submerged cells were exposed to CeO_2 NPs and ZnO NPs. For both particles the influence on metabolic processes (WST-1) as well as the cytotoxicity (LDH) and the generation of ROS was investigated. As depicted in Fig. 7, CeO_2 NPs showed no adverse effect, neither in metabolic activity, nor in cytotoxicity for all three cell lines. In addition ROS production after CeO_2 NP exposure was either equal or slightly decreased compared to the control in all cell lines used. Ce is known to change its oxidation state.[27–29] Therefore, the decrease in ROS production could be due to the antioxidative properties of CeO_2 as it is known for other cell types.[26,28] Concerning the *in vitro* toxicity of CeO_2 NPs, contradicting studies have been reported. For example, Sauer and colleagues examined the toxicity of CeO_2 NPs to rat precision-cut lung slices. They reported no cytotoxicity between 10–100 µg ml^{-1}. 1000 µg ml^{-1} was needed to reach a cytotoxic effect. Nevertheless, inflammation already occurred at 100 µg ml^{-1}.[61] Similar results were reported from another study where different CeO_2 NPs were tested on several

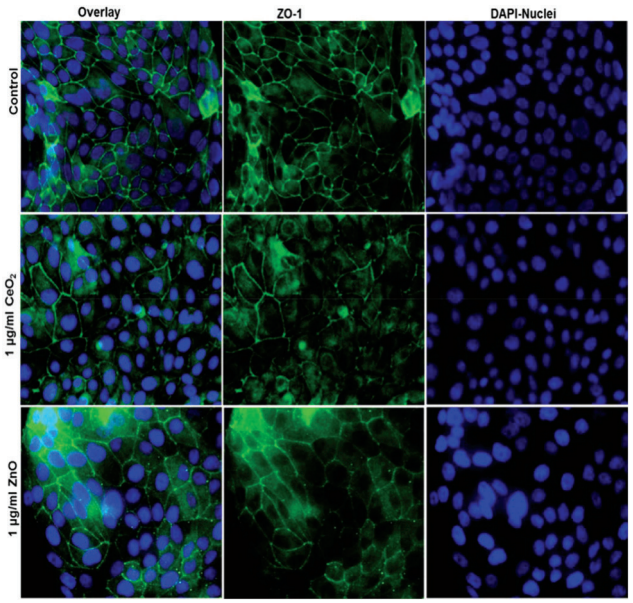

Fig. 6 Tight junction staining reveals no major effect of NPs exposure at liquid–liquid-interface (ALI) to huAEC cells The control group shown in upper row contains the overlay image of fluorescently labelled tight junction protein ZO-1 in green and nuclei in blue (DAPI) as first image, 2nd and 3rd images show ZO-1 and nuclei staining respectively. The middle row displays the overlay of ZO-1 in green and nuclei in blue after 24 h exposure to 1 µg ml^{-1} CeO_2 NPs as first image, 2nd and 3rd images show ZO-1 and nuclei staining respectively. The lower row shows the overlay of ZO-1 in green and nuclei in blue after 24 h exposure to 1 µg ml^{-1} ZnO NPs as first image, 2nd and 3rd images show ZO-1 and nuclei staining respectively.

different cell lines in submerse conditions. In a concentration range of 0.1–10 µg cm^{-2} neither a cytotoxic effect nor cell death was seen but an increase in oxidative stress occurred.[21] The generation of oxidative stress in BEAS-2B cells after CeO_2 NP exposure was also described.[19,25] Another study even revealed a protective function against oxidative stress of CeO_2 NPs for A549 after 24 hours exposure[62] which correlates with our findings (Fig. 7). These points to the fact that particle toxicity is cell type specific which was also reported by others.[19,30,63,64] Despite the broad applied concentration range in our study, the absence of an adverse/toxic effect from CeO_2 NPs exposure is not unexpected. Furthermore, our data are consistent with the findings of Shi *et al.* (2012) where the exposure of CeO_2 NPs up to 200 µg ml^{-1} showed no cytotoxicity on epithelia cells.[65] Zinc oxide NPs revealed a cytotoxicity at 10 µg ml^{-1} for all cells. For A549 cells a significant decrease in the metabolic activity was seen at 50 µg ml^{-1} whereas 10 µg ml^{-1} was sufficient to significantly decrease the metabolic activity of huAEC and hAELVi cells. Analysis of ROS production after ZnO exposure showed a strong decrease in ROS formation for hAELVi and huAEC cells at 10 µg ml^{-1}. For A549 cells such a decrease in ROS formation could not be observed. This difference might be due to the above mentioned cell line depended toxicity which needs further investigations to make a final conclusion. In contrast to CeO_2 NPs, ZnO NPs are known to be toxic to many different cell types as *e.g.* breast cancer cells[65] fibroblasts[66] and lung epithelia cells.[67] In more sophisticated systems like precision-cut lung slices, ZnO NPs induced strong toxicity based on tissue destruction as early as 10 µg ml^{-1}.[61] Therefore, our data fit with the literature and confirms a cytotoxicity of ZnO NP also for the two new cell lines hAELVi and huAEC. However, if ZnO NPs show a toxic effect on cells an increase in ROS production should be expected. This was not the case in our study. We assume that the cytotoxicity and the decrease in metabolic activity at 10 µg ml^{-1} might lead to a decrease in DCFDA uptake. This could explain the low ROS detection which especially takes place at 10 µg ml^{-1} which is similar to the detected cytotoxicity level. To sum up, WST-1, LDH and ROS assay showed similar results for all cell lines which indicates that the new developed cell lines have a similar behavior under particle exposure as the frequently used A549 cells without the disadvantages such as a carcinogenic phenotype[44,49] or the lack of a proper barrier function.[35–37] Therefore, they mimic the *in vivo* situation closer than previously used cell lines.

Model of choice

Here we reported several different lung epithelia models and showed their ability to form functional tight junction networks which is a prerequisite for a realistic *in vitro* model particularly when particle translocation is one of the challenged tasks. So, we were able to show that all new models tested here exhibit potential as pulmonary *in vitro* model to study NP cell interactions. After inhalation, most of the NPs deposit in the alveolar region.[17,68] Here they come in contact with pneumocytes type I, pneumocytes type II and alveolar macrophages; where type I cells cover about 95% of the alveolar surface.[69,70] Consequently, type I pneumocytes are the cell type which comes into the majority of contact with NPs after inhalation. Taking this into account, hAELVi are supposed to be the model of choice aside from primary cells as currently, they are the only model representing the type I human pneumocytes.[43] The bronchial epithelium is covered with a mucus layer. This respiratory mucus can promote to an agglomeration of NPs.[24] Since inhaled NPs follow the whole airway down to the alveolar region there is the possibility that some particles can deposit in the bronchial region. Thus, the huAEC cell line also represents a relevant model to study the toxicity of NPs. Moreover, huAEC cells reflect the human airway epithelium which enables microparticle studies with this cell line as well. Due to the fact that the culture conditions for huAEC and hAELVi cells are identical, further NP studies will include a co-culture model covering both cell types as well as the exposure of airborne NPs at the air–liquid interface with the aim to resemble the *in vivo* situation even closer.[56] In addition, the combination with macrophages will further increase the complexity of these models to allow more accurate *in vitro* particle translocation studies. To ensure a better representation of the *in vivo* situation different 3D models have been developed to study NP cell interaction and toxicological behavior. For instance, for the bronchial 3D model MucilAir™ a higher toxicity of CeO_2

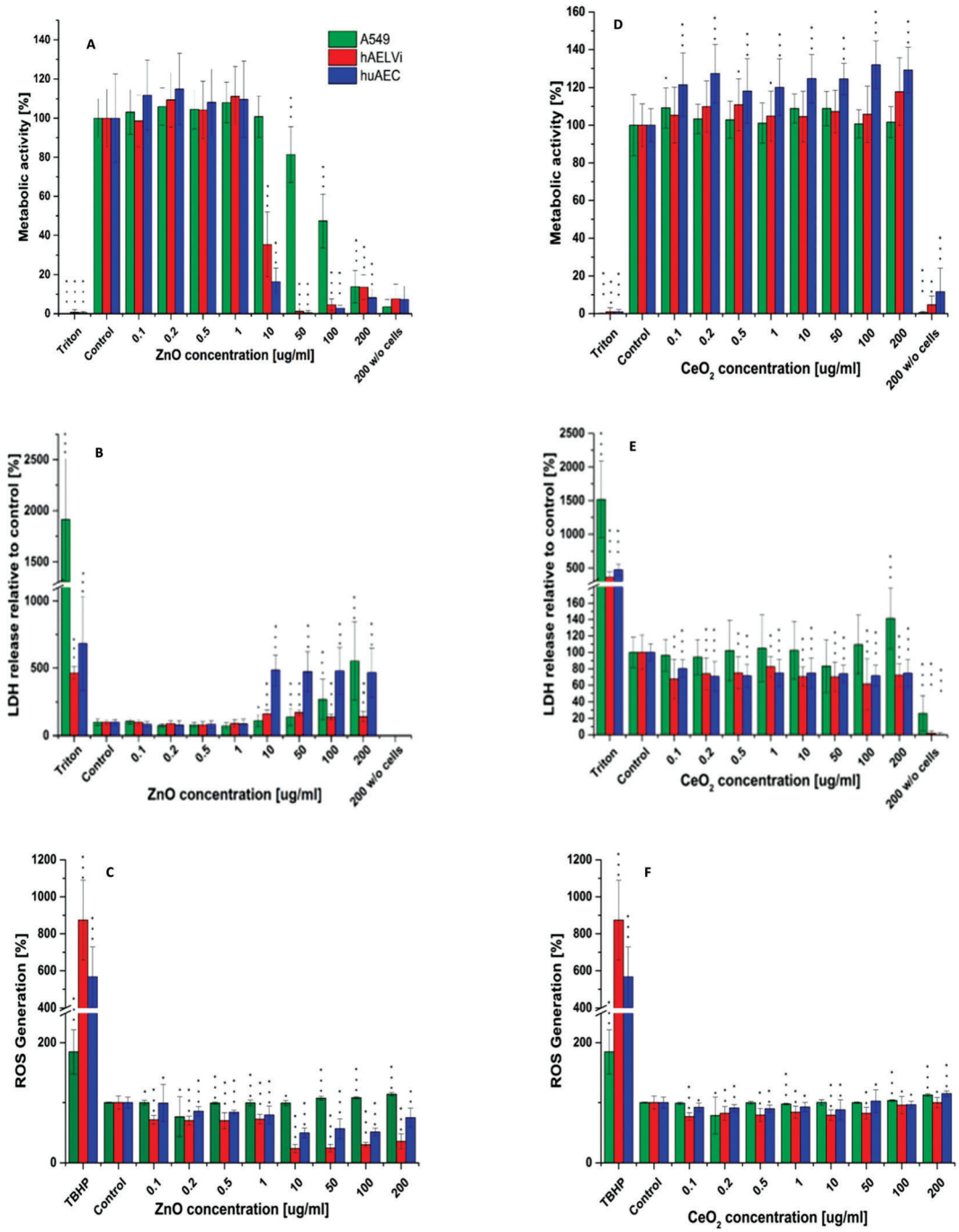

Fig. 7 Cytotoxicity, metabolic activity and ROS assay. Metabolic activity, LDH release and ROS generation after ZnO NP exposure (A–C) and CeO_2 NP exposure (C–D) in different lung epithelia cells. $n = 3$. Data are shown as mean ± SD. $^*p < 0.05$, $^{**}p < 0.01$ and $^{***}p > 0.001$ is compared to the respective control group.

NPs was reported compared to the bronchial cell line BEAS-2B in terms of oxidative stress and DNA damage.[23] The group of Brandenburger and colleagues used a co-culture model consisting of A549 cells, human blood monocyte derived macrophages and dendritic cells to investigate the effects of gold NPs.[15] Another group exposed A549 cells, BEAS-2B cells and the MucilAir™ model to CeO_2 NPs. They also reported a lower toxicity for the 3D model compared to a cellular monolayer.[24] In 2013, a tetraculture composed of A549, THP-1, HMC-1 and EA·hy 926 cells was developed to study the particle uptake of 50 nm SiO_2 NPs. The authors found that a particle uptake by macrophages[34] which is in contrast to the findings from another group where 1 μm polystyrene latex particles were found in A549 cells, macrophages and dendritic cells.[33] To the

best of our knowledge EpiAlveolar is the only commercial 3D human alveolar model so far that includes different cell types[45] which is not based on A549 cells (see above). Therefore we performed preliminary experiments to determine the barrier function with this newly developed model. Investigations regarding particle uptake and translocation will be tasks in the future. Our results showed that EpiAlveolar evolves a transepithelial resistances corresponding to primary alveolar cells *in vivo*.

Conclusions

Here we used the recently developed cell line hAELVi as an alveolar type I model[43] to investigate the effect of CeO_2 NPs and ZnO NPs. A549 cells were also exposed as they represent a human type II pneumocyte cell model. In addition, we examined the effect of these two nanomaterials on the novel developed airway epithelia cell line huAEC[44] and characterized them for the first time regarding their barrier function and applicability as *in vitro* model for NP toxicity investigations. Cultivation of lung epithelia cells at the air–liquid interface resembles the *in vivo* situation closer as submerge conditions.[56] Therefore, the barrier function was investigated under both conditions. Our data showed that both new cell lines evolve a proper tight junction network independent of if they are cultured under standard submerge conditions or at the air liquid interface. Submerged exposure to CeO_2 NPs and ZnO NPs revealed a strong toxicity for ZnO at 10 μg ml^{-1} for huAEC and hAELVi cells where A549 were only significantly affected at 50 μg ml^{-1}. CeO_2 NPs showed no toxicity in any of cell lines used. These results indicate that both new cell lines respond similarly to NP exposure as the frequently used A549 cell line. The tight junctions were not affected by the NPs. As hAELVi and huAEC cells developed tight junctions under submerge and air–liquid culture conditions they can also be used to examine the effect of airborne NPs. Taken together, these two new cell lines behave similar like the A549 cell line which is the most frequently used cell line in terms of pulmonary toxicity testing of NPs. Moreover, they can be cultivated at the air–liquid interface without losing their barrier function which makes them interesting for the future and might be helpful for various issues such as particle translocation of airborne nanomaterials or the development of respirable drugs.

Conflicts of interest

There are no conflicts to declare.

Acknowledgements

We thank Max Planck institute for solid state research, Stuttgart for transmission electron microscopy images.

Notes and references

1 Z. Ouyang, M. K. Mainali, N. Sinha, G. Strack, Y. Altundal, Y. Hao, T. A. Winningham, E. Sajo, J. Celli and W. Ngwa, Potential of using cerium oxide nanoparticles for protecting healthy tissue during accelerated partial breast irradiation (APBI), *Phys. Med.*, 2016, **32**, 631–635.

2 B. Asgharian, O. T. Price, M. Oldham, L. C. Chen, E. L. Saunders, T. Gordon, V. B. Mikheev, K. R. Minard and J. G. Teeguarden, Computational modeling of nanoscale and microscale particle deposition, retention and dosimetry in the mouse respiratory tract, *Inhalation Toxicol.*, 2014, **26**, 829–842.

3 J. S. Brown, W. E. Wilson and L. D. Grant, Dosimetric comparisons of particle deposition and retention in rats and humans, *Inhalation Toxicol.*, 2005, **17**, 355–385.

4 W. G. Kreyling, S. Andre, C. G. Collier, G. A. Ferron, H. Metivier and G. Schumann, Interspecies Comparison of Lung Clearance after Inhalation of Monodisperse, Solid Cobalt Oxide Aerosol-Particles, *J. Aerosol Sci.*, 1991, **22**, 509–535.

5 P. Demokritou, S. Gass, G. Pyrgiotakis, J. M. Cohen, W. Goldsmith, W. McKinney, D. Frazer, J. Ma, D. Schwegler-Berry, J. Brain and V. Castranova, An in vivo and in vitro toxicological characterisation of realistic nanoscale CeO2 inhalation exposures, *Nanotoxicology*, 2013, **7**, 1338–1350.

6 Y. Morimoto, H. Izumi, Y. Yoshiura, T. Tomonaga, T. Oyabu, T. Myojo, K. Kawai, K. Yatera, M. Shimada, M. Kubo, K. Yamamoto, S. Kitajima, E. Kuroda, K. Kawaguchi and T. Sasaki, Pulmonary toxicity of well-dispersed cerium oxide nanoparticles following intratracheal instillation and inhalation, *J. Nanopart. Res.*, 2015, **17**, 46.

7 W. G. Kreyling, S. Hirn, W. Moller, C. Schleh, A. Wenk, G. Celik, J. Lipka, M. Schaffler, N. Haberl, B. D. Johnston, R. Sperling, G. Schmid, U. Simon, W. J. Parak and M. Semmler-Behnke, Air-Blood Barrier Translocation of Tracheally Instilled Gold Nanoparticles Inversely Depends on Particle Size, *ACS Nano*, 2014, **8**, 222–233.

8 D. Schwotzer, H. Ernst, D. Schaudien, H. Kock, G. Pohlmann, C. Dasenbrock and O. Creutzenberg, Effects from a 90-day inhalation toxicity study with cerium oxide and barium sulfate nanoparticles in rats, *Part. Fibre Toxicol.*, 2017, **14**, 23.

9 N. V. Konduru, K. M. Murdaugh, A. Swami, R. J. Jimenez, T. C. Donaghey, P. Demokritou, J. D. Brain and R. M. Molina, Surface modification of zinc oxide nanoparticles with amorphous silica alters their fate in the circulation, *Nanotoxicology*, 2016, **10**, 720–727.

10 R. M. Molina, N. V. Konduru, H. Hirano, T. C. Donaghey, B. Adamo, B. Laurenzi, G. Pyrgiotakis and J. D. Brain, Pulmonary distribution of nanoceria: comparison of intratracheal, microspray instillation and dry powder insufflation, *Inhalation Toxicol.*, 2016, **28**, 550–560.

11 J. Keller, W. Wohlleben, L. Ma-Hock, V. Strauss, S. Groters, K. Kuttler, K. Wiench, C. Herden, G. Oberdorster, B. van

Ravenzwaay and R. Landsiedel, Time course of lung retention and toxicity of inhaled particles: short-term exposure to nano-Ceria, *Arch. Toxicol.*, 2014, **88**, 2033–2059.

12 J. G. Teeguarden, V. B. Mikheev, K. R. Minard, W. C. Forsythe, W. Wang, G. Sharma, N. Karin, S. C. Tilton, K. M. Waters, B. Asgharian, O. R. Price, J. G. Pounds and B. D. Thrall, Comparative iron oxide nanoparticle cellular dosimetry and response in mice by the inhalation and liquid cell culture exposure routes, *Part. Fibre Toxicol.*, 2014, **11**, 46.

13 D. S. Li, M. Morishita, J. G. Wagner, M. Fatouraie, M. Wooldridge, W. E. Eagle, J. Barres, U. Carlander, C. Emond and O. Jolliet, In vivo biodistribution and physiologically based pharmacokinetic modeling of inhaled fresh and aged cerium oxide nanoparticles in rats, *Part. Fibre Toxicol.*, 2016, **13**, 45.

14 M. Wiemann, A. Vennemann, U. G. Sauer, K. Wiench, L. Ma-Hock and R. Landsiedel, An in vitro alveolar macrophage assay for predicting the short-term inhalation toxicity of nanomaterials, *J. Nanobiotechnol.*, 2016, **14**, 16.

15 C. Brandenberger, B. Rothen-Rutishauser, C. Muhlfeld, O. Schmid, G. A. Ferron, K. L. Maier, P. Gehr and A. G. Lenz, Effects and uptake of gold nanoparticles deposited at the air-liquid interface of a human epithelial airway model, *Toxicol. Appl. Pharmacol.*, 2010, **242**, 56–65.

16 C. Barraud, C. Corbiere, I. Pottier, E. Estace, K. Blanchard, C. Logie, S. Lagadu, V. Keravec, D. Pottier, F. Dionnet, J. P. Morin, D. Preterre, V. Andre, C. Monteil and F. Sichel, Impact of after-treatment devices and biofuels on diesel exhausts genotoxicity in A549 cells exposed at air-liquid interface, *Toxicol. in Vitro*, 2017, **45**, 426–433.

17 G. Oberdorster, E. Oberdorster and J. Oberdorster, Nanotoxicology: an emerging discipline evolving from studies of ultrafine particles, *Environ. Health Perspect.*, 2005, **113**, 823–839.

18 R. M. Molina, N. V. Konduru, R. J. Jimenez, G. Pyrgiotakis, P. Demokritou, W. Wohlleben and J. D. Brain, Bioavailability, distribution and clearance of tracheally instilled, gavaged or injected cerium dioxide nanoparticles and ionic cerium, *Environ. Sci.: Nano*, 2014, **1**, 561–573.

19 E. J. Park, J. Choi, Y. K. Park and K. Park, Oxidative stress induced by cerium oxide nanoparticles in cultured BEAS-2B cells, *Toxicology*, 2008, **245**, 90–100.

20 K. Fytianos, S. Chortarea, L. Rodriguez-Lorenzo, F. Blank, C. von Garnier, A. Petri-Fink and B. Rothen-Rutishauser, Aerosol Delivery of Functionalized Gold Nanoparticles Target and Activate Dendritic Cells in a 3D Lung Cellular Model, *ACS Nano*, 2017, **11**, 375–383.

21 A. Kroll, C. Dierker, C. Rommel, D. Hahn, W. Wohlleben, C. Schulze-Isfort, C. Gobbert, M. Voetz, F. Hardinghaus and J. Schnekenburger, Cytotoxicity screening of 23 engineered nanomaterials using a test matrix of ten cell lines and three different assays, *Part. Fibre Toxicol.*, 2011, **8**, 9.

22 T. Loret, E. Peyret, M. Dubreuil, O. Aguerre-Chariol, C. Bressot, O. le Bihan, T. Amodeo, B. Trouiller, A. Braun, C. Egles and G. Lacroix, Air-liquid interface exposure to aerosols of poorly soluble nanomaterials induces different biological activation levels compared to exposure to suspensions, *Part. Fibre Toxicol.*, 2016, **13**, 58.

23 I. M. Kooter, M. Gröllers-Mulderij, M. Steenhof, E. Duistermaat, F. A. A. van Acker, Y. C. M. Staal, P. C. Tromp, E. Schoen, C. F. Kuper and E. van Someren, Cellular Effects in an In Vitro Human 3D Cellular Airway Model and A549/BEAS-2B In Vitro Cell Cultures Following Air Exposure to Cerium Oxide Particles at an Air–Liquid Interface, *Appl. In Vitro Toxicol.*, 2016, **2**, 56–66.

24 C. F. Kuper, M. Grollers-Mulderij, T. Maarschalkerweerd, N. M. M. Meulendijks, A. Reus, F. van Acker, E. K. Zondervan-van den Seuken, M. E. L. Wouters, S. Bijlsma and I. M. Kooter, Toxicity assessment of aggregated/agglomerated cerium oxide nanoparticles in an in vitro 3D airway model: The influence of mucociliary clearance, *Toxicol. in Vitro*, 2015, **29**, 389–397.

25 H. J. Eom and J. Choi, Oxidative stress of CeO2 nanoparticles via p38-Nrf-2 signaling pathway in human bronchial epithelial cell, Beas-2B, *Toxicol. Lett.*, 2009, **187**, 77–83.

26 R. Singh and S. Singh, Redox-dependent catalase mimetic cerium oxide-based nanozyme protect human hepatic cells from 3-AT induced acatalasemia, *Colloids Surf., B*, 2019, **175**, 625–635.

27 S. Singh, Cerium oxide based nanozymes: Redox phenomenon at biointerfaces, *Biointerphases*, 2016, **11**, 4.

28 R. Singh, A. S. Karakoti, W. Self, S. Seal and S. Singh, Redox-Sensitive Cerium Oxide Nanoparticles Protect Human Keratinocytes from Oxidative Stress Induced by Glutathione Depletion, *Langmuir*, 2016, **32**, 12202–12211.

29 T. Pirmohamed, J. M. Dowding, S. Singh, B. Wasserman, E. Heckert, A. S. Karakoti, J. E. S. King, S. Seal and W. T. Self, Nanoceria exhibit redox state-dependent catalase mimetic activity, *Chem. Commun.*, 2010, **46**, 2736–2738.

30 V. Ramalingam, S. Revathidevi, T. Shanmuganayagam, L. Muthulakshmi and R. Rajaram, Biogenic gold nanoparticles induce cell cycle arrest through oxidative stress and sensitize mitochondrial membranes in A549 lung cancer cells, *RSC Adv.*, 2016, **6**, 20598–20608.

31 X. F. Jing, J. H. Park, T. M. Peters and P. S. Thorne, Toxicity of copper oxide nanoparticles in lung epithelial cells exposed at the air-liquid interface compared with in vivo assessment, *Toxicol. in Vitro*, 2015, **29**, 502–511.

32 A. G. Lenz, E. Karg, E. Brendel, H. Hinze-Heyn, K. L. Maier, O. Eickelberg, T. Stoeger and O. Schmid, Inflammatory and oxidative stress responses of an alveolar epithelial cell line to airborne zinc oxide nanoparticles at the air-liquid interface: a comparison with conventional, submerged cell-culture conditions, *BioMed Res. Int.*, 2013, **2013**, 652632.

33 B. M. Rothen-Rutishauser, S. G. Kiama and P. Gehr, A three-dimensional cellular model of the human respiratory tract to study the interaction with particles, *Am. J. Respir. Cell Mol. Biol.*, 2005, **32**, 281–289.

34 S. G. Klein, T. Serchi, L. Hoffmann, B. Blomeke and A. C. Gutleb, An improved 3D tetraculture system mimick-

ing the cellular organisation at the alveolar barrier to study the potential toxic effects of particles on the lung, *Part. Fibre Toxicol.*, 2013, **10**, 31.

35 I. George, S. Vranic, S. Boland, A. Courtois and A. Baeza-Squiban, Development of an in vitro model of human bronchial epithelial barrier to study nanoparticle translocation, *Toxicol. in Vitro*, 2015, **29**, 51–58.

36 B. Srinivasan, A. R. Kolli, M. B. Esch, H. E. Abaci, M. L. Shuler and J. J. Hickman, TEER Measurement Techniques for In Vitro Barrier Model Systems, *JALA*, 2015, **20**, 107–126.

37 H. L. Winton, H. Wan, M. B. Cannell, D. C. Gruenert, P. J. Thompson, D. R. Garrod, G. A. Stewart and C. Robinson, Cell lines of pulmonary and non-pulmonary origin as tools to study the effects of house dust mite proteinases on the regulation of epithelial permeability, *Clin. Exp. Allergy*, 1998, **28**, 1273–1285.

38 N. V. Konduru, K. M. Murdaugh, G. A. Sotiriou, T. C. Donaghey, P. Demokritou, J. D. Brain and R. M. Molina, Bioavailability, distribution and clearance of tracheally-instilled and gavaged uncoated or silica-coated zinc oxide nanoparticles, *Part. Fibre Toxicol.*, 2014, **11**, 44.

39 C. Schleh, U. Holzwarth, S. Hirn, A. Wenk, F. Simonelli, M. Schaffler, W. Moller, N. Gibson and W. G. Kreyling, Biodistribution of Inhaled Gold Nanoparticles in Mice and the Influence of Surfactant Protein D, *J. Aerosol Med. Pulm. Drug Delivery*, 2013, **26**, 24–30.

40 S. Takenaka, E. Karg, W. G. Kreyling, B. Lentner, W. Moller, M. Behnke-Semmler, L. Jennen, A. Walch, B. Michalke, P. Schramel, J. Heyder and H. Schulz, Distribution pattern of inhaled ultrafine gold particles in the rat lung, *Inhalation Toxicol.*, 2006, **18**, 733–740.

41 N. V. Konduru, R. M. Molina, A. Swami, F. Damiani, G. Pyrgiotakis, P. Lin, P. Andreozzi, T. C. Donaghey, P. Demokritou, S. Krol, W. Kreyling and J. D. Brain, Protein corona: implications for nanoparticle interactions with pulmonary cells, *Part. Fibre Toxicol.*, 2017, **14**, 42.

42 H. S. Choi, Y. Ashitate, J. H. Lee, S. H. Kim, A. Matsui, N. Insin, M. G. Bawendi, M. Semmler-Behnke, J. V. Frangioni and A. Tsuda, Rapid translocation of nanoparticles from the lung airspaces to the body, *Nat. Biotechnol.*, 2010, **28**, 1300–1303.

43 A. Kuehn, S. Kletting, C. D. Carvalho-Wodarz, U. Repnik, G. Griffiths, U. Fischer, E. Meese, H. Huwer, D. Wirth, T. May, N. Schneider-Daum and C. M. Lehr, Human Alveolar Epithelial Cells Expressing Tight Junctions to Model the Air-Blood Barrier, *Altex-Alternatives to Animal Experimentation*, 2016, **33**, 251–260.

44 C. Lipps, F. Klein, T. Wahlicht, V. Seiffert, M. Butueva, J. Zauers, T. Truschel, M. Luckner, M. Koster, R. MacLeod, J. Pezoldt, J. Huhn, Q. G. Yuan, P. P. Muller, H. Kempf, R. Zweigerdt, O. Dittrich-Breiholz, T. Pufe, R. Beckmann, W. Drescher, J. Riancho, C. Sanudo, T. Korff, B. Opalka, V. Rebmann, J. R. Gothert, P. M. Alves, M. Ott, R. Schucht, H. Hauser, D. Wirth and T. May, Expansion of functional personalized cells with specific transgene combinations, *Nat. Commun.*, 2018, **9**, 994.

45 G. Jackson, C. Mankus, J. Oldach, M. Child, M. Spratt, H. Kandarova, S. Ayehunie and P. Hayden, A triple cell co-culture model of the air–blood barrier reconstructed from primary human cells, *Toxicol. Lett.*, 2013, **221**, S138.

46 P. Laux, C. Riebeling, A. M. Booth, J. D. Brain, J. Brunner, C. Cerrillo, O. Creutzenberg, I. Estrela-Lopis, T. Gebel, G. Johanson, H. Jungnickel, H. Kock, J. Tentschert, A. Tlili, A. Schaffer, A. Sips, R. A. Yokel and A. Luch, Biokinetics of Nanomaterials: the Role of Biopersistence, *NanoImpact*, 2017, **6**, 69–80.

47 C. R. Svensson, S. S. Ameer, L. Ludvigsson, N. Ali, A. Alhamdow, M. E. Messing, J. Pagels, A. Gudmundsson, M. Bohgard, E. Sanfins, M. Karedal, K. Broberg and J. Rissler, Validation of an air-liquid interface toxicological set-up using Cu, Pd, and Ag well-characterized nanostructured aggregates and spheres, *J. Nanopart. Res.*, 2016, **18**, 86.

48 R. Derk, D. C. Davidson, A. Manke, T. A. Stueckle, Y. Rojanasakul and L. Wang, Potential in vitro model for testing the effect of exposure to nanoparticles on the lung alveolar epithelial barrier, *Sens. Biosensing Res.*, 2015, **3**, 38–45.

49 D. J. Giard, S. A. Aaronson, G. J. Todaro, P. Arnstein, J. H. Kersey, H. Dosik and W. P. Parks, *In vitro* Cultivation of Human Tumors - Establishment of Cell Lines Derived from a Series of Solid Tumors, *J. Natl. Cancer Inst.*, 1973, **51**, 1417–1423.

50 D. W. Powell, Barrier function of epithelia, *Am. J. Physiol.*, 1981, **241**, G275–G288.

51 N. B. Hartmann, K. A. Jensen, A. Baun, K. Rasmussen, H. Rauscher, R. Tantra, D. Cupi, D. Gilliland, F. Pianella and J. M. Riego Sintes, Techniques and Protocols for Dispersing Nanoparticle Powders in Aqueous Media-Is there a Rationale for Harmonization?, *J. Toxicol. Environ. Health, Part B*, 2015, **18**, 299–326.

52 C. Singh, S. Friedrichs, G. Ceccone, N. Gibson, K. A. Jensen, M. Levin, H. G. Infante, D. Carlander and K. Rasmussen, *Cerium Dioxide, NM-211, NM-212, NM-213. Characterisation and test item preparation*, 2014.

53 S. B. Assanga-Iloki, A. A. Gil-Salido, L. M. Lewis-Luján, A. Rosas-Durazo, A. L. Acosta-Silva, E. G. Rivera-Castañeda and J. L. Rubio-Pino, Cell growth curves for different cell lines and their relationship with biological activities, *Int. J. Biotechnol. Mol. Biol. Res.*, 2013, **4**, 60–70.

54 R. Limame, A. Wouters, B. Pauwels, E. Fransen, M. Peeters, F. Lardon, O. De Wever and P. Pauwels, Comparative Analysis of Dynamic Cell Viability, Migration and Invasion Assessments by Novel Real-Time Technology and Classic Endpoint Assays, *PLoS One*, 2012, **7**, 10.

55 S. Y. Xu, X. D. Xue, K. You and J. H. Fu, Caveolin-1 regulates the expression of tight junction proteins during hyperoxia-induced pulmonary epithelial barrier breakdown, *Respir. Res.*, 2016, **17**, 50.

56 A. A. Pezzulo, T. D. Starner, T. E. Scheetz, G. L. Traver, A. E. Tilley, B. G. Harvey, R. G. Crystal, P. B. McCray and

J. Zabner, The air-liquid interface and use of primary cell cultures are important to recapitulate the transcriptional profile of in vivo airway epithelia, *Am. J. Physiol.: Lung Cell. Mol. Physiol.*, 2011, **300**, L25–L31.

57 A. Vikram Singh, T. Gharat, M. Batuwangala, B. W. Park, T. Endlein and M. Sitti, Three-dimensional patterning in biomedicine: Importance and applications in neuropharmacology, *J. Biomed. Mater. Res., Part B*, 2018, **106**, 1369–1382.

58 O. Y. F. Henry, R. Villenave, M. J. Cronce, W. D. Leineweber, M. A. Benz and D. E. Ingber, Organs-on-chips with integrated electrodes for trans-epithelial electrical resistance (TEER) measurements of human epithelial barrier function, *Lab Chip*, 2017, **17**, 2264–2271.

59 S. Kletting, S. Barthold, U. Repnik, G. Griffiths, B. Loretz, N. Schneider-Daum, C. de Souza Carvalho-Wodarz and C. M. Lehr, Co-culture of human alveolar epithelial (hAELVi) and macrophage (THP-1) cell lines, *ALTEX*, 2018, **35**, 211–222.

60 B. Rothen-Rutishauser, R. N. Grass, F. Blank, L. K. Limbach, C. Muehlfeld, C. Brandenberger, D. O. Raemy, P. Gehr and W. J. Stark, Direct Combination of Nanoparticle Fabrication and Exposure to Lung Cell Cultures in a Closed Setup as a Method To Simulate Accidental Nanoparticle Exposure of Humans, *Environ. Sci. Technol.*, 2009, **43**, 2634–2640.

61 U. G. Sauer, S. Vogel, A. Aumann, A. Hess, S. N. Kolle, L. Ma-Hock, W. Wohlleben, M. Dammann, V. Strauss, S. Treumann, S. Groters, K. Wiench, B. van Ravenzwaay and R. Landsiedel, Applicability of rat precision-cut lung slices in evaluating nanomaterial cytotoxicity, apoptosis, oxidative stress, and inflammation, *Toxicol. Appl. Pharmacol.*, 2014, **276**, 1–20.

62 L. De Marzi, A. Monaco, J. De Lapuente, D. Ramos, M. Borras, M. Di Gioacchino, S. Santucci and A. Poma, Cytotoxicity and Genotoxicity of Ceria Nanoparticles on Different Cell Lines in Vitro, *Int. J. Mol. Sci.*, 2013, **14**, 3065–3077.

63 A. M. Studer, L. K. Limbach, L. Van Duc, F. Krumeich, E. K. Athanassiou, L. C. Gerber, H. Moch and W. J. Stark, Nanoparticle cytotoxicity depends on intracellular solubility: Comparison of stabilized copper metal and degradable copper oxide nanoparticles, *Toxicol. Lett.*, 2010, **197**, 169–174.

64 B. L'Azou, J. Jorly, D. On, E. Sellier, F. Moisan, J. Fleury-Feith, J. Cambar, P. Brochard and C. Ohayon-Courtes, In vitro effects of nanoparticles on renal cells, *Part. Fibre Toxicol.*, 2008, **5**, 22.

65 J. W. Shi, H. L. Karlsson, K. Johansson, V. Gogvadze, L. S. Xiao, J. T. Li, T. Burks, A. Garcia-Bennett, A. Uheida, M. Muhammed, S. Mathur, R. Morgenstern, V. E. Kagan and B. Fadeel, Microsomal Glutathione Transferase 1 Protects Against Toxicity Induced by Silica Nanoparticles but Not by Zinc Oxide Nanoparticles, *ACS Nano*, 2012, **6**, 1925–1938.

66 X. Q. Zhang, L. H. Yin, M. Tang and Y. P. Pu, ZnO, TiO2, SiO2, and Al2O3 Nanoparticles-induced Toxic Effects on Human Fetal Lung Fibroblasts, *Biomed. Environ. Sci.*, 2011, **24**, 661–669.

67 I. S. Kim, M. Baek and S. J. Choi, Comparative Cytotoxicity of Al2O3, CeO2, TiO2 and ZnO Nanoparticles to Human Lung Cells, *J. Nanosci. Nanotechnol.*, 2010, **10**, 3453–3458.

68 M. Geiser and W. G. Kreyling, Deposition and biokinetics of inhaled nanoparticles, *Part. Fibre Toxicol.*, 2010, **7**, 2.

69 K. Luyts, D. Napierska, D. Dinsdale, S. G. Klein, T. Serchi and P. H. M. Hoet, A coculture model of the lung-blood barrier: The role of activated phagocytic cells, *Toxicol. in Vitro*, 2015, **29**, 234–241.

70 J. D. Crapo, B. E. Barry, P. Gehr, M. Bachofen and E. R. Weibel, Cell number and cell characteristics of the normal human lung, *Am. Rev. Respir. Dis.*, 1982, **126**, 332–337.

4. Discussion:

With regard to safety evaluation of chemicals, the EU adopted the REACH directive (EG 1907/2006) in 2006, which dictate that all existing chemicals on the EU market or chemical products with a volume of one ton per year or more that newly enter the EU market need to be registered [2]. By definition, NMs are covered by the REACH regulation [4] and animal studies are unfortunately still considered the gold standard for evaluating adverse or toxic effects of NMs to accomplish the REACH restrictions [143]. Developing alternative methods to reduce or even ultimately replace such *in vivo* experiments is therefore an ongoing research task. To get closer to this objective, standardization of *in vitro* methods is necessary as a first step in this development. This was the starting point of this work.

4.1 Characterization of an ALI system as a first step in standardization an *in vitro* method to assess nanoparticle toxicity

Although much *in vitro* research has been done in recent years and it is widely accepted that ALI systems are more in accordance with the *in vivo* situation as liquid exposure, there is still no standardization regarding toxicity assessment of NPs *in vitro* on a regulatory level equivalent to *in vivo* based tests like different OECD guidelines [70,176-178]. This missing standardization is due to several facts. One is that many different cellular systems are on the market. Although such variety is often an advantage, the systems are frequently only validated in house and a full characterization for the public and scientific community is not available. In addition,

reports often miss important experimental parameters like distance of aerosol entrance to the cells, the relative humidity of the aerosol or the aerosol temperature [153,164]. This not only strongly impairs the comparability of different ALI exposure setups but also hinders the standardization between data despite many recent ALI studies.

C&E (cause-and-effect) approaches help to identify major causes of a problem by visualizing them in a fishbone diagram illustrating their impact on the problem [179]. Using a C&E approach, we succeeded in characterizing a commercially available widely used ALI system based on the toxicological important parameter cell viability and developed a method to improve the robustness of current data analysis [180].

One key factor for potential regulatory application of ALI methods is their reliability. This can be proved by interlaboratory reproducibility, repeatability and robustness. Our data evaluation approach allows the analysis of day-by-day variances in cell viability measurements and is able to identify outliers easily. Therefore, this concept describes a rather uncommon analytical approach compared to those usually used in ALI studies where mostly only mean values and standard division are reported and detailed descriptions on how those data were acquired is missing. Thus, our design makes data analysis more robust to enhance reliability in these methods for regulatory purposes and research.

By using this C&E analysis, we identified four parameters; relative humidity, aerosol air temperature, flow rate and CO_2 concentration in the aerosol that are crucial for the reproducibility of cell viability under ALI exposure. Experimental parametric optimization of the system based on these parameters confirmed the estimated findings from C&E approach. All identified parameters showed a significant influence on the cell viability during ALI exposure. Those findings are partly in agreement with

recent literature where relative humidity, aerosol flow temperature and flow rate are described as important parameters influencing cell viability in ALI systems [136,181]. However, C&E analysis together the subsequent laboratory investigations revealed CO_2 supply as an additional important parameter concerning cell viability in ALI studies, especially for extended exposure durations [180]. Based on these results, an optimized exposure setup could be developed that enables cell cultures to be exposed in an ALI system under ideal environment conditions, similar to *in vivo*. This also helps to close the gap between *in vivo* and *in vitro* exposure conditions further. Therefore, it can be stated that C&E analysis is a useful tool to identify important parameters for assay characterization, which is a requirement for potential regulation applications.

4.2 Detection of CeO_2 nanoparticle dosage and their toxicity under low dose conditions

Concerning the determination of nanotoxicology and proper risk assessment of NPs, relevant exposure scenarios have to be considered. This is unfortunately not often the case in inhalation nanotoxicity, as robust data of NP air concentrations are still missing for most NPs. Acute short-term studies are commonly applied to assess the toxicity of NMs [44,98]. However, more realistic low dose NP studies gained more and more attention in the last years in both, *in vitro* [182,183] and *in vivo* [184,185]. Thus, the question of dose response relationship as an important parameter describing NP toxicity has to be reconsidered [108,186,187]. Quantitative measurements are needed to properly determine the deposited dose, but often only an estimate is taken. Instead of estimating the deposited dose by *in silico* methods or microscopy, we decided to perform a rather cost and time intense mass

spectrometry analysis. This allows an accurate quantitative determination of the intra- and extracellular CeO_2 NPs dosage used in this study, which cannot be achieved with other techniques like the ones mentioned above [180]. Furthermore, this analysis enables the investigation of non-fluorescent NPs like CeO_2 as well as their detection in a part per trillion range. When using low dose scenarios, as it was done in this study, the expected intra- and extracellularly (applied dosage) is quite low and typically not detectable with standard methods like a microbalance sensor [188]. Combining ICP-MS and TOF-SIMS allowed us to distinguish between intracellular (~ 4.5 ng/cm^2 per hour) and extracellular (~ 4 ng/cm^2 per hour) CeO_2 NPs, which depicts the dose response relationships more detailed. With this approach toxicological effects can be linked to originate either from intracellular or extracellular dose or a combination of both [180].

Cell viability and cell membrane integrity are major biomarkers in *in vitro* nanotoxicology and have been investigated extensively over the years [165,189,190]. Assays investigating these endpoints only represent an overall mean value of a cell population. Low dose exposure scenarios create significant lower dosages as acute short-term or subacute long-term studies. Typical endpoint measurements based on metabolic activity, membrane damage or oxidative stress might not detect any changes at these low dosages [180]. Nevertheless, these low concentrations can result in cellular changes on a molecular level. With this in mind, we next analyzed the membrane composition of lung epithelia cells after low dosage ALI exposure via TOF-SIMS. This technique allows the investigation of a single cell instead of whole cell population and the assessment of metabolic changes. The analysis of the gained data revealed that even at very low NP dosage of ~4.5 ng/cm^2 per hour the composition of several cell membrane lipids including phosphatidylcholines,

phosphatidylethanolamines and the sphingolipid ceramide were changed [180]. Membrane lipids accomplish multiple tasks, ranging from membrane fluidity to intracellular signaling cascades [191,192].

Especially the sphingolipid ceramide is known as a second messenger and it is involved in proliferation, inflammation as well as apoptosis [193]. A Chinese group recently reported a concentration dependent apoptosis induced by exogenous ceramide addition due to Ca^{2+} homeostasis disruption of the endoplasmic reticulum in human cancer cells [192]. Our TOF-SIMS data revealed reduced levels in different phospholipids including ceramide [180]. Therefore, a reduced apoptosis might theoretically be possible. Whether this is the case or not needs further investigation in following projects.

Taken together, the results clearly indicate that minimal CeO_2 NPs concentrations can affect the cell membrane structure of lung epithelia on a molecular level.

4.3 Comparing ALI data to *in vivo* data

The comparability of *in vitro* to *in vivo* is often considered insufficient in nanotoxicology. Sayes and coworkers investigated the toxicity of different micro- and nanoparticles *in vitro* and *in vivo* and reported only little comparison [150]. However, *in vitro* experiments were conducted under submerse conditions, whereas *in vivo* experiments were performed as instillation exposure. Both applications are limited in depicting realistic NPs inhalation toxicity [150]. The group of Demokritou compared the toxicity of CeO_2 NPs under submerse conditions to an inhalation exposure setup with rats [118]. They also reported significant discrepancies between *in vitro* and *in vivo*, which might result from protein corona formation around the NPs [118].

However, both doses, *in vitro* and in *vivo*, were only estimated to be similar. Quantitative data about tissue or cell burden was missing in this study, which makes it difficult to compare the results [118]. To overcome possible impact effects of the protein corona, Jing et al. recently compared the toxicity of cooper oxide NPs *in vitro* using a Vitrocell® ALI device to an *in vivo* inhalation study in mice. In contrast to the aforementioned studies, Jing et al. showed good agreement between *in vivo* inhalation and ALI *in vitro* regarding inflammation and cytotoxicity when using similar concentrations of copper oxide NPs [153]. This study demonstrates that ALI studies can provide meaningful data concerning *in vitro* inhalation nanotoxicity compared to *in vivo*. But studies comparing ALI to *in vivo* are still rather rare.

Moreover, *in vitro* toxicity of NPs should be tested at doses comparable to those used *in vivo.* This will enable a direct comparison between ALI *in vitro* and *in vivo* inhalation studies. Then it might be possible to further define factors that need to be considered *in vitro* to obtain equivalent results as *in vivo*. In addition to the quantitative determination of the deposited dose, the amount of particles taken up intracellularly is also of interest since these interact directly with the cells. However, in general, a detailed description of this is often not investigated. This gap was closed for CeO_2 NPs by the NANoREG project [70].

Based on the NANoREG *in vivo* data and the ALI *in vitro* exposure data presented in this thesis, it could be shown for the first time that an ALI exposure system can be used to achieve intracellular CeO_2 NP concentrations similar to *in vivo*. This represents a step in the right direction towards direct comparison between *in vitro* and *in vivo* under realistic exposure situations.

Further development of *in vitro* cell systems like 3D models, co-cultures or *ex vivo* approaches has to be done as well to enable investigations regarding inflammation,

particle clearance or particle translocation which are currently only representable *in vivo*.

4.4 Improvement of *in vitro* cell models for inhalation toxicity studies

The improvement of cellular models is an important task to further increase the validity of *in vitro* systems. Proper cell culture models help to address questions that are quite challenging right now like particle translocation from the lung to secondary organs and tissues [70]. However, ALI experiments are commonly conducted with the human alveolar cell line A549, a carcinogenic alveolar type II epithelium [171]. Unfortunately, these cells do not express functional tight junctions [143]. Thus, A549 cells are not suitable to tackle questions like particle translocation mechanisms, as a fully formed barrier would be needed to investigate translocation under *in vivo* terms. However, proper cell models to close this well-known gap are mostly limited to primary cells because available cell lines show limitation regarding a functional tight junction network. Due to limited lifetime and high costs, primary cells are not routinely used in ALI studies investigating NP toxicity. Although they would have the advantage of representing the *in vivo* situation much better than cell lines, their short lifespan limits their application for long-term experiments [174]. Even 28-day subchronic studies which are frequently used in risk assessment are difficult to perform with such models [145,194]. In 2016, Kuehn and colleagues reported a new cell line that overcame this issue. They introduced the so called hAELVi cells (human Alveolar Epithelial Lentivirus immortalized) [174]. These cells possess different advantages like a strong functional tight junction expression and a type I alveolar

epithelium phenotype [174] which is quite useful for NP toxicity assessment as more than 95 % of the alveolar surface is covered by type I cells which are responsible for gas exchange [61,79]. Hence, type I cells should be considered the primary alveolar cell type for NP toxicity investigations.

As NPs partially tend to agglomerate, deposition in the bronchial region is also of interest and should be considered for risk assessment [74-77,134,195]. Therefore, the two newly developed cell models hAELVi and huAEC (human Alveolar Epithelia Cell) were investigated concerning their suitability for testing ZnO and CeO_2 NPs toxicity under standard submerse and ALI conditions. In addition, the influence of the two NPs on the barrier function of these cell models was also investigated, as this is one of the main advantages of these two new cell lines.

The results reported in section 3.2 show that both cell lines, hAELVi and huAEC, perform similar regarding cell viability, cytotoxicity and ROS generation for both NPs, when compared to the typically used A549 cell line, suggesting good comparability with other cell systems [186]. However, as inflammation is an important parameter in nanotoxicology, this might be difficult to address with these two models as the used media contains hydrocortisone which has anti-inflammatory properties [196]. Therefore, the influence of the media on inflammation needs careful investigation in further research projects.

In contrast to A549 cells, hAELVi and huAEC evolved a strong tight junction network under submerse culture conditions as well as under ALI conditions. This was proved by immunohistochemical staining of the tight junction protein zonula occludens-1 (ZO-1) and trans epithelial electrical resistance (TEER) measurements [186]. hAELVi TEER values were in good accordance with primary alveolar epithelia cells [172].

huAEC displayed even higher TEER values compared to primary cells under submerse and ALI conditions [172].

Thus, both cell systems mimic the *in vivo* situation of the alveolar and bronchial epithelium. Both cell lines enable the examination of particle translocation under conditions more similar to the *in vivo* situation as it was previously possible.

A single monoculture just represents a small piece of the pulmonary environment. Further improvements of cell models like co-culture systems or 3D models are needed to study NP toxicity on a level as close as possible to the *in vivo* models. In 2018, Klettling et al. demonstrated that hAELVi cells are suitable for co-culturing with immune cells by combined hAELVi cells with human macrophages to mimic the interaction of human alveolar epithelium and alveolar immune cells [197].

As 3D models represent the *in vivo* situation closer than monocultures, the barrier property of the new developed 3D alveolar model EpiAlveolar was also investigated in this work. This three-dimensional co-culture consists of human alveolar epithelia cells, fibroblasts, and endothelia cells [166]. EpiAlveolar showed a good barrier evolvement with TEER values of about 2900 Ω * cm^2 which is similar to primary alveolar epithelia cells [172]. Due to the short lifetime of about one week, the usage of this model in NP toxicity testing was considered to be limited to short term studies with duration of about five days. However, the manufacturer recently published data that show a cultivation time up to 42 days with constant barrier function as well as the integration of patient derived macrophages which suggests the feasibility for subchronic studies in the future [166]. At the moment, EpiAlveolar is the only commercially available 3D human alveolar epithelia model that combines alveolar type I and type II cells. Therefore, it should be considered as a standard cell culture model for inhalation nanotoxicology studies.

To improve the complexity of in vitro systems even further, organ-on-a-chip technology represent a promising tool. This platform allows the simultaneous cultivation of different tissue compartments. As the compartments are all connected by a channel system the blood circulation can be simulated [198]. With this technology, different complex tissue compartments can be studied mimicking different parts of the body. Thus, the application of organ-on-a-chip technology might be an important part in the development of an alternative method for inhalation toxicity studies.

As EpiAlveolar and hAELVi cells can be cultivated in a transwell system, the integration in an organ-on-a-chip system is conceivable. This has not been reported so far and will be a relevant research task to push standardization and the development of an alternative method for NP inhalation toxicity in the future.

However, the complexity of an animal can certainly not be mimicked completely at present. Therefore, animal experiments will certainly be an ongoing part of nanotoxicology in the future.

4.5 Realistic exposure scenarios for risk assessment and standardization of CeO_2 nanoparticles

Current toxicological research is mostly focused on the toxic effects of NMs. In itself, this is not yet a problem as the toxicity of new substances has to be evaluated in the EU to ensure product safety. This should of course also include worst case scenarios. However, the determination of toxicity is strongly dependent on the dose of the substances and the time an individual is exposed to it. A single high dose is therefore not optimal to evaluate long-term toxicity as they can lead to a so-called overload.

This impairs the natural cleaning process of the lung leading to pathophysiological changes like fibrosis [72,166]. Whether such pathophysiological effects might also emerge under more realistic low dose long term conditions or not is still not fully understood. Fortunately, this task is getting more and more attention in the research community [50,118,148].

For most NPs, the air concentration is unknown. Therefore, occupational exposure limits (OEL) or so called no observed adverse effect levels (NOAEL) are often used instead of quantitative measured data. One disadvantage is that OELs or NOAELs are only defined for a few NPs like TiO_2 [199], carbon nanotubes [177,200] or carbon black [200]. For CeO_2, the implementation of realistic doses is difficult because no OEL value is available.

Beside industrial relevant concentrations [118], daily exposure of CeO_2 to people is mainly driven by diesel exhaust because CeO_2 has been used as diesel additive and is subsequently released into the atmosphere [157,158]. Erdakos et al. (2014) estimated 0.5 ng/m^3 as an average value and air concentrations up to 22 ng/m^3 CeO_2 at highways for the U.S. [158]. Recently, Giese and colleagues predicted a mean CeO_2 air concentration of about 5.5 ng/m^3 [159]. For the UK, quantitative measured data reporting CeO_2 values of 0.1 - 1.0 ng/m^3 [161] and 0.612 ng/m^3 [157].

A recent study from Paur and colleagues suggested a CeO_2 concentration of 0.03 ng/h*cm^2 as a realistic ambient concentration for *in vitro* studies. They also mentioned worst case scenarios with 5 ng/h*cm^2 that should be tested [50]. Our ICP-MS results demonstrated an administered dose of about 8.5 ng/h*cm^2 with a subsequent intracellular concentration of ~4.5 ng/h*cm^2. This covers the realistic exposure scenario range of Paur et al. [201]. Analysis of the membrane composition revealed that even low/environmental realistic dosages can affect the molecular

composition of the lung epithelia cell membrane. Possible long-term effects need to be examined in a further research project to better understand the interaction of NPs under realistic ambient conditions.

Examining daily relevant concentrations would therefore significantly improve the toxicity data under realistic circumstances and consequently help reduce animal experiments in general by avoiding studies with unrealistic exposure scenarios.

5. Conclusion and outlook

In vivo inhalation toxicity testing is still routinely used for regulatory decision making. One reason for this is the missing standardization of *in vitro* methods, including ALI systems. To improve this issue, reliability of ALI methods, in particular regarding dosimetry, is a key task.

By using a C&E concept we were able to characterize a commercially available ALI system concerning parameters that affect the cell viability which is a key marker in nanotoxicology. Furthermore, by developing a data analysis approach, as it is standard in analytics, we improved data analysis in biology where such an approach is normally not applied. This leads to an increased reproducibility of the obtained data, which is required for regulatory applications. However, the reliability and reproducibility should be further determined in interlaboratory and repeatability studies.

In the presented work here, it could be shown for the first time that ALI systems enable the administration of intracellular doses of CeO_2 NPs equal to *in vivo* rat studies. This demonstrates that ALI systems can provide data equal to results obtained *in vivo* (e.g., NANoREG), which is an important step in the development of an alternative method for inhalation nanotoxicology.

This work also demonstrated that environmental realistic low doses of CeO_2 NPs can affect the structural composition of alveolar epithelia cells on a molecular level. For investigating such exposure conditions in the future, it is recommended and desirable to assess the toxicity of CeO_2 NPs more realistically.

Standardization of ALI systems is just one pillar of the ultimate goal to develop an alternative method for *in vivo* nanotoxicology testing. The use of proper cell culture

models is also essential for that. Within this thesis, the two new cell lines hAELVi and huAEC have been introduced which represent suitable *in vitro* models for nanotoxicology investigation. Both form functional tight junction networks similar to *in vivo* models, a feature that was missing for most alveolar cell lines. Furthermore, hAELVi cells represent a type I model which is the most prominent cell type in the alveolar region. Thus, hAELVi cells are highly recommended to be used in future investigations. The anti-inflammatory effect of hydrocortisone in the culture medium has to be taken into account, especially when inflammation is investigated, an important marker in nanotoxicology. Further research has to be done in order to assess the usefulness of those cell lines to study the inflammatory effect of NMs.

Not even 3D cell models can fully mimic the complexity of an animal at the present. Therefore, animal experiments will certainly be an ongoing part of nanotoxicology in the future. However, standardization and further developments of *in vitro* models as well as the implementation of new methods such as organ-on-a-chips, are promising approaches in the right direction to the ultimate goal of an alternative to animal studies in inhalation nanotoxicology considering realistic doses and exposure scenarios.

In conclusion, this work provides an *in vitro* ALI exposure setup to study the toxicity of CeO_2 NPs on a realistic exposure level. Furthermore, newly developed cell models were characterized to mimic the *in vivo* situation as close as possible. We could proof that CeO_2 NP concentrations equal to *in vivo* can be achieved with *in vitro* ALI setups. The application of environmental relevant CeO_2 NP concentrations leads to the alteration of the molecular structure of alveolar epithelia cells. Possible adverse effects as results of those changes in membrane composition of NP exposed cells need further research.

This work provides a systematic approach that helps to standardize *in vitro* ALI exposure setups providing a first step towards alternative method development.

With this, a platform was created to assess the toxicity of CeO_2 NPs under realistic conditions by characterization the ALI system and new cellular systems, which should be expanded to other NPs in the future.

To further improve this system, a combination with other promising technology platforms like lungs-on-a-chip is conceivable and desirable. This would allow to add further important physiological parameters to the system like mechanical stretching (mimicking inhalation and exhalation) leading to an improved representation of the *in vivo* situation.

6. References

1. Vance, M.E.; Kuiken, T.; Vejerano, E.P.; McGinnis, S.P.; Hochella, M.F., Jr.; Rejeski, D.; Hull, M.S. Nanotechnology in the real world: Redeveloping the nanomaterial consumer products inventory. *Beilstein J Nanotechnol* **2015**, *6*, 1769-1780, doi:10.3762/bjnano.6.181.
2. Regulation (EC) No 1907/2006 of the European Parliament and of the Council of 18 December 2006 concerning the Registration, Evaluation, Authorisation and Restriction of Chemicals (REACH), establishing a European Chemicals Agency. The European Parliament and of the Council: https://eur-lex.europa.eu/legal-content/EN/TXT/?uri=CELEX%3A02006R1907-20140410, 2006; Vol. Official Journal of the European Union L 396, pp 1-520.
3. Communication from the commission to the european parliament, the council and the european economic and social commitee regulatory aspects of nanomaterials. Commision of the european communities: https://ec.europa.eu/research/industrial_technologies/pdf/policy/comm_2008_0366_en.pdf, 2008.
4. Commission recommendation of 18 October 2011 on the definition of nanomaterial. Official Journal of the European Union: https://eur-lex.europa.eu/legal-content/EN/TXT/PDF/?uri=CELEX:32011H0696&from=EN, 2011; Vol. L 275/38.
5. Regulation (EU) No 528/2012 of the european parliament and of the council of 22 May 2012 concerning the making available on the market and use of biocidal products. Official Journal of the European Union: https://eur-lex.europa.eu/legal-content/EN/TXT/PDF/?uri=CELEX:32012R0528&from=EN, 2012; Vol. L167/1.
6. Regulation (EC) No 1223/2009 of the European Parliament and of the Council of 30 November 2009 on cosmetic products. Official Journal of the European Union L 342: https://ec.europa.eu/health/sites/health/files/endocrine_disruptors/docs/cosmetic_1223_2009_regulation_en.pdf, 2009; pp 59-209
7. Regulation (EU) 2015/2283 of the european parliament and of the council of 25 November 2015 on novel foods, amending Regulation (EU) No 1169/2011 of the european parliament and of the council and repealing regulation (EC) No 258/97 of the european parliament and of the council and commission regulation (EC) No 1852/2001. Official Journal of the European Union: https://eur-lex.europa.eu/legal-content/EN/TXT/PDF/?uri=CELEX:32015R2283&from=DE, 2015; Vol. L 327/1.
8. Commission regulation (EC) No 450/2009 of 29 May 2009 on active and intelligent materials and articles intended to come into contact with food. Official Journal of the European Union: https://eur-lex.europa.eu/LexUriServ/LexUriServ.do?uri=OJ:L:2009:135:0003:0011:EN:PDF, 2009; Vol. L135/3.
9. Commission regulation (EU) No 10/2011 of 14 January 2011 on plastic materials and articles intended to come into contact with food. Official Journal of the European Union: https://eur-

lex.europa.eu/LexUriServ/LexUriServ.do?uri=OJ:L:2011:012:0001:0089:en:PDF, 2011; Vol. L12/1.

10. Regulation (EU) No 1169/2011 of the european parliament and of the council of 25 October 2011 on the provision of food information to consumers, amending Regulations (EC) No 1924/2006 and (EC) No 1925/2006 of the European Parliament and of the Council, and repealing Commission Directive 87/250/EEC, Council Directive 90/496/EEC, Commission Directive 1999/10/EC, Directive 2000/13/EC of the European Parliament and of the Council, Commission Directives 2002/67/EC and 2008/5/EC and Commission Regulation (EC) No 608/2004. Official Journal of the European Union: https://eur-lex.europa.eu/LexUriServ/LexUriServ.do?uri=OJ:L:2011:304:0018:0063:en:PDF, 2011.
11. Regulation (EC) No 1333/2008 of the European Parliament and of the council of 16 December 2008 on food additives. Official Journal of the European Union: https://eur-lex.europa.eu/LexUriServ/LexUriServ.do?uri=OJ:L:2008:354:0016:0033:en:PDF, 2008; Vol. L 354/16.
12. commission, E. Proposal for a Regulaation of the european parliament and of the council on medical devices, and amending Directive 2001/83/EC, Regulation (EC) No 178/2002 and Regulation (EC) No 1223/2009, COM (2012) 542 final, European Commission, Brussels 2012. **2012**.
13. Rauscher, H.; Rasmussen, K.; Sokull-Klüttgen, B. Regulatory Aspects of Nanomaterials in the EU. *Chemie Ingenieur Technik* **2017**, *89*, 224-231, doi:10.1002/cite.201600076.
14. W. Barthlott; Neinhuis, C. Purity of the sacred lotus, or escape from contamination in biological surfaces. *Planta* **1997**, *202*, 1-8, doi:10.1007/s004250050096.
15. Autumn, K.; Hansen, W. Ultrahydrophobicity indicates a non-adhesive default state in gecko setae. *J Comp Physiol A Neuroethol Sens Neural Behav Physiol* **2006**, *192*, 1205-1212, doi:10.1007/s00359-006-0149-y.
16. Philippe Colomban; Gouadec, G. The ideal ceramic-fibre/oxide-matrix composite: How to reconcile antagonist physical and chemical requirements ? *Annales de Chimie Science des Matériaux* **2005**, *30*, 673-688, doi:10.3166/acsm.30.673-688.
17. Johnson-McDaniel, D.; Barrett, C.A.; Sharafi, A.; Salguero, T.T. Nanoscience of an ancient pigment. *J Am Chem Soc* **2013**, *135*, 1677-1679, doi:10.1021/ja310587c.
18. Jose-Yacaman, M.; Rendon, L.; Arenas, J.; Serra Puche, M.C. Maya Blue Paint: An Ancient Nanostructured Material. *Science* **1996**, *273*, 223-225, doi:10.1126/science.273.5272.223.
19. Philippe Walter; Eléonore Welcomme; Philippe Hallégot; Nestor J. Zaluzec; Christopher Deeb; Jacques Castaing; Patrick Veyssière; René Bréniaux; Jean-Luc Lévêque; Tsoucaris, G. Early use of PbS nanotechnology for an ancient hair dyeing formula. *Nano Lett.* **2006**, *6*, 2215–2219, doi:10.1021/nl061493u.
20. Izumi Nakai; Chiya Numako; Hideo Hosono; Yamasaki, K. Origin of the Red Color of Satsuma Copper-Ruby Glass as Determined by EXAFS and Optical Absorption Spectroscopy. *Journal of the American Ceramic Society* **1999**, *82*, 689-695, doi:10.1111/J.1151-2916.1999.TB01818.X.

21. J. Delgado; M. Vilarigues; A. Ruivo; V. Corregidor; R.C. da Silva; Alves, L.C. Characterisation of medieval yellow silver stained glass from Convento de Cristo in Tomar, Portugal. *Nuclear Instruments and Methods in Physics Research Section B: Beam Interactions with Materials and Atoms* **2011**, *269*, 2383-2388, doi:10.1016/J.NIMB.2011.02.059.
22. Schaming, D.; Remita, H. Nanotechnology: from the ancient time to nowadays. *Foundations of Chemistry* **2015**, *17*, 187-205, doi:10.1007/s10698-015-9235-y.
23. Leonhardt, U. Invisibility cup. *Nature Photonics* **2007**, *1*, 207-208, doi:10.1038/nphoton.2007.38.
24. D. J. Barber; Freestone, I.C. An investigation of the origin of the colour of the Lycurgus Cup by analytical transmission electron microscopy. *Archaeometry* **1990**, *32*, 33-45, doi:10.1111/j.1475-4754.1990.tb01079.x|.
25. Krug, H.F.; Wick, P. Nanotoxicology: an interdisciplinary challenge. *Angew Chem Int Ed Engl* **2011**, *50*, 1260-1278, doi:10.1002/anie.201001037.
26. Dykman, L.A.; Khlebtsov, N.G. Gold nanoparticles in biology and medicine: recent advances and prospects. *Acta Naturae* **2011**, *3*, 34-55.
27. Hainfeld, J.F.; Slatkin, D.N.; Focella, T.M.; Smilowitz, H.M. Gold nanoparticles: a new X-ray contrast agent. *Br J Radiol* **2006**, *79*, 248-253, doi:10.1259/bjr/13169882.
28. Qian, Y.; Qiu, M.; Wu, Q.; Tian, Y.; Zhang, Y.; Gu, N.; Li, S.; Xu, L.; Yin, R. Enhanced cytotoxic activity of cetuximab in EGFR-positive lung cancer by conjugating with gold nanoparticles. *Sci Rep* **2014**, *4*, 7490, doi:10.1038/srep07490.
29. Kodiha, M.; Wang, Y.M.; Hutter, E.; Maysinger, D.; Stochaj, U. Off to the organelles - killing cancer cells with targeted gold nanoparticles. *Theranostics* **2015**, *5*, 357-370, doi:10.7150/thno.10657.
30. Valetti, S.; Maione, F.; Mura, S.; Stella, B.; Desmaele, D.; Noiray, M.; Vergnaud, J.; Vauthier, C.; Cattel, L.; Giraudo, E., et al. Peptide-functionalized nanoparticles for selective targeting of pancreatic tumor. *J Control Release* **2014**, *192*, 29-39, doi:10.1016/j.jconrel.2014.06.039.
31. Jain, S.; Coulter, J.A.; Hounsell, A.R.; Butterworth, K.T.; McMahon, S.J.; Hyland, W.B.; Muir, M.F.; Dickson, G.R.; Prise, K.M.; Currell, F.J., et al. Cell-specific radiosensitization by gold nanoparticles at megavoltage radiation energies. *Int J Radiat Oncol Biol Phys* **2011**, *79*, 531-539, doi:10.1016/j.ijrobp.2010.08.044.
32. Maksimenko, A.; Dosio, F.; Mougin, J.; Ferrero, A.; Wack, S.; Reddy, L.H.; Weyn, A.A.; Lepeltier, E.; Bourgaux, C.; Stella, B., et al. A unique squalenoylated and nonpegylated doxorubicin nanomedicine with systemic long-circulating properties and anticancer activity. *Proc Natl Acad Sci U S A* **2014**, *111*, E217-E226, doi:10.1073/pnas.1313459110.
33. Neuhaus, V.; Chichester, J.A.; Ebensen, T.; Schwarz, K.; Hartman, C.E.; Shoji, Y.; Guzman, C.A.; Yusibov, V.; Sewald, K.; Braun, A. A new adjuvanted nanoparticle-based H1N1 influenza vaccine induced antigen-specific local mucosal and systemic immune responses after administration into the lung. *Vaccine* **2014**, *32*, 3216-3222, doi:10.1016/j.vaccine.2014.04.011.
34. Brian O`Regan; Grätzel, M. A low-cost, high-efficiency solar cell based on dye-sensitized colloidal TiO_2 films. *Nature* **1991**, *353*, 737-740, doi:10.1038/353737a0.

35. Rajamanickam, N.; Ramachandran, K. Improved photovoltaic performance in nano TiO_2 based dye sensitized solar cells: Effect of $TiCl_4$ treatment and Sr doping. *J Colloid Interface Sci* **2020**, *580*, 407-418, doi:10.1016/j.jcis.2020.07.041.
36. Hsu, P.C.; Song, A.Y.; Catrysse, P.B.; Liu, C.; Peng, Y.; Xie, J.; Fan, S.; Cui, Y. Radiative human body cooling by nanoporous polyethylene textile. *Science* **2016**, *353*, 1019-1023, doi:10.1126/science.aaf5471.
37. Smulders, S.; Luyts, K.; Brabants, G.; Golanski, L.; Martens, J.; Vanoirbeek, J.; Hoet, P.H.M. Toxicity of nanoparticles embedded in paints compared to pristine nanoparticles, in vitro study. *Toxicol Lett* **2015**, *232*, 333-339, doi:10.1016/j.toxlet.2014.11.030.
38. Monteiro-Riviere, N.A.; Wiench, K.; Landsiedel, R.; Schulte, S.; Inman, A.O.; Riviere, J.E. Safety evaluation of sunscreen formulations containing titanium dioxide and zinc oxide nanoparticles in UVB sunburned skin: an in vitro and in vivo study. *Toxicol Sci* **2011**, *123*, 264-280, doi:10.1093/toxsci/kfr148.
39. Nohynek, G.J.; Dufour, E.K.; Roberts, M.S. Nanotechnology, cosmetics and the skin: is there a health risk? *Skin Pharmacol Physiol* **2008**, *21*, 136-149, doi:10.1159/000131078.
40. Ilaria Zanoni; Matteo Crosera; Simona Ortelli; Magda Blosi; Gianpiero Adami; Filon, F.L.; Costa, A.L. CuO nanoparticle penetration through intact and damaged human skin. *New Journal of Chemistry* **2019**, *43*, 17033-17039, doi:10.1039/C9NJ03373D
41. Adam C. Watkinson; Annette L. Bunge; Jonathan Hadgraft; Lane, M.E. Nanoparticles Do Not Penetrate Human Skin-A Theoretical Perspective. *Pharmaceutical Research* **2013**, *30*, 1943-1946, doi:10.1007/s11095-013-1073-9.
42. George J. Touloumes; Herdeline Ann M. Ardoña; Evan K. Casalino; John F. Zimmerman; Christophe O. Chantre; Dimitrios Bitounis; Philip Demokritou; Parker, K.K. Mapping 2D- and 3D-distributions of metal/metal oxide nanoparticles within cleared human ex vivo skin tissues. *NanoImpact* **2020**, *17*, doi:10.1016/j.impact.2020.100208.
43. Mauro, M.; Crosera, M.; Monai, M.; Montini, T.; Fornasiero, P.; Bovenzi, M.; Adami, G.; Turco, G.; Filon, F.L. Cerium Oxide Nanoparticles Absorption through Intact and Damaged Human Skin. *Molecules* **2019**, *24*, 3759, doi:10.3390/molecules24203759.
44. Ramon M. Molina; Nagarjun V. Konduru; Renato J. Jimenez; Georgios Pyrgiotakis; Philip Demokritou; Wendel Wohlleben; Brain, J.D. Bioavailability, distribution and clearance of tracheally instilled, gavaged or injected cerium dioxide nanoparticles and ionic cerium. *Environmental Science: Nano* **2014**, *1*, 561-573, doi:10.1039/C4EN00034J.
45. Alan MacNicoll; Mick Kelly; Hatice Aksoy; Evelien Kramer; Hans Bouwmeester; Chaudhry, Q. A study of the uptake and biodistribution of nano-titanium dioxide using in vitro and in vivo models of oral intake. *J Nanopart Res* **2015**, *17*, doi:10.1007/s11051-015-2862-3.
46. Warheit, D.B.; Hoke, R.A.; Finlay, C.; Donner, E.M.; Reed, K.L.; Sayes, C.M. Development of a base set of toxicity tests using ultrafine TiO_2 particles as a component of nanoparticle risk management. *Toxicol Lett* **2007**, *171*, 99-110, doi:10.1016/j.toxlet.2007.04.008.

47. Kolosnjaj-Tabi, J.; Hartman, K.B.; Boudjemaa, S.; Ananta, J.S.; Morgant, G.; Szwarc, H.; Wilson, L.J.; Moussa, F. In vivo behavior of large doses of ultrashort and full-length single-walled carbon nanotubes after oral and intraperitoneal administration to Swiss mice. *Acs Nano* **2010**, *4*, 1481-1492, doi:10.1021/nn901573w.
48. Cho, W.S.; Kang, B.C.; Lee, J.K.; Jeong, J.; Che, J.H.; Seok, S.H. Comparative absorption, distribution, and excretion of titanium dioxide and zinc oxide nanoparticles after repeated oral administration. *Part Fibre Toxicol* **2013**, *10*, 9, doi:10.1186/1743-8977-10-9.
49. Geiser, M.; Kreyling, W.G. Deposition and biokinetics of inhaled nanoparticles. *Part Fibre Toxicol* **2010**, *7*, 2, doi:10.1186/1743-8977-7-2.
50. Hanns-Rudolf Paur; Flemming R. Cassee; Justin Teeguarden; Heinz Fissan; Silvia Diabate; Michaela Aufderheide; Wolfgang G. Kreyling; Otto Hänninen; Gerhard Kasper; Michael Riediker, et al. In-vitro cell exposure studies for the assessment of nanoparticle toxicity in the lung—A dialog between aerosol science and biology. *J Aerosol Sci* **2011**, *42*, 668-692, doi:10.1016/j.jaerosci.2011.06.005.
51. Loret, T.; Peyret, E.; Dubreuil, M.; Aguerre-Chariol, O.; Bressot, C.; le Bihan, O.; Amodeo, T.; Trouiller, B.; Braun, A.; Egles, C., et al. Air-liquid interface exposure to aerosols of poorly soluble nanomaterials induces different biological activation levels compared to exposure to suspensions. *Part Fibre Toxicol* **2016**, *13*, 58, doi:10.1186/s12989-016-0171-3.
52. Chang Guo; Rachel Smith; Timothy W. Gant; Leonard, M.O. Cerium dioxide nanoparticles protect against oxidative stress induced injury through modulation of TGF-β signalling. *Toxicology Research* **2015**, *4*, 464–475.
53. Christiansen, J.; Douglas, C.G.; Haldane, J.S. The absorption and dissociation of carbon dioxide by human blood. *J Physiol* **1914**, *48*, 244-271, doi:10.1113/jphysiol.1914.sp001659.
54. Wei, Q.; Hu, Y.; Gelfand, G.; Macgregor, J.H. Segmentation of lung lobes in high-resolution isotropic CT images. *IEEE Trans Biomed Eng* **2009**, *56*, 1383-1393, doi:10.1109/TBME.2009.2014074.
55. Bierkandt, F.S.; Leibrock, L.; Wagener, S.; Laux, P.; Luch, A. The impact of nanomaterial characteristics on inhalation toxicity. *Toxicol Res (Camb)* **2018**, *7*, 321-346, doi:10.1039/c7tx00242d.
56. Scheffler, S.; Dieken, H.; Krischenowski, O.; Aufderheide, M. Cytotoxic Evaluation of e-Liquid Aerosol using Different Lung-Derived Cell Models. *Int J Environ Res Public Health* **2015**, *12*, 12466-12474, doi:10.3390/ijerph121012466.
57. Ochs, M.; Nyengaard, J.R.; Jung, A.; Knudsen, L.; Voigt, M.; Wahlers, T.; Richter, J.; Gundersen, H.J. The number of alveoli in the human lung. *Am J Respir Crit Care Med* **2004**, *169*, 120-124, doi:10.1164/rccm.200308-1107OC.
58. Jiang, P.; Gil de Rubio, R.; Hrycaj, S.M.; Gurczynski, S.J.; Riemondy, K.A.; Moore, B.B.; Omary, M.B.; Ridge, K.M.; Zemans, R.L. Ineffectual Type 2-to-Type 1 Alveolar Epithelial Cell Differentiation in Idiopathic Pulmonary Fibrosis: Persistence of the KRT8^{hi} Transitional State. *Am J Respir Crit Care Med* **2020**, *201*, 1443-1447, doi:10.1164/rccm.201909-1726LE.
59. Zacharias, W.J.; Frank, D.B.; Zepp, J.A.; Morley, M.P.; Alkhaleel, F.A.; Kong, J.; Zhou, S.; Cantu, E.; Morrisey, E.E. Regeneration of the lung alveolus by an

evolutionarily conserved epithelial progenitor. *Nature* **2018**, *555*, 251-255, doi:10.1038/nature25786.
60. Kent E. Pinkerton; Peter Gehr; Alejandro Castañeda; Crapo, J.D. Architecture and cellular composition of the air-blood tissue barrier. In *Comparative Biology of the Normal Lung: Second Edition*, Elsevier Inc.: 2015; 10.1016/B978-0-12-404577-4.00009-6pp. 105-117.
61. Macklin, C.C. The pulmonary alveolar mucoid film and the pneumonocytes. *Lancet* **1954**, *266*, 1099-1104, doi:10.1016/s0140-6736(54)92154-6.
62. Hills, B.A. Alveolar liquid lining: Langmuir method used to measure surface tension in bovine and canine lung extracts. *J Physiol* **1985**, *359*, 65-79, doi:10.1113/jphysiol.1985.sp015575.
63. Clements, J.A. Surface tension of lung extracts. *Proc Soc Exp Biol Med* **1957**, *95*, 170-172, doi:10.3181/00379727-95-23156.
64. Ochs, M.; Hegermann, J.; Lopez-Rodriguez, E.; Timm, S.; Nouailles, G.; Matuszak, J.; Simmons, S.; Witzenrath, M.; Kuebler, W.M. On Top of the Alveolar Epithelium: Surfactant and the Glycocalyx. *Int J Mol Sci* **2020**, *21*, doi:10.3390/ijms21093075.
65. Gehr, P.; Bachofen, M.; Weibel, E.R. The normal human lung: ultrastructure and morphometric estimation of diffusion capacity. *Respir Physiol* **1978**, *32*, 121-140, doi:10.1016/0034-5687(78)90104-4.
66. Graeme R. Polglase; Hooper, S.B. Role of Intra-Luminal Pressure in Regulating PBF in the Fetus and After Birth. *Current Pediatric Reviews* **2006**, *2*, 287-299, doi:10.2174/157339606778699653.
67. Jonsson, S.; Musher, D.M.; Chapman, A.; Goree, A.; Lawrence, E.C. Phagocytosis and killing of common bacterial pathogens of the lung by human alveolar macrophages. *J Infect Dis* **1985**, *152*, 4-13, doi:10.1093/infdis/152.1.4.
68. Franke-Ullmann, G.; Pförtner, C.; Walter, P.; Steinmüller, C.; Lohmann-Matthes, M.L.; Kobzik, L. Characterization of murine lung interstitial macrophages in comparison with alveolar macrophages in vitro. *J Immunol* **1996**, *157*, 3097-3104.
69. Yuan, K.; Huang, C.; Fox, J.; Laturnus, D.; Carlson, E.; Zhang, B.; Yin, Q.; Gao, H.; Wu, M. Autophagy plays an essential role in the clearance of Pseudomonas aeruginosa by alveolar macrophages. *J Cell Sci* **2012**, *125*, 507-515, doi:10.1242/jcs.094573.
70. Tentschert, J.; Laux, P.; Jungnickel, H.; Brunner, J.; Estrela-Lopis, I.; Merker, C.; Meijer, J.; Ernst, H.; Ma-Hock, L.; Keller, J., et al. Organ burden of inhaled nanoceria in a 2-year low-dose exposure study: dump or depot? *Nanotoxicology* **2020**, *14*, 554-576, doi:10.1080/17435390.2020.1736355.
71. Schwotzer, D.; Ernst, H.; Schaudien, D.; Kock, H.; Pohlmann, G.; Dasenbrock, C.; Creutzenberg, O. Effects from a 90-day inhalation toxicity study with cerium oxide and barium sulfate nanoparticles in rats. *Part Fibre Toxicol* **2017**, *14*, 23, doi:10.1186/s12989-017-0204-6.
72. Morrow, P.E. Possible mechanisms to explain dust overloading of the lungs. *Fundam Appl Toxicol* **1988**, *10*, 369-384, doi:10.1016/0272-0590(88)90284-9.
73. Li, R.; Ji, Z.; Chang, C.H.; Dunphy, D.R.; Cai, X.; Meng, H.; Zhang, H.; Sun, B.; Wang, X.; Dong, J., et al. Surface interactions with compartmentalized cellular phosphates explain rare earth oxide nanoparticle hazard and provide

opportunities for safer design. *Acs Nano* **2014**, *8*, 1771-1783, doi:10.1021/nn406166n.
74. J. Heyder; J. Gebhart; G. Rudolf; C.F. Schiller; Stahlhofen, W. Deposition of particles in the human respiratory tract in the size range 0.005–15 μm. *J Aerosol Sci* **1986**, *17*, doi:10.1016/0021-8502(86)90035-2.
75. Carvalho, T.C.; Peters, J.I.; Williams, R.O., 3rd. Influence of particle size on regional lung deposition--what evidence is there? *Int J Pharm* **2011**, *406*, 1-10, doi:10.1016/j.ijpharm.2010.12.040.
76. ICRP. *Human Respiratory Tract Model for Radiological Protection. ICRP Publication 66. Ann. ICRP 24 (1-3)*; 1994; pp 1-482.
77. Katarzyna Dobrowolska; Katarzyna Jabłczyńska; Dorota Kondej; Sosnowski, T.R. Interactions of insoluble micro- and nanoparticles with the air-liquid interface of the model pulmonary fluids. *Physicochem. Probl. Miner. Process.* **2018**, *54*, 151-162, doi:10.5277/ppmp1837
78. Fresegna, A.M.; Ursini, C.L.; Ciervo, A.; Maiello, R.; Casciardi, S.; Iavicoli, S.; Cavallo, D. Assessment of the Influence of Crystalline Form on Cyto-Genotoxic and Inflammatory Effects Induced by TiO_2 Nanoparticles on Human Bronchial and Alveolar Cells. *Nanomaterials* **2021**, *11*, 253, doi:10.3390/nano11010253.
79. Kemp, S.J.; Thorley, A.J.; Gorelik, J.; Seckl, M.J.; O'Hare, M.J.; Arcaro, A.; Korchev, Y.; Goldstraw, P.; Tetley, T.D. Immortalization of human alveolar epithelial cells to investigate nanoparticle uptake. *Am J Respir Cell Mol Biol* **2008**, *39*, 591-597, doi:10.1165/rcmb.2007-0334OC.
80. Radiom, M.; Sarkis, M.; Brookes, O.; Oikonomou, E.K.; Baeza-Squiban, A.; Berret, J.F. Pulmonary surfactant inhibition of nanoparticle uptake by alveolar epithelial cells. *Sci Rep* **2020**, *10*, 19436, doi:10.1038/s41598-020-76332-7.
81. Weiss, M.; Fan, J.; Claudel, M.; Lebeau, L.; Pons, F.; Ronzani, C. Combined In Vitro and In Vivo Approaches to Propose a Putative Adverse Outcome Pathway for Acute Lung Inflammation Induced by Nanoparticles: A Study on Carbon Dots. *Nanomaterials* **2021**, *11*, 180, doi:10.3390/nano11010180.
82. Bustamante-Marin, X.M.; Ostrowski, L.E. Cilia and Mucociliary Clearance. *Cold Spring Harb Perspect Biol* **2017**, *9*, doi:10.1101/cshperspect.a028241.
83. Schuster, B.S.; Suk, J.S.; Woodworth, G.F.; Hanes, J. Nanoparticle diffusion in respiratory mucus from humans without lung disease. *Biomaterials* **2013**, *34*, 3439-3446, doi:10.1016/j.biomaterials.2013.01.064.
84. Oberdörster, G. Lung Clearance of Inhaled Insoluble and Soluble Particles. *Journal of Aerosol Medicine,* **1988**, *1*, 289-330, doi:10.1089/jam.1988.1.289.
85. Stuart, B.O. Deposition and clearance of inhaled particles. *Environ Health Perspect* **1984**, *55*, 369-390, doi:10.1289/ehp.8455369.
86. Frieke Kuper, C.; Grollers-Mulderij, M.; Maarschalkerweerd, T.; Meulendijks, N.M.; Reus, A.; van Acker, F.; Zondervan-van den Beuken, E.K.; Wouters, M.E.; Bijlsma, S.; Kooter, I.M. Toxicity assessment of aggregated/agglomerated cerium oxide nanoparticles in an in vitro 3D airway model: the influence of mucociliary clearance. *Toxicol in Vitro* **2015**, *29*, 389-397, doi:10.1016/j.tiv.2014.10.017.
87. Nemmar, A.; Vanbilloen, H.; Hoylaerts, M.F.; Hoet, P.H.; Verbruggen, A.; Nemery, B. Passage of intratracheally instilled ultrafine particles from the lung into the systemic circulation in hamster. *Am J Respir Crit Care Med* **2001**, *164*, 1665-1668, doi:10.1164/ajrccm.164.9.2101036.

88. Schleh, C.; Holzwarth, U.; Hirn, S.; Wenk, A.; Simonelli, F.; Schaffler, M.; Moller, W.; Gibson, N.; Kreyling, W.G. Biodistribution of inhaled gold nanoparticles in mice and the influence of surfactant protein D. *J Aerosol Med Pulm Drug Deliv* **2013**, *26*, 24-30, doi:10.1089/jamp.2011.0951.
89. Liu, J.; Wong, H.L.; Moselhy, J.; Bowen, B.; Wu, X.Y.; Johnston, M.R. Targeting colloidal particulates to thoracic lymph nodes. *Lung Cancer* **2006**, *51*, 377-386, doi:10.1016/j.lungcan.2005.11.006.
90. Kim, J.K.; Kim, H.P.; Park, J.D.; Ahn, K.; Kim, W.Y.; Gulumian, M.; Oberdorster, G.; Yu, I.J. Lung retention and particokinetics of silver and gold nanoparticles in rats following subacute inhalation co-exposure. *Part Fibre Toxicol* **2021**, *18*, doi:10.1186/s12989-021-00397-z.
91. Li, D.; Morishita, M.; Wagner, J.G.; Fatouraie, M.; Wooldridge, M.; Eagle, W.E.; Barres, J.; Carlander, U.; Emond, C.; Jolliet, O. In vivo biodistribution and physiologically based pharmacokinetic modeling of inhaled fresh and aged cerium oxide nanoparticles in rats. *Part Fibre Toxicol* **2016**, *13*, 45, doi:10.1186/s12989-016-0156-2.
92. Molina, R.M.; Konduru, N.V.; Queiroz, P.M.; Figueroa, B.; Fu, D.; Ma-Hock, L.; Groeters, S.; Schaudien, D.; Brain, J.D. Fate of Barium Sulfate Nanoparticles Deposited in the Lungs of Rats. *Sci Rep* **2019**, *9*, 8163, doi:10.1038/s41598-019-44551-2.
93. Laux, P.; Riebeling, C.; Booth, A.M.; Brain, J.D.; Brunner, J.; Cerrillo, C.; Creutzenberg, O.; Estrela-Lopis, I.; Gebel, T.; Johanson, G., et al. Biokinetics of Nanomaterials: the Role of Biopersistence. *NanoImpact* **2017**, *6*, 69-80, doi:10.1016/j.impact.2017.03.003.
94. Driscoll, K.E.; Borm, P.J.A. Expert workshop on the hazards and risks of poorly soluble low toxicity particles. *Inhal Toxicol* **2020**, *32*, 53-62, doi:10.1080/08958378.2020.1735581.
95. Borm, P.J.A.; Driscoll, K.E. The hazards and risks of inhaled poorly soluble particles - where do we stand after 30 years of research? *Part Fibre Toxicol* **2019**, *16*, doi:10.1186/s12989-019-0294-4.
96. Gosens, I.; Cassee, F.R.; Zanella, M.; Manodori, L.; Brunelli, A.; Costa, A.L.; Bokkers, B.G.; de Jong, W.H.; Brown, D.; Hristozov, D., et al. Organ burden and pulmonary toxicity of nano-sized copper (II) oxide particles after short-term inhalation exposure. *Nanotoxicology* **2016**, *10*, 1084-1095, doi:10.3109/17435390.2016.1172678.
97. Takenaka, S.; Karg, E.; Roth, C.; Schulz, H.; Ziesenis, A.; Heinzmann, U.; Schramel, P.; Heyder, J. Pulmonary and systemic distribution of inhaled ultrafine silver particles in rats. *Environ Health Perspect* **2001**, *109 Suppl 4*, 547-551, doi:10.1289/ehp.01109s4547.
98. Konduru, N.V.; Murdaugh, K.M.; Sotiriou, G.A.; Donaghey, T.C.; Demokritou, P.; Brain, J.D.; Molina, R.M. Bioavailability, distribution and clearance of tracheally-instilled and gavaged uncoated or silica-coated zinc oxide nanoparticles. *Part Fibre Toxicol* **2014**, *11*, 44, doi:10.1186/s12989-014-0044-6.
99. Sulotto, F.; Romano, C.; Berra, A.; Botta, G.C.; Rubino, G.F.; Sabbioni, E.; Pietra, R. Rare-earth pneumoconiosis: a new case. *Am J Ind Med* **1986**, *9*, 567-575, doi:10.1002/ajim.4700090609.
100. Pairon, J.C.; Roos, F.; Sebastien, P.; Chamak, B.; Abd-Alsamad, I.; Bernaudin, J.F.; Bignon, J.; Brochard, P. Biopersistence of cerium in the human respiratory

tract and ultrastructural findings. *Am J Ind Med* **1995**, *27*, 349-358, doi:10.1002/ajim.4700270304.
101. Pairon, J.C.; Roos, F.; Iwatsubo, Y.; Janson, X.; Billon-Galland, M.A.; Bignon, J.; Brochard, P. Lung retention of cerium in humans. *Occup Environ Med* **1994**, *51*, 195-199, doi:10.1136/oem.51.3.195.
102. Oberdörster, G.; Ferin, J.; Lehnert, B.E. Correlation between particle size, in vivo particle persistence, and lung injury. *Environ Health Perspect* **1994**, *102 Suppl 5*, 173-179, doi:10.1289/ehp.102-1567252.
103. Ma, J.Y.; Mercer, R.R.; Barger, M.; Schwegler-Berry, D.; Scabilloni, J.; Ma, J.K.; Castranova, V. Induction of pulmonary fibrosis by cerium oxide nanoparticles. *Toxicol Appl Pharmacol* **2012**, *262*, 255-264, doi:10.1016/j.taap.2012.05.005.
104. Li, M.; Zhu, L.; Lin, D. Toxicity of ZnO nanoparticles to Escherichia coli: mechanism and the influence of medium components. *Environ Sci Technol* **2011**, *45*, 1977-1983, doi:10.1021/es102624t.
105. Gliga, A.R.; Skoglund, S.; Wallinder, I.O.; Fadeel, B.; Karlsson, H.L. Size-dependent cytotoxicity of silver nanoparticles in human lung cells: the role of cellular uptake, agglomeration and Ag release. *Part Fibre Toxicol* **2014**, *11*, 11, doi:10.1186/1743-8977-11-11.
106. Foldbjerg, R.; Dang, D.A.; Autrup, H. Cytotoxicity and genotoxicity of silver nanoparticles in the human lung cancer cell line, A549. *Arch Toxicol* **2011**, *85*, 743-750, doi:10.1007/s00204-010-0545-5.
107. Annangi, B.; Rubio, L.; Alaraby, M.; Bach, J.; Marcos, R.; Hernandez, A. Acute and long-term in vitro effects of zinc oxide nanoparticles. *Arch Toxicol* **2016**, *90*, 2201-2213, doi:10.1007/s00204-015-1613-7.
108. Heng, B.C.; Zhao, X.; Xiong, S.; Ng, K.W.; Boey, F.Y.; Loo, J.S. Toxicity of zinc oxide (ZnO) nanoparticles on human bronchial epithelial cells (BEAS-2B) is accentuated by oxidative stress. *Food Chem Toxicol* **2010**, *48*, 1762-1766, doi:10.1016/j.fct.2010.04.023.
109. El Yamani, N.; Collins, A.R.; Runden-Pran, E.; Fjellsbo, L.M.; Shaposhnikov, S.; Zienolddiny, S.; Dusinska, M. In vitro genotoxicity testing of four reference metal nanomaterials, titanium dioxide, zinc oxide, cerium oxide and silver: towards reliable hazard assessment. *Mutagenesis* **2017**, *32*, 117-126, doi:10.1093/mutage/gew060.
110. V. Ramalingam; S. Revathidevi; T. Shanmuganayagam; L. Muthulakshmi; Rajaram, R. Biogenic gold nanoparticles induce cell cycle arrest through oxidative stress and sensitize mitochondrial membranes in A549 lung cancer cells *Rsc Adv* **2016**, *6*, 20598-20608, doi:10.1039/C5RA26781A.
111. Park, E.J.; Yi, J.; Chung, K.H.; Ryu, D.Y.; Choi, J.; Park, K. Oxidative stress and apoptosis induced by titanium dioxide nanoparticles in cultured BEAS-2B cells. *Toxicol Lett* **2008**, *180*, 222-229, doi:10.1016/j.toxlet.2008.06.869.
112. Park, E.J.; Choi, J.; Park, Y.K.; Park, K. Oxidative stress induced by cerium oxide nanoparticles in cultured BEAS-2B cells. *Toxicology* **2008**, *245*, 90-100, doi:10.1016/j.tox.2007.12.022.
113. Eom, H.J.; Choi, J. Oxidative stress of CeO_2 nanoparticles via p38-Nrf-2 signaling pathway in human bronchial epithelial cell, Beas-2B. *Toxicol Lett* **2009**, *187*, 77-83, doi:10.1016/j.toxlet.2009.01.028.
114. Gabelova, A.; El Yamani, N.; Alonso, T.I.; Buliakova, B.; Srancikova, A.; Babelova, A.; Pran, E.R.; Fjellsbo, L.M.; Elje, E.; Yazdani, M., et al. Fibrous

shape underlies the mutagenic and carcinogenic potential of nanosilver while surface chemistry affects the biosafety of iron oxide nanoparticles. *Mutagenesis* **2017**, *32*, 193-202, doi:10.1093/mutage/gew045.
115. Ishida, T.; Fujihara, N.; Nishimura, T.; Funabashi, H.; Hirota, R.; Ikeda, T.; Kuroda, A. Live-cell imaging of macrophage phagocytosis of asbestos fibers under fluorescence microscopy. *Genes Environ* **2019**, *41*, 14, doi:10.1186/s41021-019-0129-4.
116. Donaldson, K.; Murphy, F.A.; Duffin, R.; Poland, C.A. Asbestos, carbon nanotubes and the pleural mesothelium: a review of the hypothesis regarding the role of long fibre retention in the parietal pleura, inflammation and mesothelioma. *Part Fibre Toxicol* **2010**, *7*, 5, doi:10.1186/1743-8977-7-5.
117. Hartung, T.; Rovida, C. Chemical regulators have overreached. *Nature* **2009**, *460*, 1080-1081, doi:10.1038/4601080a.
118. Demokritou, P.; Gass, S.; Pyrgiotakis, G.; Cohen, J.M.; Goldsmith, W.; McKinney, W.; Frazer, D.; Ma, J.; Schwegler-Berry, D.; Brain, J., et al. An in vivo and in vitro toxicological characterisation of realistic nanoscale CeO_2 inhalation exposures. *Nanotoxicology* **2013**, *7*, 1338-1350, doi:10.3109/17435390.2012.739665.
119. Otmar Schmid; Stoeger, T. Surface area is the biologically most effective dose metric for acute nanoparticle toxicity in the lung. *J Aerosol Sci* **2016**, *99*, 133-143, doi:10.1016/j.jaerosci.2015.12.006.
120. Kasai, T.; Umeda, Y.; Ohnishi, M.; Kondo, H.; Takeuchi, T.; Aiso, S.; Nishizawa, T.; Matsumoto, M.; Fukushima, S. Thirteen-week study of toxicity of fiber-like multi-walled carbon nanotubes with whole-body inhalation exposure in rats. *Nanotoxicology* **2015**, *9*, 413-422, doi:10.3109/17435390.2014.933903.
121. Loomis, D.; Dement, J.; Richardson, D.; Wolf, S. Asbestos fibre dimensions and lung cancer mortality among workers exposed to chrysotile. *Occup Environ Med* **2010**, *67*, 580-584, doi:10.1136/oem.2009.050120.
122. Aalapati, S.; Ganapathy, S.; Manapuram, S.; Anumolu, G.; Prakya, B.M. Toxicity and bio-accumulation of inhaled cerium oxide nanoparticles in CD1 mice. *Nanotoxicology* **2014**, *8*, 786-798, doi:10.3109/17435390.2013.829877.
123. W. M. S. Russell; Burch, R.L. *The Principles of Humane Experimental Technique*; Methuen: 1959.
124. Mülhopt, S.; Dilger, M.; Diabate, S.; Schlager, C.; Krebs, T.; Zimmermann, R.; Buters, J.; Oeder, S.; Wascher, T.; Weiss, C., et al. Toxicity testing of combustion aerosols at the air-liquid interface with a self-contained and easy-to-use exposure system. *J Aerosol Sci* **2016**, *96*, 38-55, doi:10.1016/j.jaerosci.2016.02.005.
125. Pezzulo, A.A.; Starner, T.D.; Scheetz, T.E.; Traver, G.L.; Tilley, A.E.; Harvey, B.G.; Crystal, R.G.; McCray, P.B., Jr.; Zabner, J. The air-liquid interface and use of primary cell cultures are important to recapitulate the transcriptional profile of in vivo airway epithelia. *Am J Physiol Lung Cell Mol Physiol* **2011**, *300*, L25-31, doi:10.1152/ajplung.00256.2010.
126. Jiang Bing; Xu Xiao; David Julian McClements; Yuan Biao; Chongjiang, C. Protein corona formation around inorganic nanoparticles: Food plant proteins-TiO_2 nanoparticle interactions. *Food Hydrocolloids* **2021**, *115*, doi:10.1016/j.foodhyd.2021.106594.

127. Kim, H.; Roth, D.; Isoe, Y.; Hayashi, K.; Mochizuki, C.; Kalkum, M.; Nakamura, M. Protein corona components of polyethylene glycol-conjugated organosilica nanoparticles modulates macrophage uptake. *Colloids Surf B Biointerfaces* **2020**, *199*, doi:10.1016/j.colsurfb.2020.111527.
128. Chortarea, S.; Barosova, H.; Clift, M.J.D.; Wick, P.; Petri-Fink, A.; Rothen-Rutishauser, B. Human Asthmatic Bronchial Cells Are More Susceptible to Subchronic Repeated Exposures of Aerosolized Carbon Nanotubes At Occupationally Relevant Doses Than Healthy Cells. *Acs Nano* **2017**, *11*, 7615-7625, doi:10.1021/acsnano.7b01992.
129. Savi, M.; Kalberer, M.; Lang, D.; Ryser, M.; Fierz, M.; Gaschen, A.; Ricka, J.; Geiser, M. A novel exposure system for the efficient and controlled deposition of aerosol particles onto cell cultures. *Environ Sci Technol* **2008**, *42*, 5667-5674, doi:10.1021/es703075q.
130. Mertes, P.; Praplan, A.P.; Kunzi, L.; Dommen, J.; Baltensperger, U.; Geiser, M.; Weingartner, E.; Ricka, J.; Fierz, M.; Kalberer, M. A compact and portable deposition chamber to study nanoparticles in air-exposed tissue. *J Aerosol Med Pulm Drug Deliv* **2013**, *26*, 228-235, doi:10.1089/jamp.2012.0985.
131. Brandenberger, C.; Rothen-Rutishauser, B.; Muhlfeld, C.; Schmid, O.; Ferron, G.A.; Maier, K.L.; Gehr, P.; Lenz, A.G. Effects and uptake of gold nanoparticles deposited at the air-liquid interface of a human epithelial airway model. *Toxicol Appl Pharmacol* **2010**, *242*, 56-65, doi:10.1016/j.taap.2009.09.014.
132. Seagrave, J.; McDonald, J.D.; Mauderly, J.L. In vitro versus in vivo exposure to combustion emissions. *Exp Toxicol Pathol* **2005**, *57*, 233-238, doi:10.1016/j.etp.2005.05.011.
133. Ingeborg M. Kooter; Mariska Gröllers-Mulderij; Maaike Steenhof; Evert Duistermaat; Frederique A.A. van Acker; Yvonne C.M. Staal; Peter C. Tromp; Eric Schoen; C. Frieke Kuper; Someren, E.v. Cellular Effects in an In Vitro Human 3D Cellular Airway Model and A549/BEAS-2B In Vitro Cell Cultures Following Air Exposure to Cerium Oxide Particles at an Air–Liquid Interface. *APPLIED IN VITRO TOXICOLOGY* **2016**, *2*, 56-66, doi:10.1089/aivt.2015.0030.
134. Durantie, E.; Vanhecke, D.; Rodriguez-Lorenzo, L.; Delhaes, F.; Balog, S.; Septiadi, D.; Bourquin, J.; Petri-Fink, A.; Rothen-Rutishauser, B. Biodistribution of single and aggregated gold nanoparticles exposed to the human lung epithelial tissue barrier at the air-liquid interface. *Part Fibre Toxicol* **2017**, *14*, 49, doi:10.1186/s12989-017-0231-3.
135. Lenz, A.G.; Karg, E.; Lentner, B.; Dittrich, V.; Brandenberger, C.; Rothen-Rutishauser, B.; Schulz, H.; Ferron, G.A.; Schmid, O. A dose-controlled system for air-liquid interface cell exposure and application to zinc oxide nanoparticles. *Part Fibre Toxicol* **2009**, *6*, doi:10.1186/1743-8977-6-32.
136. Kim, J.S.; Peters, T.M.; O'Shaughnessy, P.T.; Adamcakova-Dodd, A.; Thorne, P.S. Validation of an in vitro exposure system for toxicity assessment of air-delivered nanomaterials. *Toxicol in Vitro* **2013**, *27*, 164-173, doi:10.1016/j.tiv.2012.08.030.
137. Fytianos, K.; Chortarea, S.; Rodriguez-Lorenzo, L.; Blank, F.; von Garnier, C.; Petri-Fink, A.; Rothen-Rutishauser, B. Aerosol Delivery of Functionalized Gold Nanoparticles Target and Activate Dendritic Cells in a 3D Lung Cellular Model. *Acs Nano* **2017**, *11*, 375-383, doi:10.1021/acsnano.6b06061.
138. Doryab, A.; Taskin, M.B.; Stahlhut, P.; Schroppel, A.; Orak, S.; Voss, C.; Ahluwalia, A.; Rehberg, M.; Hilgendorff, A.; Stoger, T., et al. A Bioinspired in

vitro Lung Model to Study Particokinetics of Nano-/Microparticles Under Cyclic Stretch and Air-Liquid Interface Conditions. *Front Bioeng Biotechnol* **2021**, *9*, 616830, doi:10.3389/fbioe.2021.616830.

139. Noel, A.; Hossain, E.; Perveen, Z.; Zaman, H.; Penn, A.L. Sub-ohm vaping increases the levels of carbonyls, is cytotoxic, and alters gene expression in human bronchial epithelial cells exposed at the air-liquid interface. *Respir Res* **2020**, *21*, 305, doi:10.1186/s12931-020-01571-1.
140. Giralt, A.; Iskandar, A.R.; Martin, F.; Moschini, E.; Serchi, T.; Kondylis, A.; Marescotti, D.; Leroy, P.; Ortega-Torres, L.; Majeed, S., et al. Comparison of the biological impact of aerosol of e-vapor device with MESH® technology and cigarette smoke on human bronchial and alveolar cultures. *Toxicol Lett* **2021**, *337*, 98-110, doi:10.1016/j.toxlet.2020.11.006.
141. Diabate, S.; Armand, L.; Murugadoss, S.; Dilger, M.; Fritsch-Decker, S.; Schlager, C.; Beal, D.; Arnal, M.E.; Biola-Clier, M.; Ambrose, S., et al. Air-Liquid Interface Exposure of Lung Epithelial Cells to Low Doses of Nanoparticles to Assess Pulmonary Adverse Effects. *Nanomaterials* **2020**, *11*, 65, doi:10.3390/nano11010065.
142. A. Tippe; U. Heinzmann; Roth, C. Deposition of fine and ultrafine aerosol particles during exposure at the air/cell interface. *Aerosol Science* **2002**, *33*, 207–218, doi:10.1016/S0021-8502(01)00158-6.
143. Lacroix, G.; Koch, W.; Ritter, D.; Gutleb, A.C.; Larsen, S.T.; Loret, T.; Zanetti, F.; Constant, S.; Chortarea, S.; Rothen-Rutishauser, B., et al. Air–Liquid Interface In Vitro Models for Respiratory Toxicology Research: Consensus Workshop and Recommendations. *Applied In Vitro Toxicology* **2018**, *4*, 91-106, doi:10.1089/aivt.2017.0034.
144. Steiner, S.; Majeed, S.; Kratzer, G.; Hoeng, J.; Frentzel, S. A new fluorescence-based method for characterizing in vitro aerosol exposure systems. *Toxicol in Vitro* **2017**, *38*, 150-158, doi:10.1016/j.tiv.2016.09.018.
145. Gosens, I.; Mathijssen, L.E.; Bokkers, B.G.; Muijser, H.; Cassee, F.R. Comparative hazard identification of nano- and micro-sized cerium oxide particles based on 28-day inhalation studies in rats. *Nanotoxicology* **2014**, *8*, 643-653, doi:10.3109/17435390.2013.815814.
146. Pfuhler, S.; Pirow, R.; Downs, T.R.; Haase, A.; Hewitt, N.; Luch, A.; Merkel, M.; Petrick, C.; Said, A.; Schafer-Korting, M., et al. Validation of the 3D reconstructed human skin Comet assay, an animal-free alternative for following-up positive results from standard in vitro genotoxicity assays. *Mutagenesis* **2021**, *36*, 19-35, doi:10.1093/mutage/geaa009.
147. Wang, H.; He, L.; Liu, B.; Feng, Y.; Zhou, H.; Zhang, Z.; Wu, Y.; Wang, J.; Gan, Y.; Yuan, T., et al. Establishment and comparison of air-liquid interface culture systems for primary and immortalized swine tracheal epithelial cells. *BMC Cell Biol* **2018**, *19*, doi:10.1186/s12860-018-0162-3.
148. Loretta Müller; Michael Gasser; David O. Raemy; Fabian Herzog; Christina Brandenberger; Otmar Schmid; Peter Gehr; Barbara Rothen-Rutishauser; Clift, M.J.D. Realistic Exposure Methods for Investigating the Interaction of Nanoparticles with the Lung at the Air-Liquid Interface In Vitro. *Insciences J.* **2011**, *1*, 30-36, doi:10.5640/insc.010130.
149. Upadhyay, S.; Palmberg, L. Air-Liquid Interface: Relevant In Vitro Models for Investigating Air Pollutant-Induced Pulmonary Toxicity. *Toxicol Sci* **2018**, *164*, 21-30, doi:10.1093/toxsci/kfy053.

150. Sayes, C.M.; Reed, K.L.; Warheit, D.B. Assessing toxicity of fine and nanoparticles: Comparing in vitro measurements to in vivo pulmonary toxicity profiles. *Toxicol Sci* **2007**, *97*, 163-180, doi:10.1093/toxsci/kfm018.
151. Barbara Drasler; Phil Sayre; Klaus Günter Steinhäuser; Alke Petri-Fink; Rothen-Rutishauser, B. In vitro approaches to assess the hazard of nanomaterials. *NanoImpact* **2017**, *8*, 99-116, doi:10.1016/j.impact.2017.08.002.
152. Teeguarden, J.G.; Mikheev, V.B.; Minard, K.R.; Forsythe, W.C.; Wang, W.; Sharma, G.; Karin, N.; Tilton, S.C.; Waters, K.M.; Asgharian, B., et al. Comparative iron oxide nanoparticle cellular dosimetry and response in mice by the inhalation and liquid cell culture exposure routes. *Part Fibre Toxicol* **2014**, *11*, doi:10.1186/s12989-014-0046-4.
153. Jing, X.F.; Park, J.H.; Peters, T.M.; Thorne, P.S. Toxicity of copper oxide nanoparticles in lung epithelial cells exposed at the air-liquid interface compared with in vivo assessment. *Toxicol in Vitro* **2015**, *29*, 502-511, doi:10.1016/j.tiv.2014.12.023.
154. Gangwal, S.; Brown, J.S.; Wang, A.; Houck, K.A.; Dix, D.J.; Kavlock, R.J.; Hubal, E.A. Informing selection of nanomaterial concentrations for ToxCast in vitro testing based on occupational exposure potential. *Environ Health Perspect* **2011**, *119*, 1539-1546, doi:10.1289/ehp.1103750.
155. Erdely, A.; Dahm, M.; Chen, B.T.; Zeidler-Erdely, P.C.; Fernback, J.E.; Birch, M.E.; Evans, D.E.; Kashon, M.L.; Deddens, J.A.; Hulderman, T., et al. Carbon nanotube dosimetry: from workplace exposure assessment to inhalation toxicology. *Part Fibre Toxicol* **2013**, *10*, 53, doi:10.1186/1743-8977-10-53.
156. Cassee, F.R.; Campbell, A.; Boere, A.J.; McLean, S.G.; Duffin, R.; Krystek, P.; Gosens, I.; Miller, M.R. The biological effects of subacute inhalation of diesel exhaust following addition of cerium oxide nanoparticles in atherosclerosis-prone mice. *Environ Res* **2012**, *115*, 1-10, doi:10.1016/j.envres.2012.03.004.
157. Park, B.; Donaldson, K.; Duffin, R.; Tran, L.; Kelly, F.; Mudway, I.; Morin, J.P.; Guest, R.; Jenkinson, P.; Samaras, Z., et al. Hazard and risk assessment of a nanoparticulate cerium oxide-based diesel fuel additive - A case study. *Inhal Toxicol* **2008**, *20*, 547-566, doi:10.1080/08958370801915309.
158. Erdakos, G.B.; Bhave, P.V.; Pouliot, G.A.; Simon, H.; Mathur, R. Predicting the Effects of Nanoscale Cerium Additives in Diesel Fuel on Regional-Scale Air Quality. *Environ Sci Technol* **2014**, *48*, 12775-12782, doi:10.1021/es504050g.
159. Giese, B.; Klaessig, F.; Park, B.; Kaegi, R.; Steinfeldt, M.; Wigger, H.; von Gleich, A.; Gottschalk, F. Risks, Release and Concentrations of Engineered Nanomaterial in the Environment. *Sci Rep-Uk* **2018**, *8*, 1565, doi:10.1038/s41598-018-19275-4.
160. Liu, H.H.; Cohen, Y. Multimedia environmental distribution of engineered nanomaterials. *Environ Sci Technol* **2014**, *48*, 3281-3292, doi:10.1021/es405132z.
161. Gantt, B.; Hoque, S.; Willis, R.D.; Fahey, K.M.; Delgado-Saborit, J.M.; Harrison, R.M.; Erdakos, G.B.; Bhave, P.V.; Zhang, K.M.; Kovalcik, K., et al. Near-road modeling and measurement of cerium-containing particles generated by nanoparticle diesel fuel additive use. *Environ Sci Technol* **2014**, *48*, 10607-10613, doi:10.1021/es502169p.
162. George, I.; Vranic, S.; Boland, S.; Courtois, A.; Baeza-Squiban, A. Development of an in vitro model of human bronchial epithelial barrier to study

nanoparticle translocation. *Toxicol in Vitro* **2015**, *29*, 51-58, doi:10.1016/j.tiv.2014.08.003.
163. Rothen-Rutishauser, B.M.; Kiama, S.G.; Gehr, P. A three-dimensional cellular model of the human respiratory tract to study the interaction with particles. *Am J Respir Cell Mol Biol* **2005**, *32*, 281-289, doi:10.1165/rcmb.2004-0187OC.
164. Klein, S.G.; Serchi, T.; Hoffmann, L.; Blomeke, B.; Gutleb, A.C. An improved 3D tetraculture system mimicking the cellular organisation at the alveolar barrier to study the potential toxic effects of particles on the lung. *Part Fibre Toxicol* **2013**, *10*, 31, doi:10.1186/1743-8977-10-31.
165. Sauer, U.G.; Vogel, S.; Hess, A.; Kolle, S.N.; Ma-Hock, L.; van Ravenzwaay, B.; Landsiedel, R. In vivo-in vitro comparison of acute respiratory tract toxicity using human 3D airway epithelial models and human A549 and murine 3T3 monolayer cell systems. *Toxicol in Vitro* **2013**, *27*, 174-190, doi:10.1016/j.tiv.2012.10.007.
166. Barosova, H.; Maione, A.G.; Septiadi, D.; Sharma, M.; Haeni, L.; Balog, S.; O'Connell, O.; Jackson, G.R.; Brown, D.; Clippinger, A.J., et al. Use of EpiAlveolar Lung Model to Predict Fibrotic Potential of Multiwalled Carbon Nanotubes. *Acs Nano* **2020**, *14*, 3941-3956, doi:10.1021/acsnano.9b06860.
167. Huh, D.; Matthews, B.D.; Mammoto, A.; Montoya-Zavala, M.; Hsin, H.Y.; Ingber, D.E. Reconstituting organ-level lung functions on a chip. *Science* **2010**, *328*, 1662-1668, doi:10.1126/science.1188302.
168. Stucki, A.O.; Stucki, J.D.; Hall, S.R.; Felder, M.; Mermoud, Y.; Schmid, R.A.; Geiser, T.; Guenat, O.T. A lung-on-a-chip array with an integrated bio-inspired respiration mechanism. *Lab Chip* **2015**, *15*, 1302-1310, doi:10.1039/c4lc01252f.
169. Hirn, S.; Haberl, N.; Loza, K.; Epple, M.; Kreyling, W.G.; Rothen-Rutishauser, B.; Rehberg, M.; Krombach, F. Proinflammatory and cytotoxic response to nanoparticles in precision-cut lung slices. *Beilstein J Nanotechnol* **2014**, *5*, 2440-2449, doi:10.3762/bjnano.5.253.
170. Sauer, U.G.; Vogel, S.; Aumann, A.; Hess, A.; Kolle, S.N.; Ma-Hock, L.; Wohlleben, W.; Dammann, M.; Strauss, V.; Treumann, S., et al. Applicability of rat precision-cut lung slices in evaluating nanomaterial cytotoxicity, apoptosis, oxidative stress, and inflammation. *Toxicol Appl Pharmacol* **2014**, *276*, 1-20, doi:10.1016/j.taap.2013.12.017.
171. Giard, D.J.; Aaronson, S.A.; Todaro, G.J.; Arnstein, P.; Kersey, J.H.; Dosik, H.; Parks, W.P. In vitro cultivation of human tumors: establishment of cell lines derived from a series of solid tumors. *J Natl Cancer Inst* **1973**, *51*, 1417-1423, doi:10.1093/jnci/51.5.1417.
172. Srinivasan, B.; Kolli, A.R.; Esch, M.B.; Abaci, H.E.; Shuler, M.L.; Hickman, J.J. TEER measurement techniques for in vitro barrier model systems. *J Lab Autom* **2015**, *20*, 107-126, doi:10.1177/2211068214561025.
173. Winton, H.L.; Wan, H.; Cannell, M.B.; Gruenert, D.C.; Thompson, P.J.; Garrod, D.R.; Stewart, G.A.; Robinson, C. Cell lines of pulmonary and non-pulmonary origin as tools to study the effects of house dust mite proteinases on the regulation of epithelial permeability. *Clin Exp Allergy* **1998**, *28*, 1273-1285, doi:10.1046/j.1365-2222.1998.00354.x.
174. Kuehn, A.; Kletting, S.; de Souza Carvalho-Wodarz, C.; Repnik, U.; Griffiths, G.; Fischer, U.; Meese, E.; Huwer, H.; Wirth, D.; May, T., et al. Human alveolar

epithelial cells expressing tight junctions to model the air-blood barrier. *ALTEX* **2016**, *33*, 251-260, doi:10.14573/altex.1511131.
175. Crapo, J.D.; Barry, B.E.; Gehr, P.; Bachofen, M.; Weibel, E.R. Cell number and cell characteristics of the normal human lung. *Am Rev Respir Dis* **1982**, *126*, 332-337, doi:10.1164/arrd.1982.126.2.332.
176. Movia, D.; Bruni-Favier, S.; Prina-Mello, A. In vitro Alternatives to Acute Inhalation Toxicity Studies in Animal Models-A Perspective. *Front Bioeng Biotechnol* **2020**, *8*, doi:10.3389/fbioe.2020.00549.
177. Lee, Y.S.; Sung, J.H.; Song, K.S.; Kim, J.K.; Choi, B.S.; Yu, I.J.; Park, J.D. Derivation of occupational exposure limits for multi-walled carbon nanotubes and graphene using subchronic inhalation toxicity data and a multi-path particle dosimetry model. *Toxicology Research* **2019**, *8*, 580-586, doi:10.1039/c9tx00026g.
178. Keller, J.; Wohlleben, W.; Ma-Hock, L.; Strauss, V.; Groters, S.; Kuttler, K.; Wiench, K.; Herden, C.; Oberdorster, G.; van Ravenzwaay, B., et al. Time course of lung retention and toxicity of inhaled particles: short-term exposure to nano-Ceria. *Arch Toxicol* **2014**, *88*, 2033-2059, doi:10.1007/s00204-014-1349-9.
179. Petersen, E.J.; Sharma, M.; Clippinger, A.J.; Gordon, J.; Katz, A.; Laux, P.; Leibrock, L.B.; Luch, A.; Matheson, J.; Stucki, A.O., et al. Use of Cause-and-Effect Analysis to Optimize the Reliability of In Vitro Inhalation Toxicity Measurements Using an Air-Liquid Interface. *Chem Res Toxicol* **2021**, *34*, 1370-1385, doi:10.1021/acs.chemrestox.1c00080.
180. Leibrock, L.B.; Jungnickel, H.; Tentschert, J.; Katz, A.; Toman, B.; Petersen, E.J.; Bierkandt, F.S.; Singh, A.V.; Laux, P.; Luch, A. Parametric Optimization of an Air-Liquid Interface System for Flow-Through Inhalation Exposure to Nanoparticles: Assessing Dosimetry and Intracellular Uptake of CeO_2 Nanoparticles. *Nanomaterials* **2020**, *10*, 2369, doi:10.3390/nano10122369.
181. Zavala, J.; Greenan, R.; Krantz, Q.T.; DeMarini, D.M.; Higuchi, M.; Gilmour, M.I.; White, P.A. Regulating temperature and relative humidity in air-liquid interface in vitro systems eliminates cytotoxicity resulting from control air exposures. *Toxicology Research* **2017**, *6*, 448-459, doi:10.1039/c7tx00109f.
182. House, J.S.; Bouzos, E.; Fahy, K.M.; Francisco, V.M.; Lloyd, D.T.; Wright, F.A.; Motsinger-Reif, A.A.; Asuri, P.; Wheeler, K.E. Low-Dose Silver Nanoparticle Surface Chemistry and Temporal Effects on Gene Expression in Human Liver Cells. *Small* **2020**, *16*, e2000299, doi:10.1002/smll.202000299.
183. Duval, K.E.A.; Vernice, N.A.; Wagner, R.J.; Fiering, S.N.; Petryk, J.D.; Lowry, G.J.; Tau, S.S.; Yin, J.; Houde, G.R.; Chaudhry, A.S., et al. Immunogenetic effects of low dose (CEM43 30) magnetic nanoparticle hyperthermia and radiation in melanoma cells. *Int J Hyperthermia* **2019**, *36*, 37-46, doi:10.1080/02656736.2019.1627433.
184. Skalska, J.; Dabrowska-Bouta, B.; Frontczak-Baniewicz, M.; Sulkowski, G.; Struzynska, L. A Low Dose of Nanoparticulate Silver Induces Mitochondrial Dysfunction and Autophagy in Adult Rat Brain. *Neurotox Res* **2020**, *38*, 650-664, doi:10.1007/s12640-020-00239-4.
185. De, A.; Ghosh, S.; Chakrabarti, M.; Ghosh, I.; Banerjee, R.; Mukherjee, A. Effect of low-dose exposure of aluminium oxide nanoparticles in Swiss albino mice: Histopathological changes and oxidative damage. *Toxicol Ind Health* **2020**, *36*, 567-579, doi:10.1177/0748233720936828.

186. Leibrock, L.; Wagener, S.; Singh, A.V.; Laux, P.; Luch, A. Nanoparticle induced barrier function assessment at liquid–liquid and air–liquid interface in novel human lung epithelia cell lines. *Toxicology Research* **2019**, *8*, 1016-1027, doi:10.1039/c9tx00179d.
187. Morimoto, Y.; Izumi, H.; Yoshiura, Y.; Tomonaga, T.; Oyabu, T.; Myojo, T.; Kawai, K.; Yatera, K.; Shimada, M.; Kubo, M., et al. Pulmonary toxicity of well-dispersed cerium oxide nanoparticles following intratracheal instillation and inhalation. *J Nanopart Res* **2015**, *17*, 442, doi:10.1007/s11051-015-3249-1.
188. Ding, Y.; Weindl, P.; Lenz, A.G.; Mayer, P.; Krebs, T.; Schmid, O. Quartz crystal microbalances (QCM) are suitable for real-time dosimetry in nanotoxicological studies using VITROCELL ® Cloud cell exposure systems. *Part Fibre Toxicol* **2020**, *17*, doi:10.1186/s12989-020-00376-w.
189. Phuyal, S.; Kasem, M.; Rubio, L.; Karlsson, H.L.; Marcos, R.; Skaug, V.; Zienolddiny, S. Effects on human bronchial epithelial cells following low-dose chronic exposure to nanomaterials: A 6-month transformation study. *Toxicol in Vitro* **2017**, *44*, 230-240, doi:10.1016/j.tiv.2017.07.016.
190. Luyts, K.; Napierska, D.; Dinsdale, D.; Klein, S.G.; Serchi, T.; Hoet, P.H. A coculture model of the lung-blood barrier: the role of activated phagocytic cells. *Toxicol in Vitro* **2015**, *29*, 234-241, doi:10.1016/j.tiv.2014.10.024.
191. Ballweg, S.; Sezgin, E.; Doktorova, M.; Covino, R.; Reinhard, J.; Wunnicke, D.; Hanelt, I.; Levental, I.; Hummer, G.; Ernst, R. Regulation of lipid saturation without sensing membrane fluidity. *Nat Commun* **2020**, *11*, doi:10.1038/s41467-020-14528-1.
192. Liu, Z.; Xia, Y.; Li, B.; Xu, H.; Wang, C.; Liu, Y.; Li, Y.; Li, C.; Gao, N.; Li, L. Induction of ER stress-mediated apoptosis by ceramide via disruption of ER Ca(2+) homeostasis in human adenoid cystic carcinoma cells. *Cell Biosci* **2014**, *4*, doi:10.1186/2045-3701-4-71.
193. Haimovitz-Friedman, A.; Kolesnick, R.N.; Fuks, Z. Ceramide signaling in apoptosis. *Br Med Bull* **1997**, *53*, 539-553, doi:10.1093/oxfordjournals.bmb.a011629.
194. Geraets, L.; Oomen, A.G.; Schroeter, J.D.; Coleman, V.A.; Cassee, F.R. Tissue distribution of inhaled micro- and nano-sized cerium oxide particles in rats: results from a 28-day exposure study. *Toxicol Sci* **2012**, *127*, 463-473, doi:10.1093/toxsci/kfs113.
195. Yaobo Ding; Riediker, M. A system to assess the stability of airborne nanoparticle agglomerates under aerodynamic shear. *J Aerosol Sci* **2015**, *88*, 98-108, doi:10.1016/j.jaerosci.2015.06.001.
196. Blauer, M.; Sand, J.; Laukkarinen, J. Regulation of p38 MAPK and glucocorticoid receptor activation by hydrocortisone in mono-and co-cultured pancreatic acinar and stellate cells. *Pancreatology* **2021**, *21*, 384-389, doi:10.1016/j.pan.2020.12.024.
197. Kletting, S.; Barthold, S.; Repnik, U.; Griffiths, G.; Loretz, B.; Schneider-Daum, N.; de Souza Carvalho-Wodarz, C.; Lehr, C.M. Co-culture of human alveolar epithelial (hAELVi) and macrophage (THP-1) cell lines. *ALTEX* **2018**, *35*, 211-222, doi:10.14573/altex.1607191.
198. Maschmeyer, I.; Lorenz, A.K.; Schimek, K.; Hasenberg, T.; Ramme, A.P.; Hubner, J.; Lindner, M.; Drewell, C.; Bauer, S.; Thomas, A., et al. A four-organ-chip for interconnected long-term co-culture of human intestine, liver, skin and kidney equivalents. *Lab Chip* **2015**, *15*, 2688-2699, doi:10.1039/c5lc00392j.

199. Mihalache, R.; Verbeek, J.; Graczyk, H.; Murashov, V.; van Broekhuizen, P. Occupational exposure limits for manufactured nanomaterials, a systematic review. *Nanotoxicology* **2017**, *11*, 7-19, doi:10.1080/17435390.2016.1262920.
200. Schulte, P.A.; Kuempel, E.D.; Drew, N.M. Characterizing risk assessments for the development of occupational exposure limits for engineered nanomaterials. *Regul Toxicol Pharm* **2018**, *95*, 207-219, doi:10.1016/j.yrtph.2018.03.018.
201. Paur, H.R.; Cassee, F.R.; Teeguarden, J.; Fissan, H.; Diabate, S.; Aufderheide, M.; Kreyling, W.G.; Hanninen, O.; Kasper, G.; Riediker, M., et al. In-vitro cell exposure studies for the assessment of nanoparticle toxicity in the lung-A dialog between aerosol science and biology. *J Aerosol Sci* **2011**, *42*, 668-692, doi:10.1016/j.jaerosci.2011.06.005.

7. List of publications

7.1 Publications integrated in the cumulative dissertation

1. **Lars Leibrock**, Sandra Wagener, Ajay Vikram Singh, Peter Laux and Andreas Luch: Nanoparticle induced barrier function assessment at liquid–liquid and air–liquid interface in novel human lung epithelia cell lines. *Toxicol. Res.*, 2019, **8**, 1016-1027, https://doi.org/10.1039/c9tx00179d

2. **Lars B. Leibrock,** Harald Jungnickel, Jutta Tentschert, Aaron Katz, Blaza Toman, Elijah J. Petersen, Frank S. Bierkandt, Ajay Vikram Singh, Peter Laux and Andreas Luch: Parametric Optimization of an Air–Liquid Interface System for Flow-Through Inhalation Exposure to Nanoparticles Assessing Dosimetry and Intracellular Uptake of CeO_2 Nanoparticles. *Nanomaterials* **2020**, *10*, 2369, https://doi.org/10.3390/nano10122369

7.2 Other Publications

1. Frank S. Bierkandt, **Lars Leibrock**, Sandra Wagener, Peter Laux and Andreas Luch: The impact of nanomaterial characteristics on inhalation toxicity. Toxicol. Res., 2018, **7**, 321-346, https://doi.org/10.1039/c7tx00242d

2. Ajay Vikram Singh, Harald Jungnickel, **Lars Leibrock**, Jutta Tentschert, Philipp Reichardt, Aaron Katz, Peter Laux & Andreas Luch: ToF-SIMS 3D imaging unveils important insights on the cellular microenvironment during biomineralization of gold nanostructures. *Sci Rep* (2020) **10**:261, https://doi.org/10.1038/s41598-019-57136-w

3. Elijah J Petersen, Monita Sharma, Amy J Clippinger, John Gordon, Aaron Katz, Peter Laux, **Lars B Leibrock**, Andreas Luch, Joanna Matheson, Andreas O Stucki, Jutta Tentschert, Frank S Bierkand: Use of Cause-and-Effect Analysis to Optimize the Reliability of *In Vitro* Inhalation Toxicity Measurements Using an Air-Liquid Interface. *Chem Res Toxicol.* 2021; **34**(6):1370-1385, https://doi.org/10.1021/acs.chemrestox.1c00080

4. Ajay Vikram Singh, Anthony Romeo, Kassandra Scott, Sandra Wagener, **Lars Leibrock**, Peter Laux, Andreas Luch, Pranali Kerkar, Shidin Balakrishnan, Sarada Prasad Dakua, Byung-Wook Park: Emerging Technologies for In Vitro Inhalation Toxicology, Adv. Healthcare Mater. 2021, **10**, 22100633 https://doi.org/10.1002/adhm.202100633

7.3 Conferences

1. Poster: 11th International particle toxicology conference (IPTC), 26-29 September 2016, Singapore: Dosimetry establishment for *in vitro* inhalation toxicity studies at the air-liquid interface

2. Poster: 20th International Congress on *In Vitro* Toxicology (ESTIV), 15-18 October 2018, Berlin: New human cell models mimicking various respiratory regions for nanoparticle toxicology - which is the more suitable?

Annex I

Supplementary Data

Parametric Optimization of an Air–Liquid Interface System for Flow-Through Inhalation Exposure to Nanoparticles Assessing Dosimetry and Intracellular Uptake of CeO_2 Nanoparticles

Lars B. Leibrock, Harald Jungnickel, Jutta Tentschert, Aaron Katz, Blaza Toman, Elijah J. Petersen, Frank S. Bierkandt, Ajay Vikram Singh, Peter Laux and Andreas Luch

This chapter was published online on 28.11.2020 in:

Nanomaterials **2020**, *10(12)*, 2369 by MDPI

https://doi.org/10.3390/nano10122369

Supplemental Information

Supplemental Methods

R-Code:

```
#The code requires that both R and OpenBUGS be installed, both are free to download.
#R can be obtained at http://www.R-project.org/ ,
#OpenBUGS at http://www.openbugs.net/w/Downloads.
#The only input to the program that is needed are the values in linedata.NP is the number of plates, NI is the number of inserts.
#Pasting the entire program below into an R window will produce the estimates of the statistics.
# If you run it with the debug =T in the bugs statement you can see if the MCMC has converged by looking at the trace plots.

################################################################################
library(R2OpenBUGS)

############## type data here:
linedata<-list(Solvent=c(0.1331,0.1323,0.1275,0.1275,0.1184,0.1237,0.116,0.0995,0.0995,0.0968,0.0997,0.0921,0.1016,0.0973,0.1008,0.1028,0.1937,0.1931,0.1945,0.1924,0.1936,0.1922),
Biorep=c(1,1,1,1,1,1,1,2,2,2,2,2,2,2,2,2,3,3,3,3,3,3),
NC=c(1.0665,0.9889,1.0056,0.9939,0.9718,0.9285,1.0537,1.0043,1.0278,1.1171,1.1137,1.1465,1.1589,1.1212,1.0924,1.2295,1.1762,1.2322,0.7171,0.7085,0.7259,0.6816,0.6819,0.6831,0.7026,0.7024,0.6986),
PlateNC=c(1,1,1,1,1,1,1,1,1,2,2,2,2,2,2,2,2,2,2,3,3,3,3,3,3,3,3,3),InsertNC=c(1,1,1,2,2,2,3,3,3,1,1,1,2,2,2,3,3,3,1,1,1,2,2,2,3,3,3),
measure=c(1.0684,1.0537,0.9642,1.0677,0.9511,0.9423,1.0096,1.0502,1.0162,0.9863,0.966,0.929,1.1151,1.0027,1.0638,1.0827,1.155,1.1005,0.7306,0.7318,0.736,0.7489,0.7512,0.7497,0.6063,0.6063,0.6021,1.0684,1.0537,0.9642,1.0677,0.9511,0.9423,1.0096,1.0502,1.0162,0.9863,0.966,0.929,1.1151,1.0027,1.0638,1.0827,1.155,1.1005,0.7306,0.7318,0.736,0.7489,0.7512,0.7497,0.6063,0.6063,0.6021),
parameter=c(1,1,1,1,1,1,1,1,1,1,1,1,1,1,1,1,1,1,1,1,1,1,1,1,2,2,2,2,2,2,2,2,2,2,2,2,2,2,2,2,2,2,2,2,2,2,2,2),
Plate=c(1,1,1,1,1,1,1,1,1,2,2,2,2,2,2,2,2,2,2,3,3,3,3,3,3,3,3,3,1,1,1,1,1,1,1,1,1,2,2,2,2,2,2,2,2,2,3,3,3,3,3,3,3,3),
Insert=c(1,1,1,2,2,2,3,3,3,1,1,1,2,2,2,3,3,3,1,1,1,2,2,2,3,3,3,1,1,1,2,2,2,3,3,3,1,1,1,2,2,2,3,3,3,1,1,1,2,2,2,3,3,3),NP=3,NI=3)
###############
##### OpenBUGS code and inits

lineinits<-function(){list(slvmu=c(0,0,0))}

linemodel <- function() {xinsig~dnorm(0,0.0016)%_%I(0.001,)
                         chsqnsig~dgamma(0.5,0.5)
                        sigNC<-xinsig/sqrt(chsqnsig)
```

```
for(i in 1:NP){slvmu[i]~dnorm(0,1.0E-5)
                        xins[i]~dnorm(0,0.0016)%_%I(0.001,)
                        chsqns[i]~dgamma(0.5,0.5)
                        slvtau[i]<-xins[i]/sqrt(chsqns[i])}
for(i in 1:22){Solvent[i]~dnorm(slvmu[Biorep[i]],slvtau[Biorep[i]])}

for(i in 1:NP){xinsNC[i]~dnorm(0,0.0016)%_%I(0.001,)
                        chsqnsNC[i]~dgamma(0.5,0.5)
                       tauNC[i]<-xinsNC[i]/sqrt(chsqnsNC[i])
                       NCmu[i]~dnorm(0,1.0E-5)}
for(i in 1:NP){
for(j in 1:NI){NCmean[i,j]~dnorm(NCmu[i],sigNC)}}
for(i in 1:27){
NC[i]~dnorm(NCmean[PlateNC[i],InsertNC[i]],tauNC[PlateNC[i]])}

for(i in 1:1){xinsigm[i]~dnorm(0,0.0016)%_%I(0.001,)
                        chsqnsigm[i]~dgamma(0.5,0.5)
                       sigm[i]<-xinsigm[i]/sqrt(chsqnsigm[i])
for(j in 1:NP){xinsmeas[i,j]~dnorm(0,0.0016)%_%I(0.001,)
                        chsqnsmeas[i,j]~dgamma(0.5,0.5)
                       taumeas[i,j]<-xinsmeas[i,j]/sqrt(chsqnsmeas[i,j])
                       measmu[i,j]~dnorm(0,1.0E-5)}}
for(i in 1:1){
for(j in 1:NP){
for(k in 1:NI){measmean[i,j,k]~dnorm(measmu[i,j],sigm[i])}}}

for(i                                                                                    in
1:27){measure[i]~dnorm(measmean[parameter[i],Plate[i],Insert[i]],taumeas[parameter[i],Plate[i]])}
for(i in 1:1){
for(j in 1:NP){
                        viabmu[i,j]<-(measmu[i,j]-slvmu[j])/(NCmu[j]-slvmu[j])*100}}
#for(i in 1:NP){viabdif[i]<-viabmu[1,i]-viabmu[2,i]}

##########################################

#Tf~dcat(Pf[])
#Pf[1:NP]~ddirich(alphaf[])
#for(i in 1:NP){alphaf[i]<-1}
#viabdiffin<-viabdif[Tf]

T~dcat(P[])
P[1:NP]~ddirich(alpha[])
```

```
for(i in 1:NP){alpha[i]<-1}
for(i in 1:1){viabmufin[i]<-viabmu[i,T]}

}

  ###### run the OpenBUGS
lineout<-bugs(data=linedata,inits=lineinits,digits=5,parameters=c("viabmu","viabmufin","measmean
","measmu"),model.file=linemodel,n.chains=1,n.iter=40000,n.burnin=25000,n.thin=10,debug=T)
##### print output
attach.bugs(lineout) ## imports the statistics
## in the output: viabmu are the % viability values for the two parameters, viabdif is the difference,
## viabmufin and viabdiffin are the Linear Pool consensus values for these parameters.
#####
print (lineout, digits=3)
```

Supplemental Results

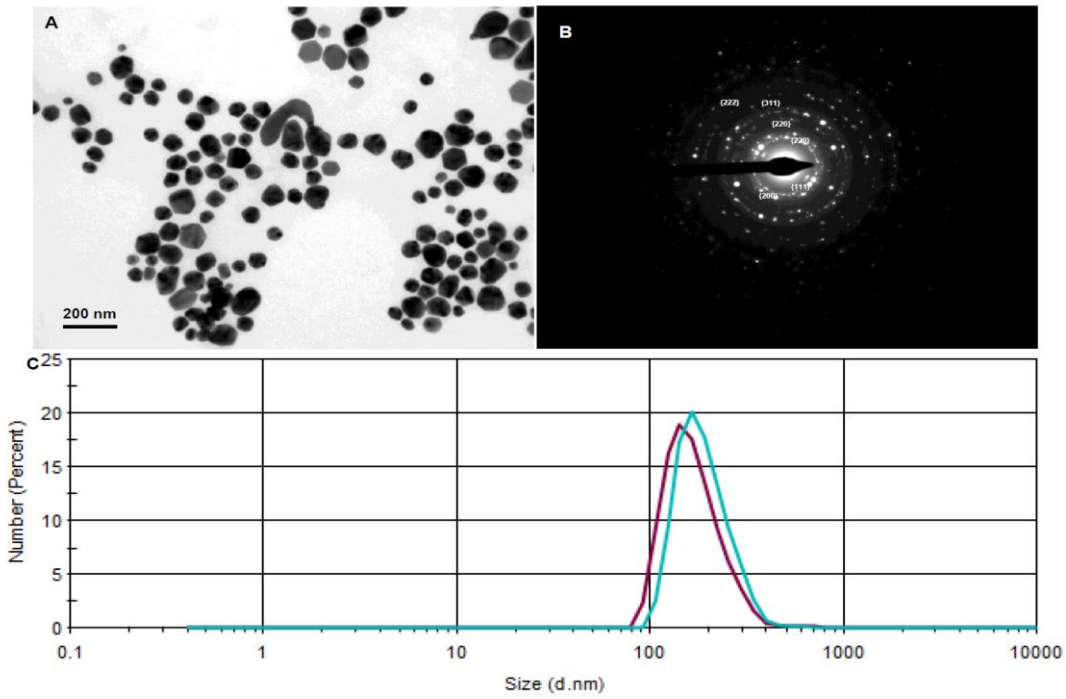

Figure S1. Nanoparticle size characterization. (A) TEM image shows the size and shape of CeO_2 NPs. (B) Selected area electron diffraction (SAED) of CeO_2 NPs. (C) Dynamic light scattering (DLS) analysis of the particle diameter calculated via size distribution by numbers. (n = 3 = three independent experiments, each experiment was performed in triplicates). Out of three, two of them were overlapping and the 3rd one covered the purple one.

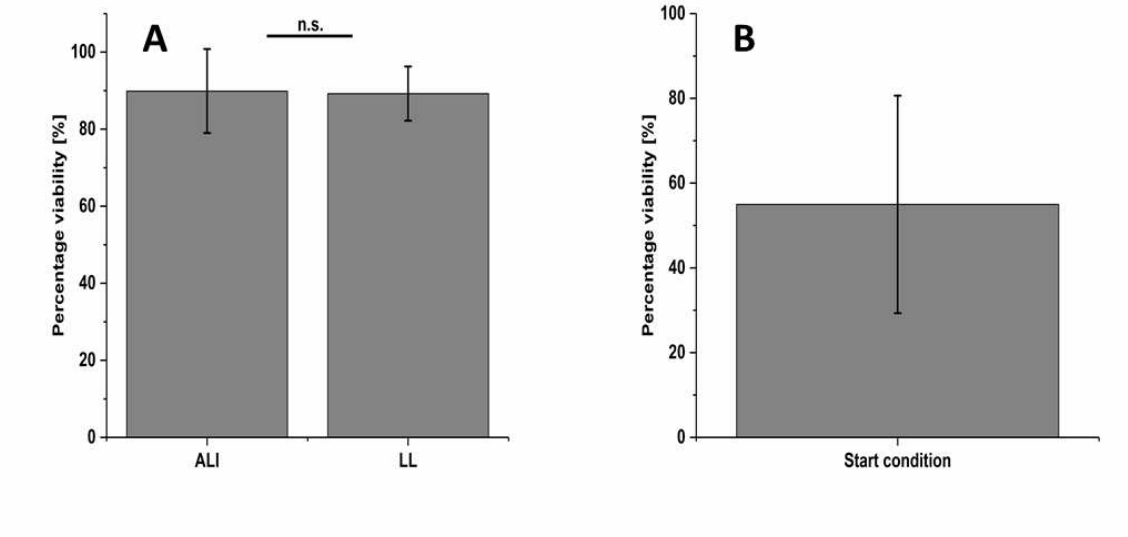

Figure S2. A549 cell viability. (A) shows cell viability under ALI and submerged (LL) culture conditions (no ALI exposure) compared to ALI cultured cells. (B) exhibits the cell viability after 1 h ALI clean air exposure compared to the incubator control without any optimization of the ALI system (initial conditions). Percentage viability values are the consensus values calculated for each of the three plates using the Bayesian modeling. The values are the means and the error bars the standard deviations.

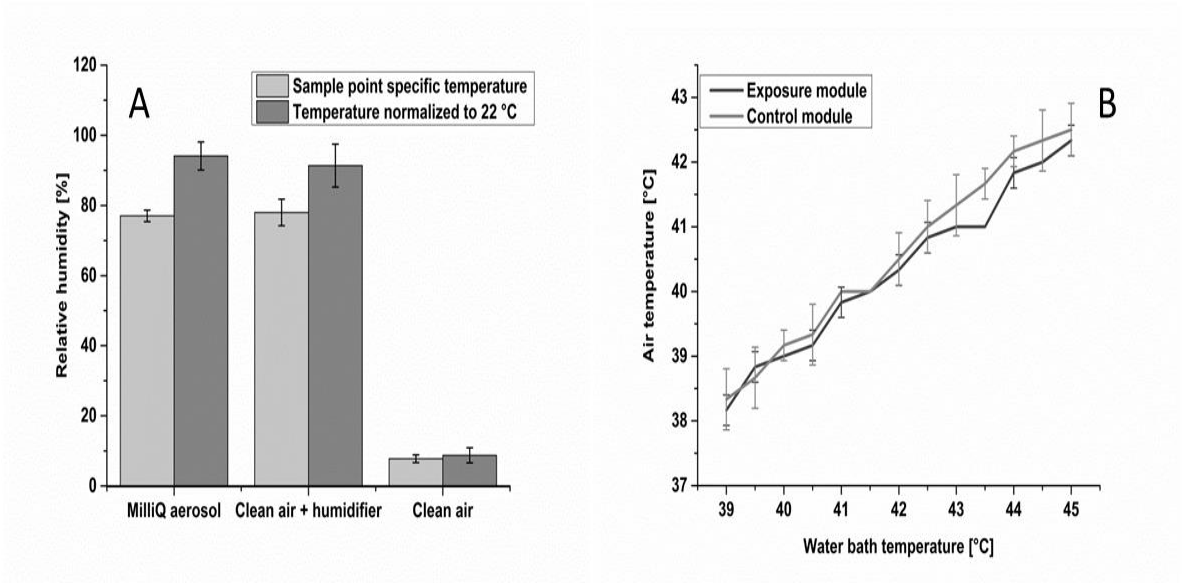

Figure S3. Characterization of the Vitrocell exposure 12/3 CF module. The relative humidity of the exposure air with and without humidification of the clean air, or a water droplet aerosol (MilliQ aerosol), which was used for particle exposure, is shown in (A). Heating the lid temperature to a certain degree does not necessarily mean that the aerosol flow temperature is equal to the lid temperature. Therefore, the relationship between the temperature of the air flow and the water bath temperature, which was used to heat the lid, is shown in part (B) for the particle exposure module and the control module (clean air only). n = 3 independent experiments with 1 technical replicate each. The values are the means and the error bars the standard deviations.

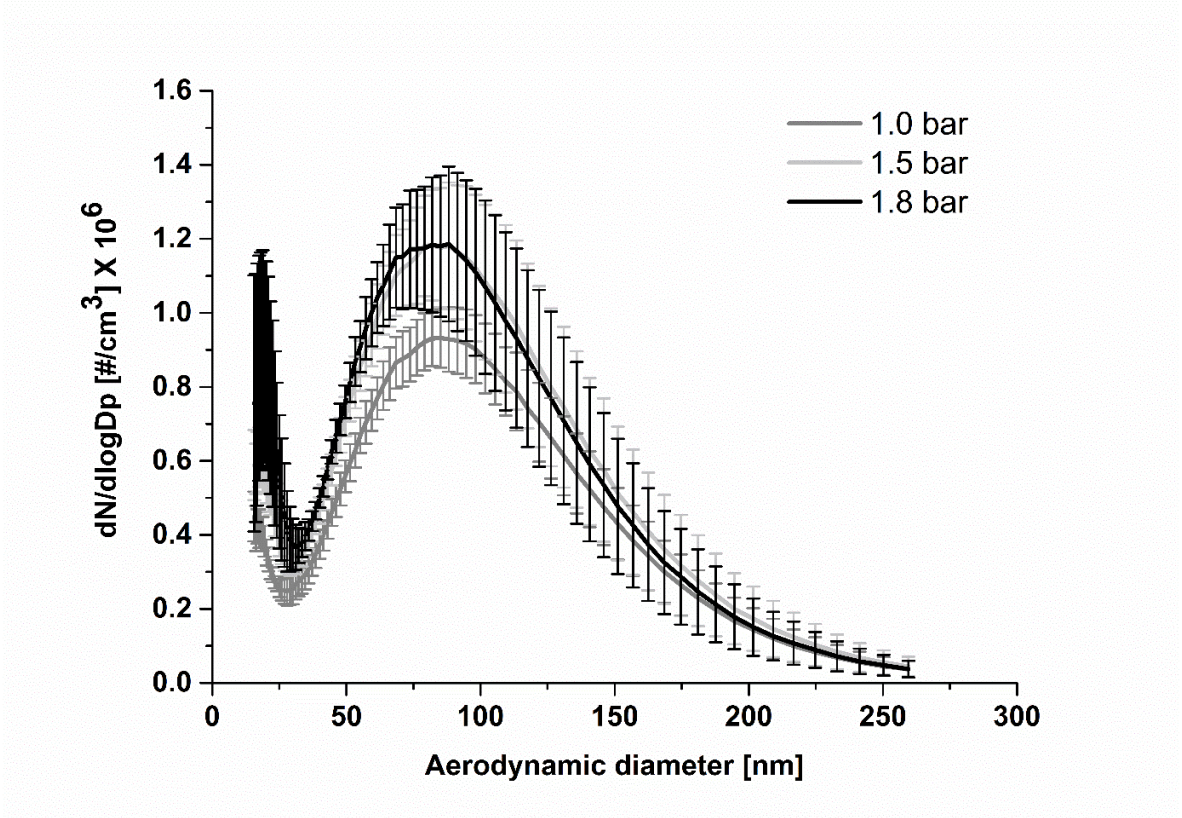

Figure S4. The particle size distribution of NM-212 as a function of the inlet pressure of the aerosol generator (n = 9 = three independent experiments with 3 data points each. Data from each experiment are combined and shown as mean ± SD).

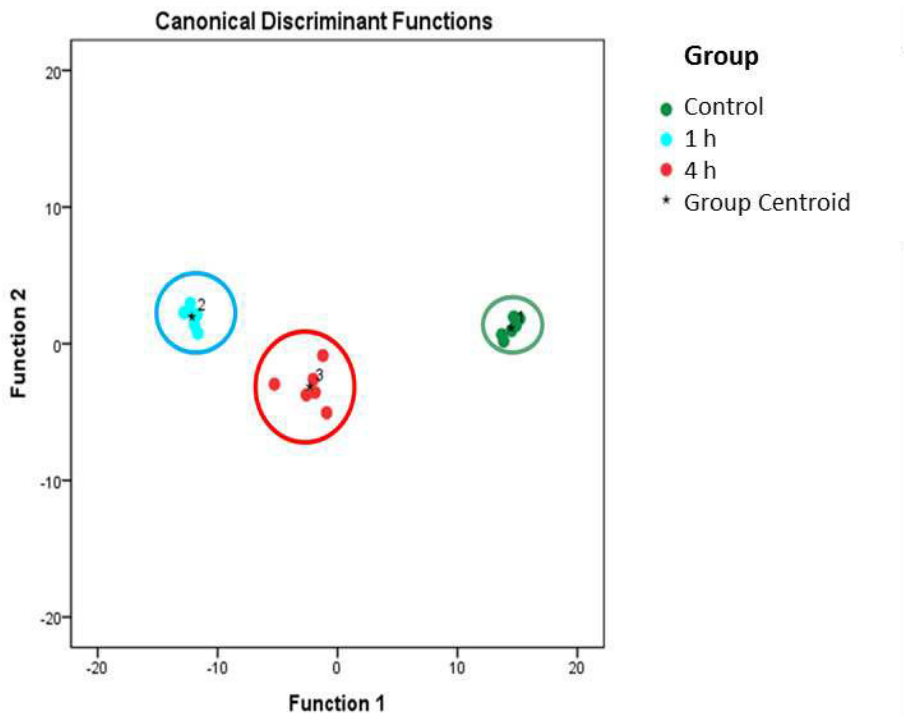

Figure S5. Fisher's linear discriminant of ToF-SIMS analysis (n = 6). Different groups show distinct differences.

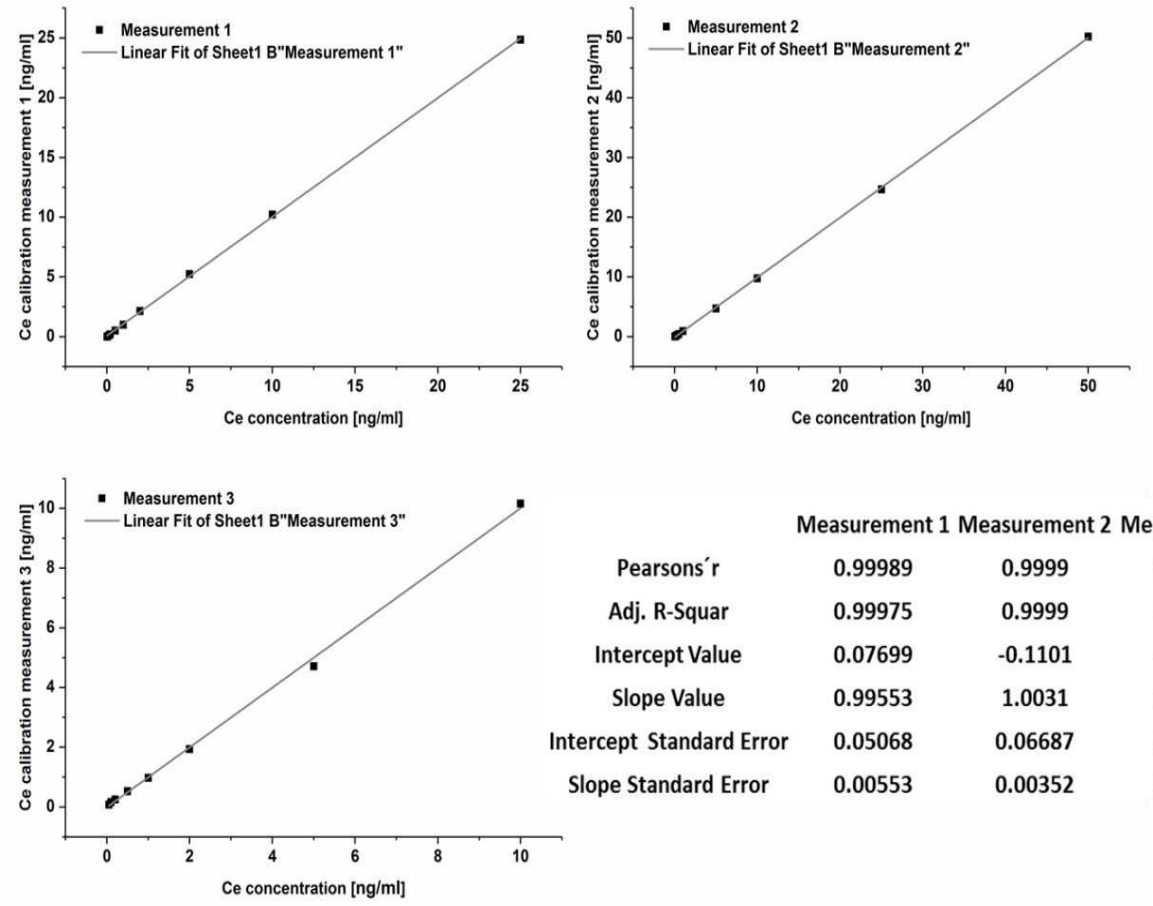

	Measurement 1	Measurement 2	Measurement 3
Pearsons´r	0.99989	0.9999	0.99931
Adj. R-Squar	0.99975	0.9999	0.99838
Intercept Value	0.07699	-0.1101	-0.00713
Slope Value	0.99553	1.0031	1.00104
Intercept Standard Error	0.05068	0.06687	0.06145
Slope Standard Error	0.00553	0.00352	0.01523

Figure S6. ICP-MS calibration curves of the three different measurements. The solid lines indicate a linear regression fit to the data.

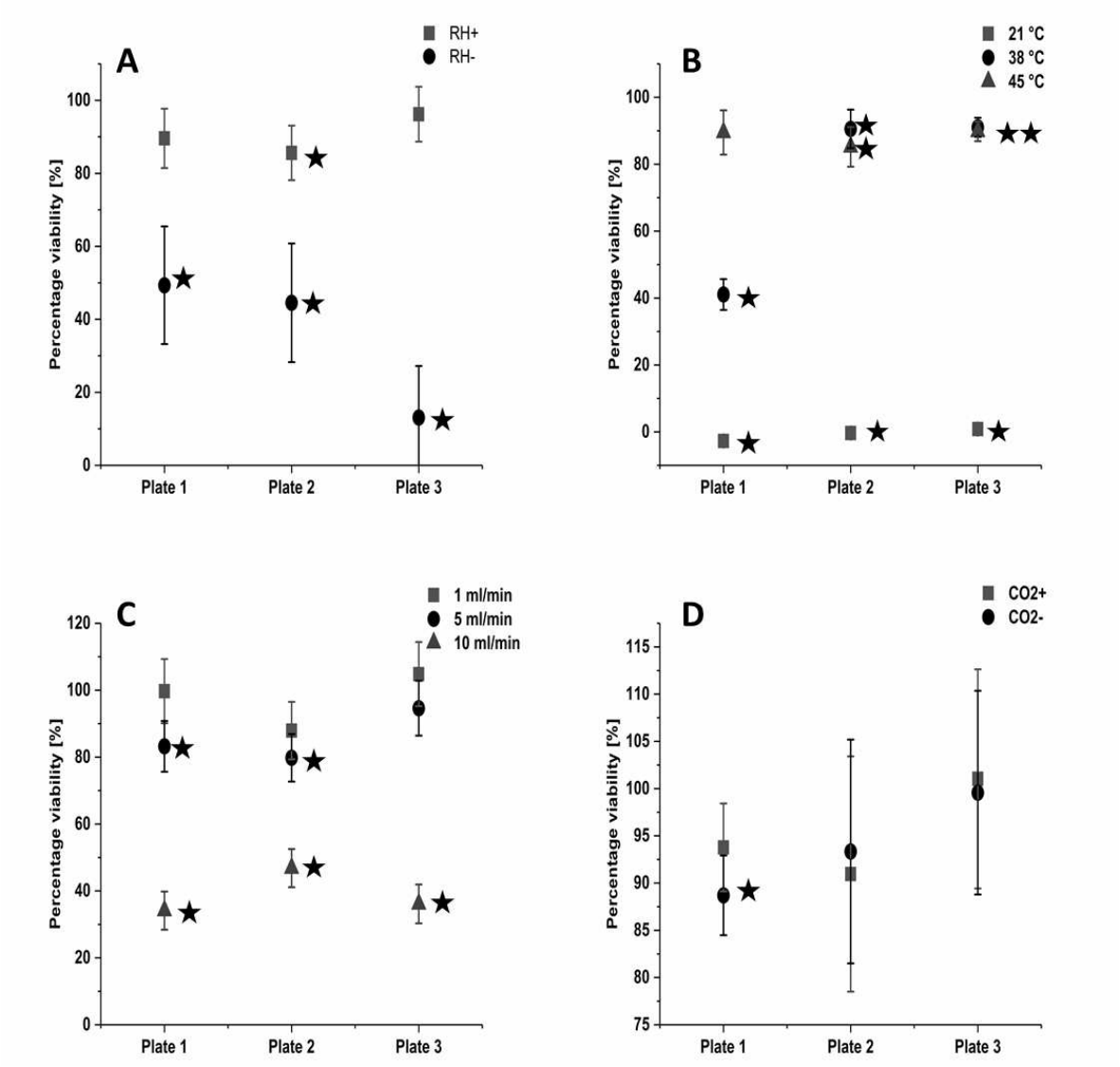

Figure S7. Plate to plate analysis of consensus values for the different parameters affecting cell viability: Relative humidity (A), lid temperature (B), flow rates (C) and 5 % CO_2 supply (D). Percentage viability values are the consensus values calculated for each of the three plates using the Bayesian modeling. The values are the means and the error bars the standard deviation. Black asterisks indicate that the consensus value is significantly less than the incubator control with a 95 % likelihood using the Bayesian modeling.

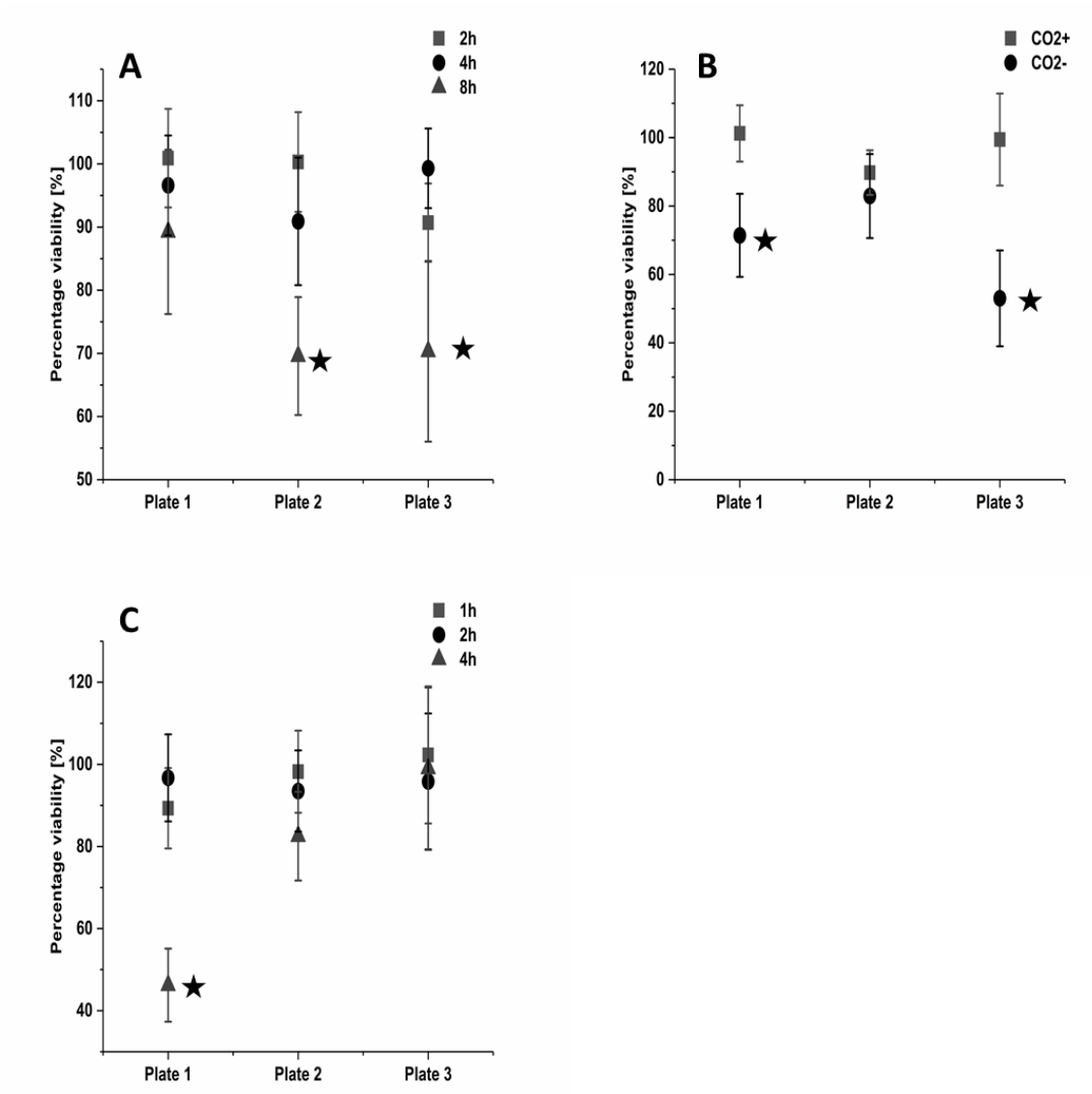

Figure S8. Plate to plate analysis of consensus values for the different parameters affecting cell viability: (A) Time-dependent cell viability for MilliQ water aerosol exposure (without ENM) using the optimized Vitrocell setup. (B) Effect of 5 % CO_2 supply to the air on the cell viability after 4 h MilliQ water aerosol exposure using the optimized Vitrocell exposure setup. (C) A time-dependent NM-212 exposure compared to MilliQ water aerosol (without NP) exposed cells. Percentage viability values are the consensus values calculated for each of the three plates using the Bayesian modeling. The values are the means and the error bars the standard deviation. Black asterisks indicate that the consensus value is significantly less than the incubator control with a 95 % likelihood using the Bayesian modeling.

50 Table S1. Mycoplasma test, PCR compounds.

Material	Manufacture	Article number	Sequence
TaqDNA polymerase	New England Biolabs	M0320L	
Forward Primer			5′-ggC GAA Tgg gTg AgT AAC ACg-3′
Reverse Primer			5′-Cgg ATA ACg CTT gCg ACC TAT g-3′
dNTP set (nuleotides)	Fermentas	R0182	
Genomic DNA extract from mycoplasma fermentans (positive control)	Minerva	51-0117	
GeneRuler™ 1 kb Plus DNA Ladder	Fermentas	SM1331	

51

52 Table S2. Mycoplasma test, PCR conditions and protocol.

Temperature [°C]	Time [seconds]	Comment
94	300	Initial denaturation
55	105	Initial denaturation
72	45	Initial denaturation
3 cycles of the following three steps		
94	45	
55	105	
72	180	
40 cycles of the following two steps		
94	45	
55	45	
1 cycles of the following three steps		
72	10	
27	10	
4	infinite	

53 Table S3. ICP-MS LOD/LOQ levels of the three different measurements.

Measurement	LOD [ng/ml]	LOQ [ng/ml]	Background levels [ng/ml]	R-values
1	1.22×10^{-4}	2.75×10^{-4}	5.10×10^{-5}	0.99969
2	6.29×10^{-3}	1.73×10^{-2}	1.57×10^{-3}	0.99969
3	7.19×10^{-2}	7.30×10^{-2}	7.15×10^{-2}	0.99931

54

55 Table S4. Possible pitfalls during an ALI exposure experiment.

Pitfalls	Troubleshooting/Advise
Chamber incompletely/not fully closed.	Connect all gas exit tubes together and check flow rates. The flow rate entering the system should be equal to the sum of the three insert flow rates. Check the seal ring for any damage as well as its correct position. Check/correct tightness of seal clamps.
Retention of cleaning solution (ethanol, H_2O) inside the chamber.	Wash two times with 5 ml medium before adding medium for the exposure to remove ethanol completely.
Too much medium inside the chamber or inhomogeneous membrane covering of the medium at basolateral side.	If medium is rising above the insert at the edges, remove excessive medium, and then check whether the chamber is leveled.
Not enough medium inside the chamber.	Check whether membrane is in contact with the medium, and then add medium if needed.
Incomplete cell monolayer.	If microscopic analyses before transferring into ALI exposure system reveals that the monolayer is not complete; consider adjusting the ALI culture protocol (extending growth time, increasing number of cells).
Low cell viability because of incorrect flow rate or no flow into the exposure chamber.	Flow rate should be checked before placing cells inside the chamber (valve positions of the vacuum pump can change day to day between experiments due to strong vibration of the vacuum pump). The connection has to be proven after checking for any leakages every time before starting the exposure.
Low cell viability because of no humidifier connection.	The connection should be proven after checking for any leakages every time before starting the exposure.
Gas supply runs out during exposure.	If possible, switch from gas bottles to house gas lines to avoid disruption of gases due to empty bottles during exposure. Filter house gas by a hydrocarbon filter and a molecular sieve to remove generator oil.

	Alternatively, replace the gas bottle earlier to avoid running out during a cellular exposure.
The gas has an overly high pressure in the chamber.	Reduce generator pressure/aerosol flow to avoid mechanical cell damage by the air flow.
Cell monolayer is not present in the center of the monolayer after exposure.	One potential cause is that the air inlet is too close to the cells. In this case, adjust inlet height until no cell damage is visually observed (i.e., cells may not be present in the middle of the insert). Another potential cause is that the insert flow rate is too high. In this case, reduce the flow rate until no cell damage is visually observable. A third potential cause is insufficient humidity. In this case, check the relative humidity.
Contamination of cells occurs during the exposure experiment.	Routinely clean the chamber before and after use. Add antibiotics and fungicides to the cell culture medium. Perform the whole experiment under sterile conditions if possible.
SMPS particle contamination observed.	Before measuring a particle size distribution, a control clearance check by performing a standard measurement with a HEPES filter in front of the SMPS air inlet should be performed. If particles are detected, then clean device to remove old particles by setting the sheath flow to 30 ml/min using the HEPA filter in front of the SMPS air inlet. Then, conduct a control clearance check again. No particles should be detected after the system is cleaned. Clean device after use by setting the sheath flow to 30 ml/min for a minimum of 30 minutes, using the HEPA filter in front of the SMPS air inlet.
No deposition detectable.	Air inlet possibly too far away from the cells. Try performing deposition measurements on an empty insert and quantifying the deposition.

56

Annex II

Supplementary Data

Nanoparticle induced barrier function assessment at liquid–liquid and air–liquid interface in novel human lung epithelia cell lines

Lars Leibrock, Sandra Wagener, Ajay Vikram Singh, Peter Laux, and Andreas Luch

This chapter was published online on 19.11.2019 in:

Toxicology Research, 2019, **8**, 1016-1027 by Oxford University Press

https://doi.org/10.1039/C9TX00179D

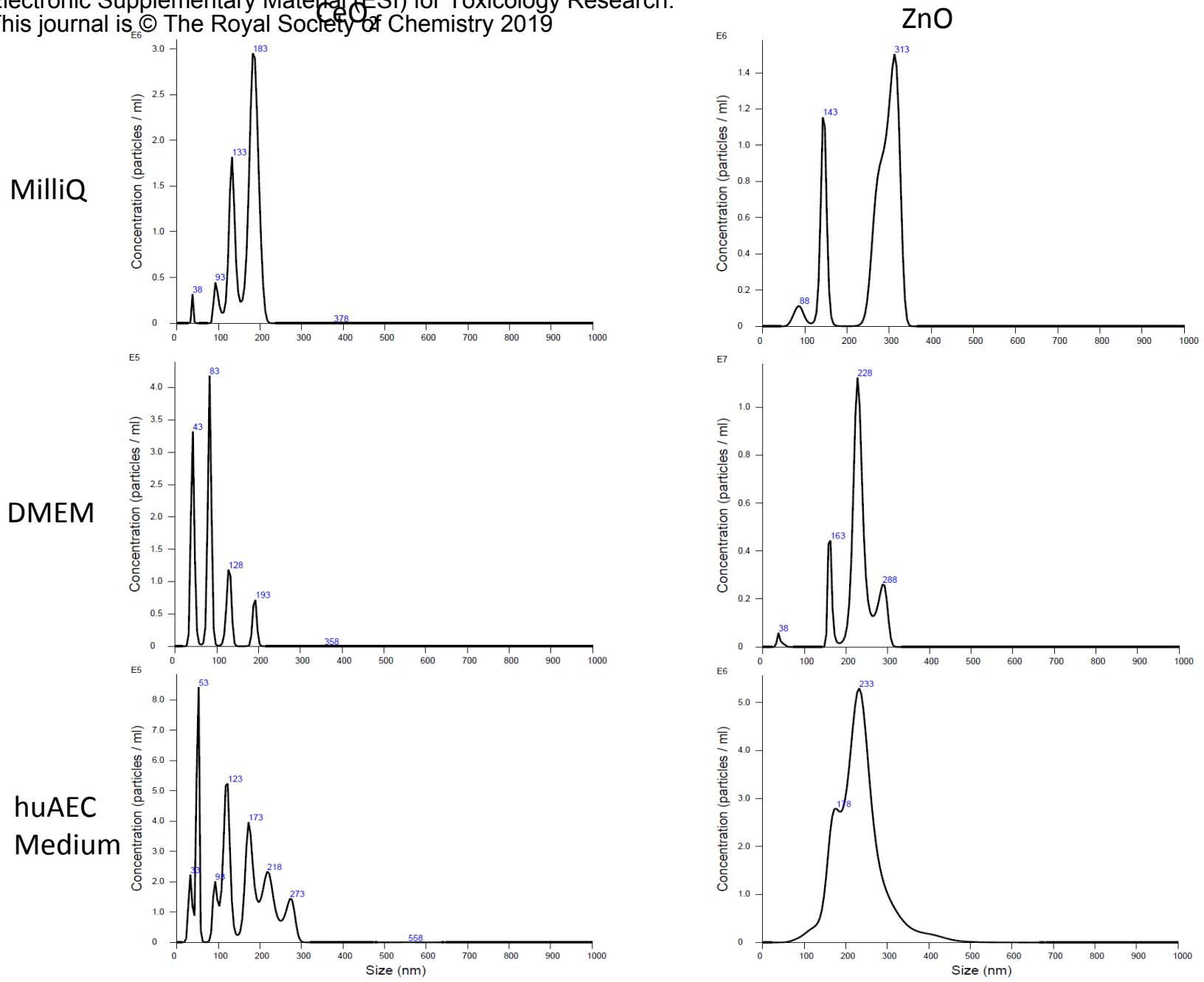

Supplemental figure 1: Particle size distribution of CeO_2 and ZnO NPs analyzed by NTA.

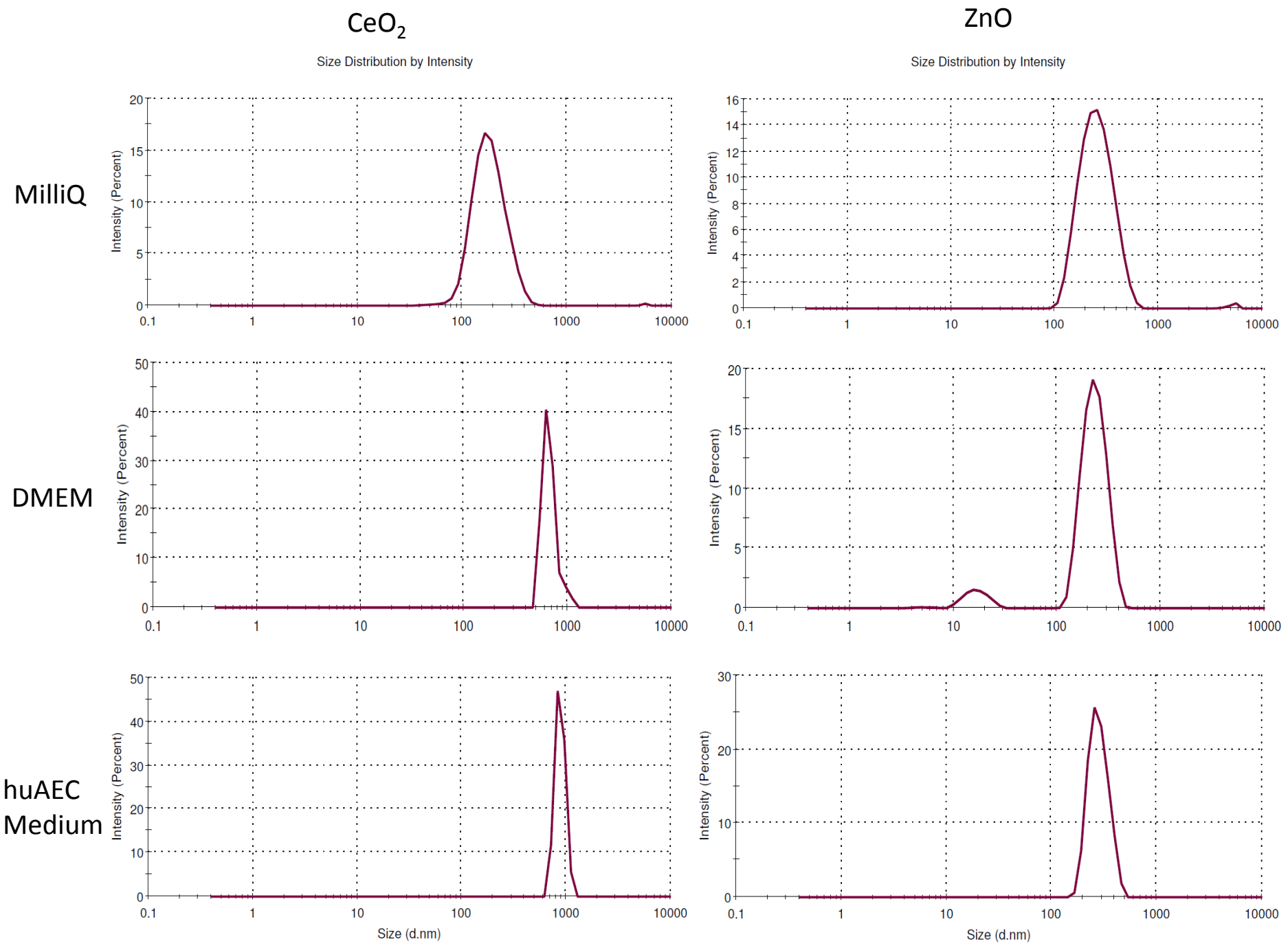

Supplemental figure 2: Particle size distribution of CeO_2 and ZnO NPs analyzed by DLS.